Technical Report Documentation Page

1. Report No.	2. Government Accession No.	3. Recipient's Catalog No.
7-1982-2		

4. Title and Subtitle	5. Report Date
Effects of Traffic and Wind Loads on a Tied-Arch Bridge	December 1994
	6. Performing Organization Code
7. Author(s)	8. Performing Organization Report No.
Partha P. Sarkar, W. Pennington Vann, et.al.	7-1982-2
9. Performing Organization Name and Address	10. Work Unit No. (TRAIS)
Department of Civil Engineering Texas Tech University Box 41023 Lubbock, Texas 79409-1023	11. Contract or Grant No. 7-1982-2
	13. Type of Report and Period Covered
12. Sponsoring Agency Name and Address	Interim February 1994 - December 1994
Texas Department of Transportation Research & Technology Transfer Office Austin, Texas 78763	14. Sponsoring Agency Code

15. Supplementary Notes

This study was conducted in cooperation with the U.S. Department of Transportation

16. Abstract

The purpose of this study is to assess the sensitivity of four highway bridges to wind and live loadings. The bridges are planned for construction on U.S. 59 in Houston, Texas. Each bridge will be of the tied-arch type and will be constructed on-grade over cut areas with clear spans in excess of 61 meters (200 feet). To expedite construction, unique procedures are planned which use existing bridges as platforms for final fabrication of the tied arches. This procedure requires consideration of wind loading on the arches during construction.

In this study, the bridge design is analyzed under the expected wind loadings based on assumed aerodynamic parameters and the bridge details furnished by the Texas Department of Transportation. A geometrically-scaled wind tunnel model of a typical bridge was built and tested to determine the actual aerodynamic parameters. The wind tunnel test results and the traffic loading results are presented. The analytical study shows that the completed bridge is aerodynamically stable and will not have any major problems due to dynamic vibrations. The same is true for the partially constructed state where the two arches are braced together without the deck. Vortex shedding excitation emerged as more critical than buffeting excitation of the deck and, therefore, was more closely examined. Dynamic stresses and dynamic deflections due to traffic loads are too small to cause structural fatigue or driver discomfort. It is concluded that the proposed arch bridges over U.S. 59 in Houston should not have any problems with wind or traffic loadings.

17. Key Words	18. Distribution Statement
Wind loadings, dynamic analyses, vortex shedding, buffeting, flutter, highway bridges, wind tunnel testing	NO RESTRICTIONS This document is available to the public through the National Technical Information Service, Springfield, VA 22161

19. Security Classif. (of this report)	20. Security Classif. (of this page)	21. No. of Pages	22. Price
UNCLASSIFIED	UNCLASSIFIED		

Effects of Traffic and Wind Loads on a Tied-Arch Bridge

by

Partha P. Sarkar
W. Pennington Vann
Phillip T. Nash
Kishor C. Mehta
J. Walt Oler
Wendong Wang
Himanshu Gupta
Jianmin Yin

Final Research Report Number 7-1982-2

conducted for the
Texas Department of Transportation

by the
DEPARTMENT OF CIVIL ENGINEERING
TEXAS TECH UNIVERSITY

DECEMBER, 1994

IMPLEMENTATION STATEMENT

Analytical and experimental results will provide guidance for final bridge designs and erection procedures.

FEDERAL/DEPARTMENT CREDIT

Prepared in cooperation with the Texas Department of Transportation and the U.S. Department of Transportation.

DISCLAIMER

Any opinions, findings, and conclusions or recommendations expressed in this material are those of the authors and do not necessarily reflect the views or policies of the Texas Department of Transportation (TxDOT). This report does not constitute a standard, specification or regulation.

There was no invention or discovery conceived or first actually reduced to practice in the course of or under this contract, including any art, method, process, machine, manufacture, design or composition of matter, or any new and useful improvement thereof, or any variety of plant which is or may be patentable under the patent laws of the United States of America or any foreign country.

METRIC CONVERSION FACTORS

Approximate Conversions to Metric Measures

Symbol	When You Know	Multiply by	To Find	Symbol
	LENGTH			
in	inches	*2.5	centimeters	cm
ft	feet	30	centimeters	cm
yd	yards	0.9	meters	m
mi	miles	1.6	kilometers	km
	AREA			
in^2	square inches	6.5	square centimeters	cm^2
ft^2	square feet	0.09	square meters	m^2
yd^2	square yards	0.8	square meters	m^2
mi^2	square miles	2.6	square kilometers	km^2
	acres	0.4	hectares	ha
	MASS (weight)			
oz	ounces	28	grams	g
lb	pounds	0.45	kilograms	kg
	short tons (2000 lb)	0.9	tonnes	t
	VOLUME			
tsp	teaspoons	5	milliliters	ml
Tbsp	tablespoons	15	milliliters	ml
fl oz	fluid ounces	30	milliliters	ml
c	cups	0.24	liters	l
pt	pints	0.47	liters	l
qt	quarts	0.95	liters	l
gal	gallons	3.8	liters	l
ft^3	cubic feet	0.03	cubic meters	m^3
yd^3	cubic yards	0.76	cubic meters	m^3
	TEMPERATURE (exact)			
°F	Fahrenheit temperature	5/9 (after subtracting 32)	Celsius temperature	°C

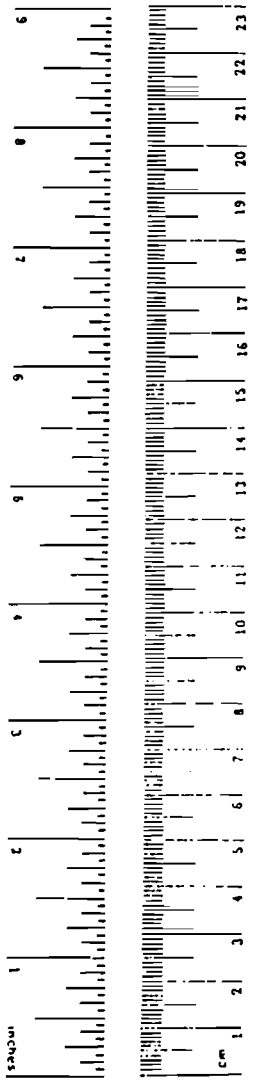

Approximate Conversions from Metric Measures

Symbol	When You Know	Multiply by	To Find	Symbol
	LENGTH			
mm	millimeters	0.04	inches	in
cm	centimeters	0.4	inches	in
m	meters	3.3	feet	ft
m	meters	1.1	yards	yd
km	kilometers	0.6	miles	mi
	AREA			
cm^2	square centimeters	0.16	square inches	in^2
m^2	square meters	1.2	square yards	yd^2
km^2	square kilometers	0.4	square miles	mi^2
ha	hectares (10,000 m^2)	2.5	acres	
	MASS (weight)			
g	grams	0.035	ounces	oz
kg	kilograms	2.2	pounds	lb
t	tonnes (1000 kg)	1.1	short tons	
	VOLUME			
ml	milliliters	0.03	fluid ounces	fl oz
l	liters	2.1	pints	pt
l	liters	1.06	quarts	qt
l	liters	0.26	gallons	gal
m^3	cubic meters	35	cubic feet	ft^3
m^3	cubic meters	1.3	cubic yards	yd^3
	TEMPERATURE (exact)			
°C	Celsius temperature	9/5 (then add 32)	Fahrenheit temperature	°F

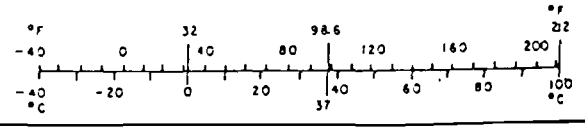

METRIC CONVERSION FACTORS

TABLE OF CONTENTS

Page

Implementation Statement iv
Federal/Department Credit v
Disclaimer vi
List of Figures x
List of Tables xii
Summary xiii

1. Introduction 1
    1.1. Background 1
    1.2. Statement of the Problem 3
    1.3. Objectives 3

2. Bridge Designs and Loadings 5
    2.1. Design Information 5
    2.2. Expected Wind Loading 5
    2.3. Expected Traffic Loading 14

3. Wind Tunnel Studies 18
    3.1. Deck Model Description 18
    3.2. Wind Tunnel Facility 18
    3.3. Experimental Results 22

4. Static Analysis 24
    4.1. Finite Element Model Description 24
    4.2. Comparison to TxDOT Vertical Loading Results 27
    4.3. Design Wind Loading 31
    4.4. Mean Wind Loading 32

5. Natural Frequencies and Modes of Vibration 35

6. Time Domain Analysis of Response to Buffeting Winds 40

7. Time Domain Analysis of Response to Traffic Loading 48
    7.1. Static Response 48
    7.2. Dynamic Response 52

8. Frequency Domain Analysis 74
    8.1. Flutter Instability 74
        8.1.1. Background 74
        8.1.2. Expermental Results 74
        8.1.3. Flutter Analysis 75

8.2. Buffeting Response of the Deck 80
8.2.1. Background 80
8.2.2. Expermental Results 80
8.2.3. Buffeting Analysis 81
8.3. Vortex-Induced Response of the Deck 86
8.3.1. Background 86
8.3.2. Expermental Results 87
8.3.3. Vortex-Shedding Analysis 87
8.4. Vortex-Induced Response of Deck Hangers 90
8.4.1. Background 90
8.4.2. Analysis of Vortex-Induced Responses of Deck Hangers 91

9. Conclusions 93
10. References 95

LIST OF FIGURES

No.	Title	Page
1.1	Photographs of a Typical Existing Bridge	2
2.1	Model of a Typical Tied Arch Bridge (Houston Disrtict, TxDOT)	6
2.2	Plan and Elevation of a Typical Tied Arch Bridge (Houston District, TxDOT)	7
2.3	Cross-section of the Deck of a Typical Tied Arch Bridge (Houston District,TxDOT)	8
2.4	Cross-Section of the Deck of a Typical Tied Arch Bridge	9
2.5	Aerial View Showing an Existing Bridge on U.S. 59 in Houston, TX	10
2.6	Correlation Coefficients for the Bridge	15
2.7	Model of HS20-44 Truck	17
3.1	Details of the Bridge Deck Section Model	19
3.2	Hollowed out Aluminum Block for the Section Model	20
3.3	Full View of the Bridge Deck Section Model	21
3.4	Texas Tech Wind-Tunnel Facility	23
4.1	First Level Model of Completed Bridge (77 nodes) Using STARDYNE	25
4.2	Second Level Model of Completed Bridge (341 nodes) Using STARDYNE	26
4.3	First Level Model of Partially Completed Bridge Using STARDYNE	28
4.4	Deflections of Completed Bridge Under Dead Load Plus Prestress	30
4.5	Static Wind Deflections Under 75 psf (3.6 KPa) for the Partially Completed Bridge	33
5.1	First Ten Frequencies and Mode Shapes of the Completed Bridge	37
5.2	First Ten Frequencies and Mode Shapes of the Partially Completed Bridge	38
6.1	Time History of Buffeting Wind Loading at the Top of the Arch	41
6.2	Assumed Along-Wind and Vertical Power Spectra for the Arch and Deck	43
6.3	Dynamic Lateral Deflections at the Top of the Arch	44
6.4	Dynamic Vertical Deflections of the Deck at Midspan due to Lift and Moment	47
7.1	Computer Model of the Bridge for Traffic Analysis	49
7.2	Static Deflection Shapes due to a Single Truck	50
7.3	Influence Line of Quarter Span Point due to a Single Truck	51
7.4	Time History of Truck Loading at Midspan for 30 mph Vehicle Speed	53
7.5	Time History of Truck Loading at Midspan for 60 mph Vehicle Speed	55
7.6	Dynamic Response of Quarter Span Point for One Truck Traveling at 30 mph	56
7.7	Dynamic Response of Quarter Span Point for One Truck Traveling at 60 mph	57
7.8	Dynamic Response of Midspan Point for One Truck Traveling at 30 mph	58
7.9	Dynamic Response of Midspan Point for One Truck Traveling at 60 mph	59

LIST OF FIGURES (CONTINUED)

No.	Title	Page
7.10	Dynamic Response of Quarter Span Point for Two Trucks Following with Full Separation at 30 mph	62
7.11	Dynamic Response of Quarter Span Point for Two Trucks Following with Full Separation at 60 mph	63
7.12	Dynamic Response of Quarter Span Point for Two Trucks Following with Half Separation at 30 mph	65
7.13	Dynamic Response of Quarter Span Point for Two Trucks Following with Half Separation at 60 mph	66
7.14	Dynamic Response of Quarter Point for Two Trucks Meeting at Midspan at 30 mph	67
7.15	Dynamic Response of Quarter Point for Two Trucks Meeting at Midspan at 60 mph	68
7.16	Dynamic Response of Quarter Span Point for Two Trucks Meeting There at 30 mph	69
7.17	Dynamic Response of Quarter Span Point for Two Trucks Meeting There at 60 mph	70
7.18	Comparison of Deflections of Quarter Span Point Between Static and Dynamic Responses	72
8.1(a)	Flutter Derivatives A_2^* vs. Wind Speed	76
8.1(b)	Flutter Derivatives A_3^* vs. Wind Speed	77
8.1(c)	Flutter Derivatives H_1^* vs. Wind Speed	78
8.1(d)	Flutter Derivatives H_4^* vs. Wind Speed	79
8.2	Two Different Grids for Wind Tunnel Turbulence	82
8.3	Comparison of Standard Deviations Between Time and Frequency Domain Analyses	85
8.4	Span-wise Correlation of Vortices Shed from the Deck	88

LIST OF TABLES

No.	Title	Page
4.1	Comparison of Static Midspan Vertical Deflection with TxDOT Results	29
4.2	Static Deflections and Stresses Due to Design Wind Loading (75 psf = 3.6 KPa)	31
4.3	Static Deflections and Stresses Due to Mean Wind Loading	34
4.4	Deflections at Midspan Due to Mean Wind Lift and Moment Loading	34
5.1	First Ten Frequencies of the Completed Bridge	36
5.2	First Ten Frequencies of the Partially Completed Bridge	36
6.1	Peak Dynamic Deflections and Stresses Due to Buffeting Wind Loading for Partially Completed Bridge	42
6.2	Peak Dynamic Deflections and Stresses Due to Buffeting Wind Loading for Completed Bridge	45
6.3	Peak Dynamic Deflections at Midspan Due to Fully Correlated Lift and Moment	46
6.4	Peak Dynamic Deflections at Midspan Due to Partially Correlated Lift and Moment	46
7.1	Static Normal Stresses Due to a Single Truck at the Quarter Span Point	52
7.2	Peak Dynamic Centerline Deflection Due to Traffic Loading	71
8.1	Static Aerodynamic Coefficients	80
8.2	Standard Deviation of the Vertical Buffeting Response (σ_h) and Torsional Buffeting Response (σ_α) of the Deck by the Frequency Domain Method	83
8.3	Vertical Deflection of the Deck due to Vortex-Shedding (with Traffic Signs)	89
8.4	Dynamic Response of the Hangers	91

SUMMARY

The purpose of this study is to assess the sensitivity of four highway bridges to wind and traffic loadings. Each bridge will be construction on-grade over a depressed section of U.S. 59 in Houston, Texas. Each bridge will be of the tied arch type with a clear span of approximately 69.5 m (228 feet). To expedite construction, unique procedures are planned using existing bridges as platforms for final fabrication of the tied arches. Final design and erection plans require consideration of wind loading on the arches during construction as well as on the completed bridges.

In this study, the bridge design is analyzed under the expected static and dynamic wind and traffic loadings. Structural systems considered under wind loading include the final configuration and the partially constructed state in which the tied arches will be braced together without the deck. Completed bridges with traffic signs in different positions are also considered under wind effects. Wind tunnel tests on a geometrically scaled model of the bridge deck provide information on aerodynamic parameters required for predicting wind loads.

Analytical results indicate that the peak dynamic stresses due to buffeting from a turbulent wind with a basic wind speed of 40 m/s (90 mph) as per ASCE 7-88 acting perpendicular to the completed bridge will only be of the order of 14 MPa (2 ksi). Stresses of this magnitude should not create fatigue problems in the bridge. For the stage of partial construction, when the existing bridge has been removed but the new deck has not been installed, buffeting wind stresses may be considerably larger, or as much as 104 MPa (15 ksi), but there still should be no fatigue problem because of the very short time when this stage of construction may be subjected to the wind.

Flutter analysis of the deck shows that with and without attached traffic signs it is aeroelastically stable.

Maximum excursions of the deck in vertical deflection and in angular rotation from the position of static equilibrium are calculated due to both vortex shedding and buffeting. Vortex shedding response could be greater than the buffeting response at the design wind speed, but it is less likely to develop because it will not occur except near the calculated lock-in wind speed of 36 m/s (81 mph). In the calculations for the worst vortex shedding

deflection a lower bound damping ratio of 0.5% is assumed for conservative purposes. The maximum vertical deck deflection due to vortex shedding is calculated to be 0.24 m (0.79 ft) at a wind speed of 36 m/s (81 mph).

The maximum vertical deck deflection due to buffeting corresponding to a mean wind speed at the deck level of 27.6 m/s (62 mph), which is based on the basic wind speed of 40 m/s (90 mph), is calculated to be 0.09 m (0.31 ft). The maximum deck rotation due to buffeting at this wind speed is calculated to be 0.021 radians, which corresponds to a vertical deflection at the edge of 0.19 m (0.63 ft). Very small maximum dynamic deflections are calculated for the hanger cables, indicating that they will not suffer fatigue problems or have a noisy hum.

Dynamic stresses due to moving traffic loads are calculated to be less than 27.22 MPa (3.945 ksi), or too small to cause fatigue problems. The dynamic deflections due to traffic loading will be less than 19.2 mm (0.063 ft), which should not cause user discomfort. Maximum impact factors from traffic loads are found to be less than 1.10.

The overall conclusion from this project is that the proposed arch bridges over US59 in Houston should not have any problems with wind or traffic loadings.

1. INTRODUCTION

1.1. Background

The Texas Department of Transportation (TxDOT) plans to construct four bridges over U.S. 59 in Houston, Texas. The four bridges will cross U.S. 59 at Hazard, Woodhead, Dunlavy, and Mandell streets. Existing bridges at those locations (see Figure 1.1) have piers in the middle and vertical clearances above U.S. 59 of about 4.4 m (14.5 feet). These clearances must be increased to 5.03 m (16.5 feet) and the intermediate piers must be eliminated so that the existing medians can become high occupancy vehicle (HOV) lanes. Thus the bridge spans will be roughly doubled, further increasing the demand on the structural systems supporting the prestressed decks.

The surface elevations of U.S. 59 cannot be lowered because of a 1.83 m (72-inch) diameter storm sewer under the present bridges. The storm sewer is required to prevent flooding, and its removal would create the need for two additional pumping stations. At the bridge locations, U.S. 59 lacks sufficient width to accommodate traffic during removal of the existing bridges. In addition, the bridge surface levels cannot be raised appreciably because of their need to connect to existing city streets, driveways and buildings. In order to increase the clearances and keep the surface levels roughly the same, the depths of the deck structures need to be decreased. Virtually the only design option is a variable depth, two-way prestressed slab supported from above the deck.

The support of the deck can be accomplished by one of the following systems: spline beams, trusses, arches, cable stays, or suspension cables. Cable stays and suspension cables have been eliminated because there are no feasible locations for the necessary towers and tie backs. Of the remaining structural options, arches have been selected by TxDOT on the basis of aesthetics. In summary, the arches are needed to provide a bridge with an effective deck depth of only 0.305 m (1 foot) and a clear span of 69.5 m (228 feet) that can be built over traffic with a minimum time of closure of the lanes below.

The vibrational characteristics of long-span bridges make them particularly sensitive to wind and other live loadings. Depending upon the dynamic characteristics of a bridge, wind loads can affect individual elements or the structure as a whole. Vortex shedding around individual elements such as hangers can induce vibration and consequent fatigue failure. Buffeting wind loads can cause horizontal, vertical or torsional vibrations of major portions of tied arch bridges. Wind loadings could be critical both during and after construction. Similarly, live loadings from traffic can create vibration of the bridge and its elements. Vibrations depend upon the dynamic characteristics of the bridge and the frequencies of the wind and traffic loads. Loadings in near-phase with the natural

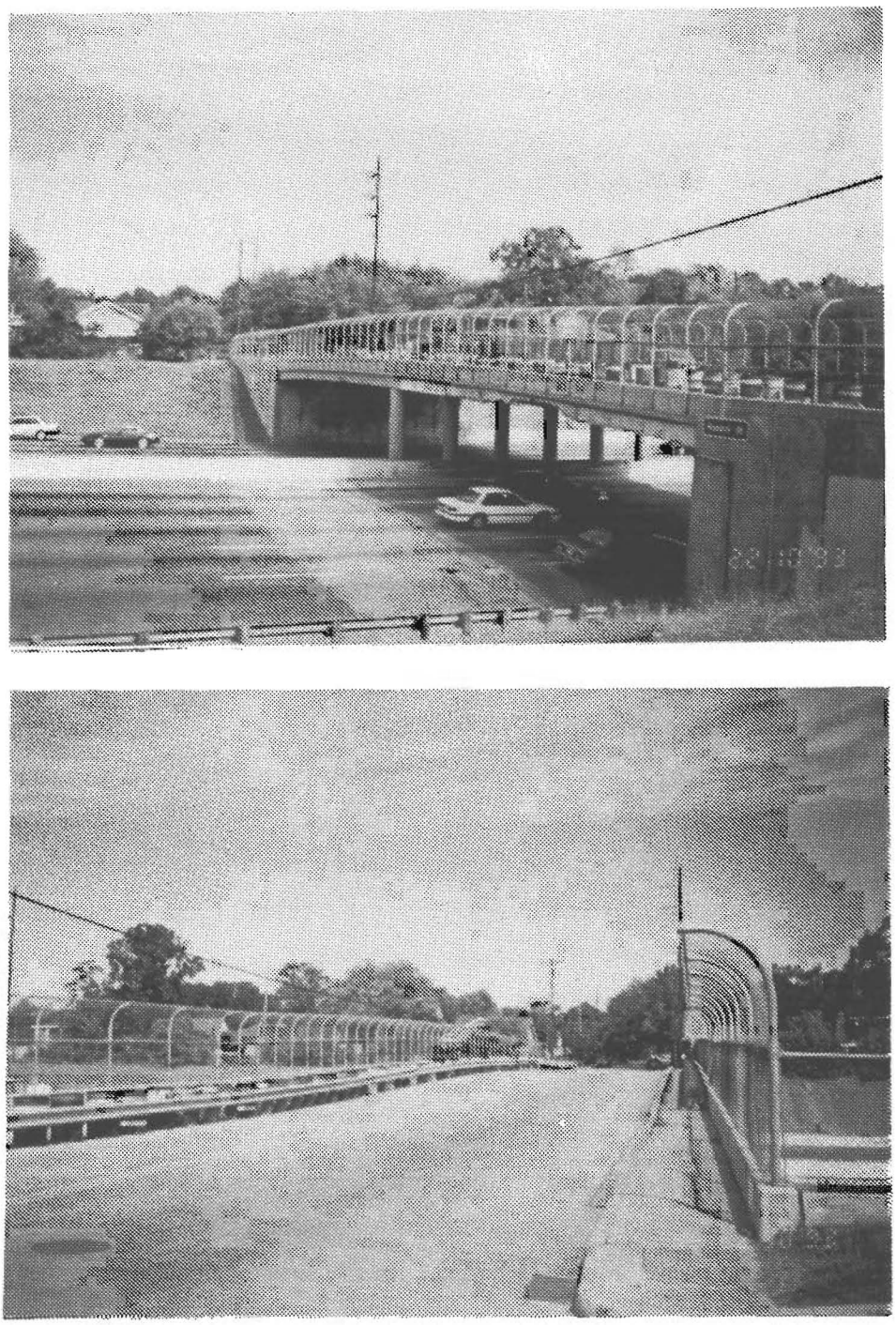

Figure 1.1: Photographs of a Typical Existing Bridge

periods of the bridge can lead to element fatigue or excessive movement of the bridge. By identifying the expected wind and traffic loadings and the dynamic characteristics of the bridge, it can be designed or altered to mitigate undesirable dynamic responses.

1.2. Statement of the Problem

Each of the four bridges which are planned for construction over U.S. 59 will be on-grade over cut areas with clear spans of 69.5 m (228 feet). The long spans of the bridges increase their susceptibility to vibration problems from wind or traffic loads. Vibrations from wind loads are also a concern during bridge erection. The bridge designs are tied arches and the designs of some components and appurtenances are not final. Changes in these designs can affect the wind loads from buffeting, flutter, or vortex shedding. Other bridges of similar design have experienced vibration problems in hanger elements. Analytical assessments, including wind tunnel experiments, are needed to determine possible static and dynamic responses of the bridges under wind and traffic loadings. If vibration problems are discovered, mitigation strategies should be designed.

1.3. Objectives

The central objective of the present study, as indicated earlier, is to determine if there are potential problems with the tied arch bridge designs due to wind loads. A secondary objective is to analyze the bridges dynamically under moving traffic loads. In both cases the dynamics of the bridges are important. TxDOT has already checked the design for 3.6 KPa (75 psf) static wind loading. The types of wind effects that are considered in this project are as follows:

- static wind loading (the steady state response to the mean wind)
- buffeting (dynamic response to turbulence in the wind)
- vortex shedding by the deck
- aeroelastic instability (flutter) of the deck
- hanger vibration due to vortex shedding

For a thorough check of possible problems, some of these analyses will be carried out for the bridge in a critical stage of its construction as well as in its final configuration.

The project includes both experimental and analytical studies. Experiments are performed on a section model of the bridge deck in the Texas Tech wind tunnel to verify whether or not there are potential problems regarding vortex shedding, buffeting, and/or aeroelastic instability (flutter). Analytical studies include finite element computations of the static response of the bridge to wind and traffic loadings, determination of the lowest

natural frequencies and modes of vibration, and computation of the bridge's dynamic response to wind buffeting, vortex shedding, and traffic loading.

2. Bridge Designs and Loadings

2.1. Design Information

The tied arch bridges considered have been designed by the Bridge Section of the Houston District of the Texas Department of Transportation. A model of the bridges built by TxDOT is shown in Figure 2.1. Only the basic features of the bridges are presented here to help the reader understand the contents of this report. Further details can be obtained from the Texas Department of Transportation. TxDOT plan and elevation drawings for one bridge are shown in Figure 2.2. The bridge is 69.5 m (228 feet) long and has a 12.2 m (40 feet) rise from the line joining the end support points to the center of the arch at midspan. There is also a small rise of 0.46 m (1.5 feet) in the deck from the ends to midspan. The deck hangs from each arch by means of nine double wire ropes that are equally spaced along the span. The steel superstructure of each arch, including the steel construction beam and all the cables, will be constructed on the deck of the existing bridge, hoisted into position on its end supports, and cross-braced to the other arch before the existing bridge is demolished.

Department of Transportation drawings of the cross-section of the deck are shown in Figure 2.3. Including the overlay, the deck varies in thickness from 305 mm (12 inches) to 438 mm (17.25 inches). The full width of the deck is 18.3 m (60 feet), and it extends 2.29 m (7.5 feet) outside the centerline of each arch to provide a pedestrian walkway. The precast concrete units will be hung from steel construction beams, as shown, and then grouted and post-tensioned before the construction beams are encased in concrete and post-tensioned as well. The final step will be placement of the overlay on the precast deck units. Curved chain link fences will be mounted to the outside curbs, to which 3.05 m (10 feet) high signs may be attached along diagonally opposite half-spans, as seen in Figure 2.4.

2.2. Expected Wind Loading

The terrain over which the wind approaches the bridge is assumed to be Exposure B (Urban and Suburban area, ASCE 1990). An aerial view in the vicinity of the existing bridges is shown in Figure 2.5, revealing a typical suburban surrounding. The design windspeed is taken as being able to approach the bridge from any possible direction, and the worst case of its approaching the bridge broadside is taken in most of the calculations. There is no "prevailing wind direction" to be considered when dealing with maximum extreme winds.

Figure 2.1: Model of a Typical Tied Arch Bridge (Houston District, TxDOT)

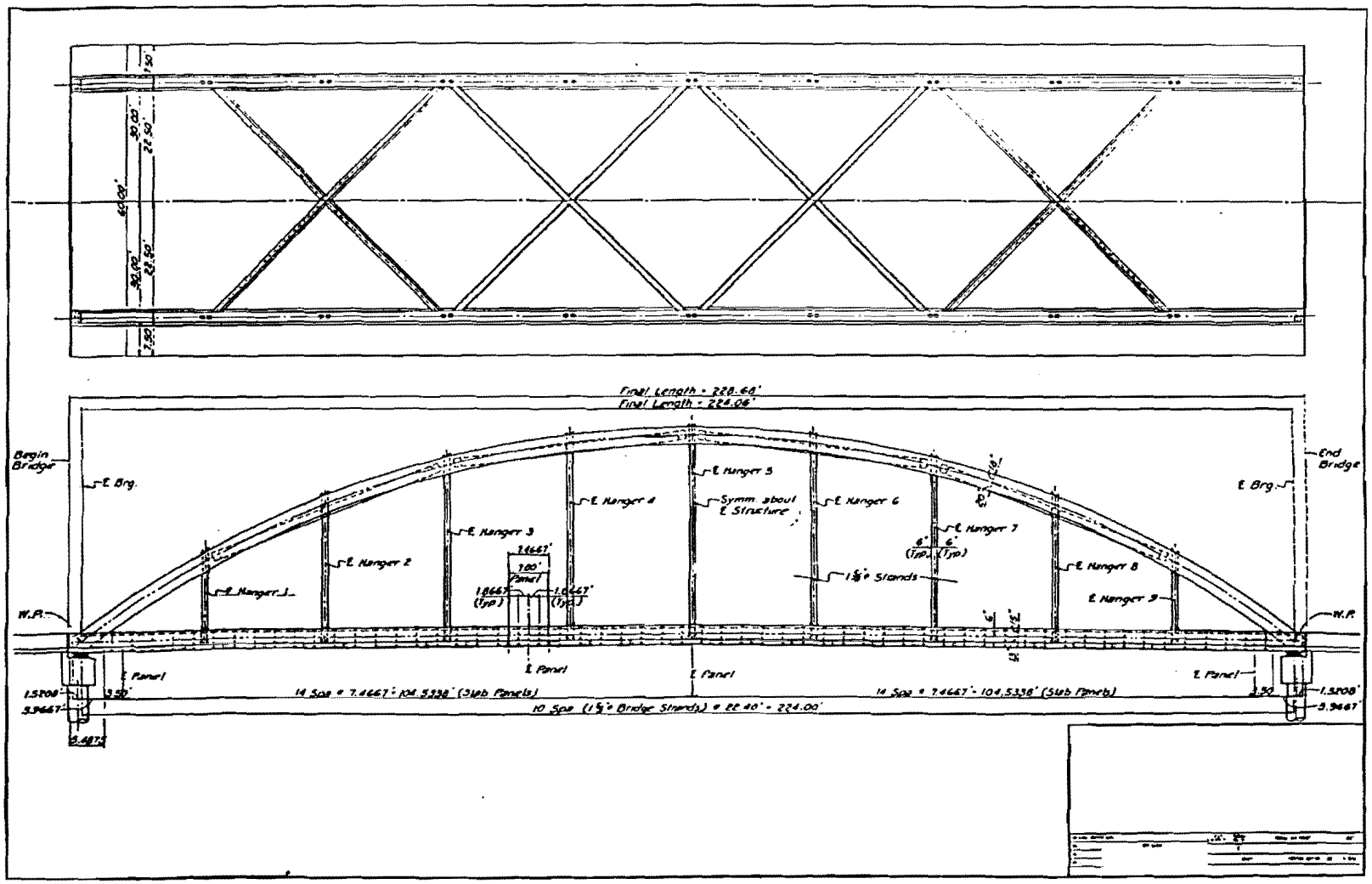

Figure 2.2: Plan and Elevation of a Typical Tied Arch Bridge (Houston District, TxDOT)

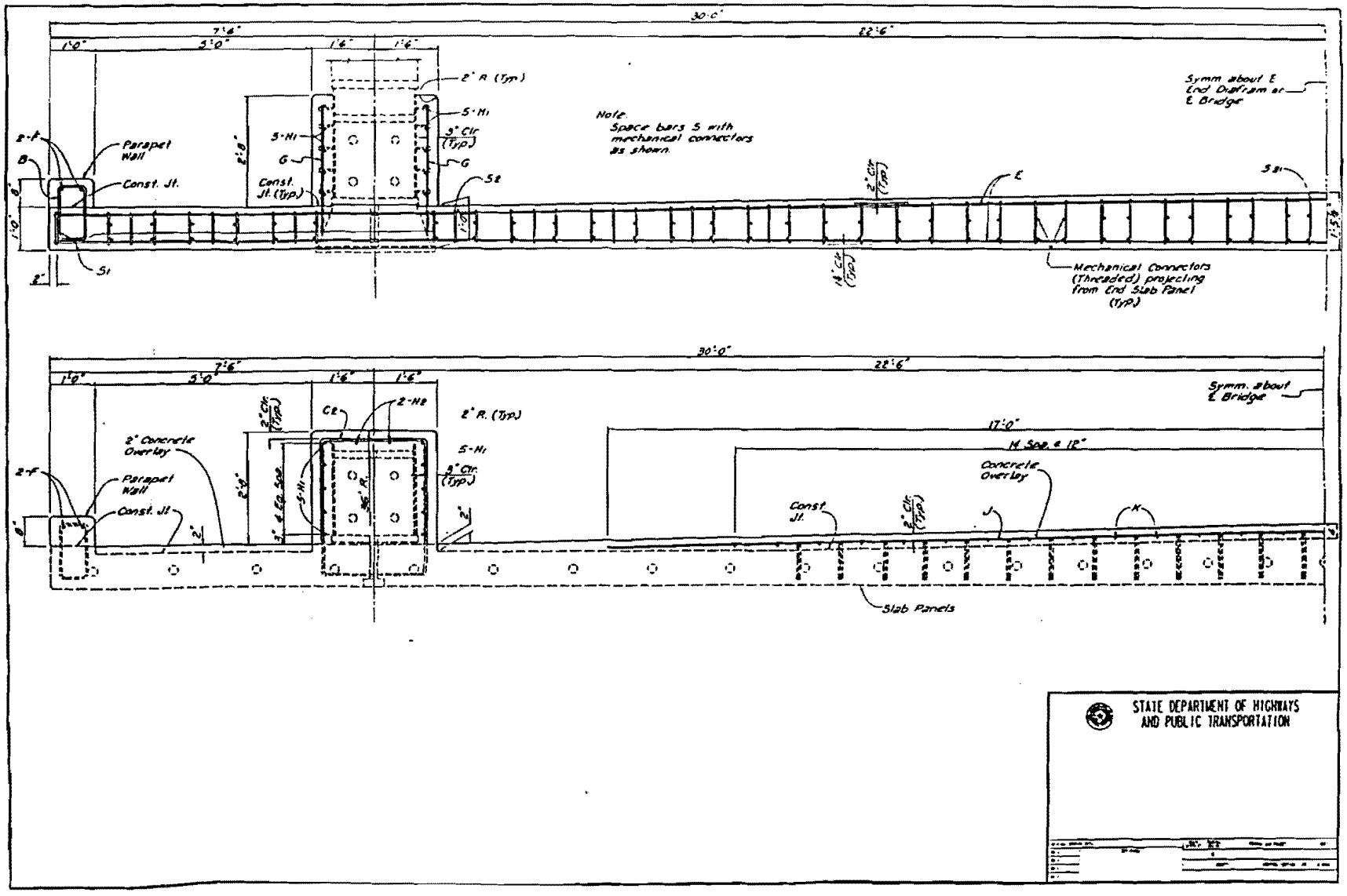

Figure 2.3: Cross-section of the Deck of a Typical Tied Arch Bridge (Houston District, TxDOT)

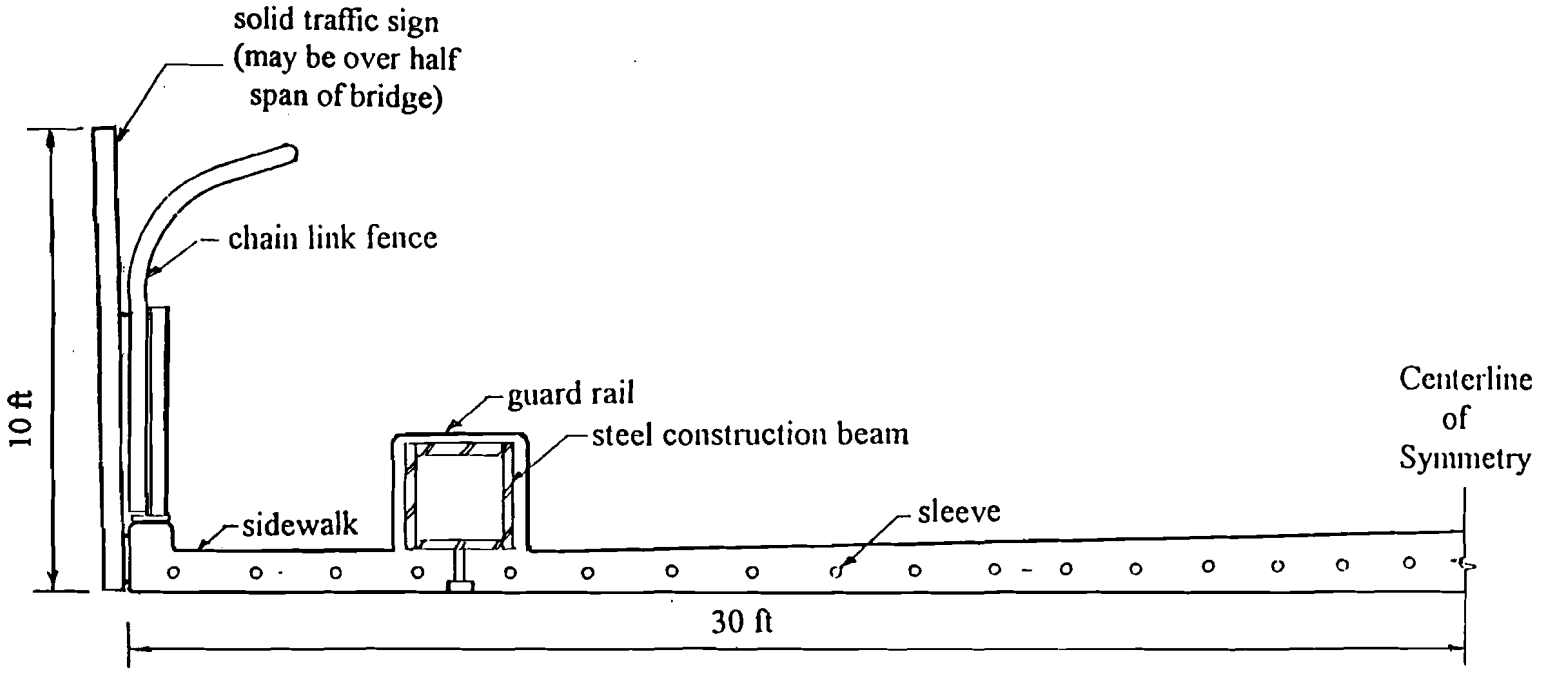

Figure 2.4: Cross-Section of the Deck of a Typical Tied Arch Bridge

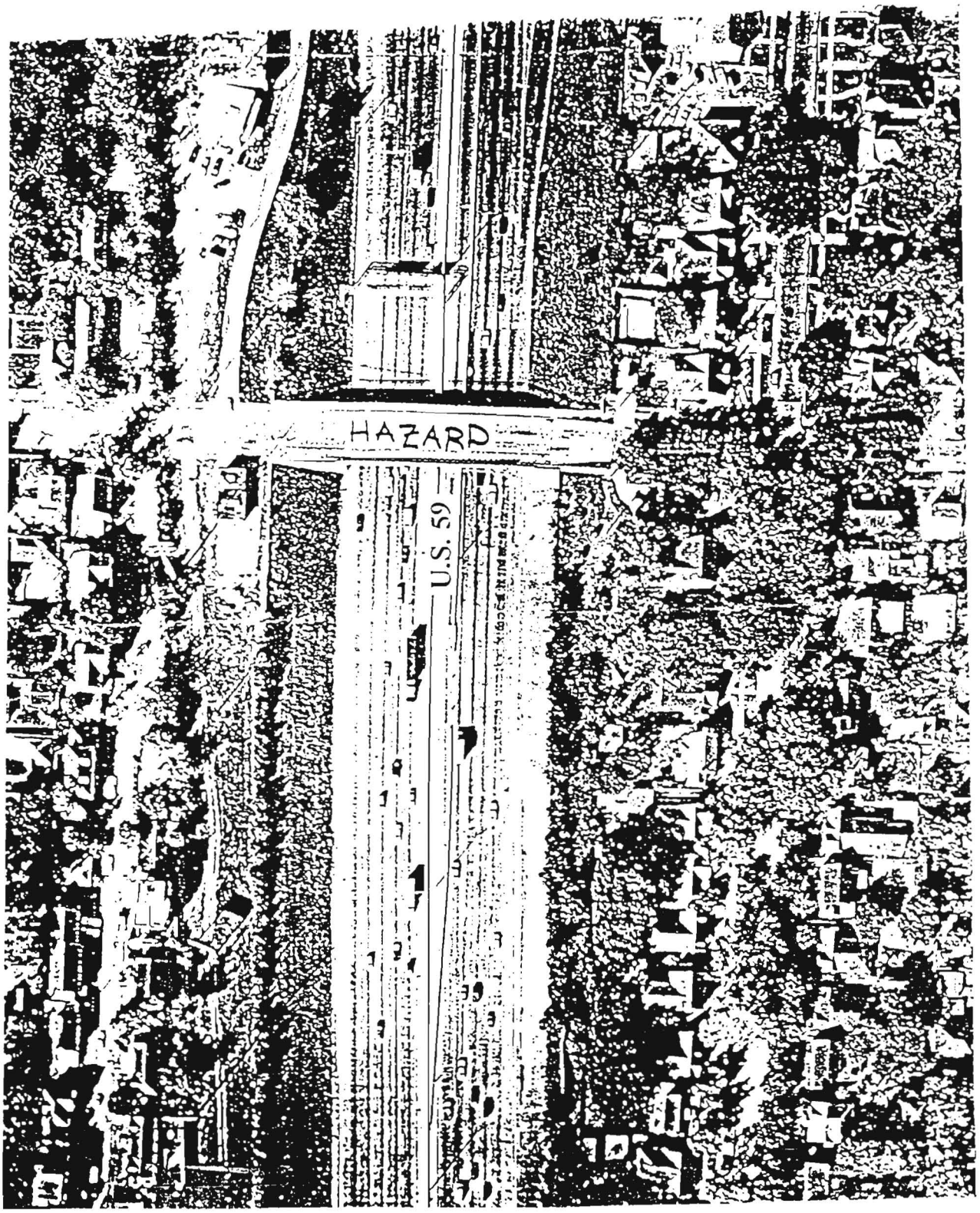

Figure 2.5: Aerial View Showing an Existing Bridge on U.S. 59 in Houston, TX

Empirical formulae of the wind spectra $S_{uu}(z,n)$ for the along-wind turbulence component u and $S_{ww}(z,n)$ for the vertical-wind turbulence component w at any height z are assumed as follows (Simiu and Scanlan 1986):

$$\frac{nS_{uu}(z,n)}{u_*^2} = \frac{200f}{(1+50f)^{5/3}}, \quad \text{(Kaimal Spectrum)} \tag{2.1}$$

$$\frac{nS_{ww}(z,n)}{u_*^2} = \frac{3.36f}{1+10f^{5/3}}, \quad \text{(Lumley and Panofsky Spectrum)} \tag{2.2}$$

where $f = nz/U$, n = frequency in Hz, z = height in ft, U = mean wind speed in ft/s, and u_* = friction velocity in ft/s. u_* can be calculated using the mean square value of u ($\overline{u^2}$) which is equal to βu_*^2, where β is assumed as 4.85 for the densely built-up suburban terrain around the bridge. Usually, $I_u(z) = \frac{\overline{u^2(z)}^{1/2}}{U(z)}$ = turbulence intensity of the u component is assumed for calculating u_*.

Calculations are made for the deck with two values of $I_u(z)$, i.e., 25% and 40%, and for the arch with one value of $I_u(z)$ = 25%. The turbulence intensity $I_w(z)$ of the w component is taken as $0.3I_u(z)$. Since the deck is nearer to the ground it will be subjected to higher turbulence. In the wind velocity calculations, the height z of the deck from the ground is assumed as 5.03 m (16.5 feet), and the height of the arch from the ground is taken as 17.4 m (57.0 feet). The actual height of the arch from the ground varies, but the maximum height is considered for conservative results.

The design codes for wind loads are based on steady-state winds. The effects of fluctuations in the wind and dynamic characteristic of the structure are accounted for in the wind design codes through gust response factors. Since turbulence and dynamics are accounted for separately in the present buffeting analysis, the gust response factor is taken as unity in the code formulae for calculating the equivalent mean wind speed for dynamic analysis. The following calculations show the derivation of the mean wind speeds U for the deck and for the arch in the buffeting analysis, based upon the ASCE 1990 code. Later the wind pressure values are compared with the 3.6 KPa (75 psf) pressures used in the design by TxDOT as per the code of The American Association of State Highway and Transportation Officials (AASHTO).

$$q_z = 0.00256K_z(IV)^2 = \tfrac{1}{2}\rho U^2 \tag{2.3}$$

$$P = q_z G_h C_f = \tfrac{1}{2}\rho U^2 G_h C_f \tag{2.4}$$

where q_z is the velocity pressure in psf at height z; K_z is the exposure coefficient, which is a function of height z and type of exposure or terrain; I is the importance factor, which depends upon the importance and use of the structure; V is the basic (fastest mile) wind speed in mph for a 50-year return period at 10 m (33 feet) as measured at weather stations; ρ is the air density; U is the equivalent mean wind speed; P is the design wind pressure; G_h is the gust response factor, which is a function of wind turbulence, dynamic characteristics of the structure, and total structure height, h; and C_f is an appropriate pressure or force coefficient.

The value of G_h is taken as 1.0 for the present calculation for reasons mentioned earlier. The other values assumed are as follows:

K_Z for the deck at z = 5.03 m (16.5 ft) = 0.385 (Table 6, ASCE 1990)
K_Z for the arch at z = 17.4 m (57.0 ft) = 0.665 (Table 6, ASCE 1990)
I for a Category III structure = 1.11 (Table 5, ASCE 1990) at hurricane oceanline
V for Houston, Texas = 40 m/s or 90 mph (Figure 1, ASCE 1990).

An expression for U can be written using Equation 2.3, as follows:

$$= \sqrt{\frac{2q_z}{\rho}}. \qquad (2.5)$$

This equation and the above values yield U = 27.6 m/s (62.0 mph) for the deck and U = 36.5 m/s (81.5 mph) for the arch.

Equation 2.4 can be used to calculate the design static pressure (P) on the arch taking U = 36.5 m/s (81.5 mph), G_h as 1.40 corresponding to z = 17.4 m (57 ft) and Exposure B (ASCE 1990), and the coefficient of force $C_f = C_D$ = 2.90 (normalized by the arch depth D = 0.965 m or (3.17 ft). With these values P = 3.3 KPa (69.0 lb/ft$^{2)}$, which compares very well with the design pressure of 3.6 KPa (75 lb/ft$^{2)}$ used by TxDOT. However, for the deck where the equivalent mean design wind speed U is only 27.6 m/s (62.0 mph) instead of 36.5 m/s (81.5 mph), G_h is 1.63 corresponding to z = 5.0 m (16.5 ft) and Exposure B instead of G_h = 1.40, and the drag coefficient C_D is only 1.64 (normalized with deck depth D = 1.12 m or (3.66 ft) instead of 2.90, the design wind pressure of 3.6 KPa (75 psf) used by TxDOT for equivalent static analysis is very much on the high side. For the deck, Equation 2.4 with U, G_h, and C_D values just mentioned gives a design pressure of only 1.3 KPa (26.3 lb/ft$^{2)}$.

Buffeting forces act on a bluff body like a bridge deck or arch because of fluctuations in the wind speed, i.e., wind turbulence. These forces are also influenced by turbulence induced by the bluff body itself. To account for the body-induced turbulence, an aerodynamic admittance function, $\chi^2(K)$, is needed for each of the three forces, i.e., the lift, moment, and drag forces. In general, the admittance functions vary with the reduced frequency $K = \omega B / U$, where ω is the frequency in radians per second, B is the width of the deck, and U is the local wind speed. For the present analysis the admittance functions are determined in the wind tunnel, but only at one wind speed, and are assumed to be the same for all other frequencies.

Auto-spectra of the lift, moment, and drag forces at any location, x, along the span of the bridge, neglecting cross-spectral components of velocity, can be obtained from the previously defined quantities and the auto-spectra of the longitudinal and vertical wind fluctuations. Denoting the longitudinal (u) and vertical (w) wind spectra by $S_{uu}(x,K)$ and $S_{ww}(x,K)$, respectively (Scanlan, 1988), the lift (L), moment (M) and drag (D) force auto-spectra are as follows:

$$
\begin{aligned}
S_{L,L}(x,K) &= (\tfrac{1}{2}\rho U^2 B)^2 \left[4C_L^2 \frac{S_{uu}(x,K)}{U^2} + (C_L' + C_D)^2 \frac{S_{ww}(x,K)}{U^2}\right](\chi^L(K))^2 \\
S_{M,M}(x,K) &= (\tfrac{1}{2}\rho U^2 B^2)^2 \left[4C_M^2 \frac{S_{uu}(x,K)}{U^2} + (C_M')^2 \frac{S_{ww}(x,K)}{U^2}\right](\chi^M(K))^2 \qquad (2.6) \\
S_{D,D}(x,K) &= (\tfrac{1}{2}\rho U^2 B)^2 \left[4C_D^2 \frac{S_{uu}(x,K)}{U^2}\right](\chi^D(K))^2,
\end{aligned}
$$

where C_L, C_M and C_D are static coefficients of lift, moment and drag, respectively; $C_L' = dC_L / d\alpha$, $C_M' = dC_M / d\alpha$, and $C_D' = dC_D / d\alpha$., where α is the angle of attack; B is the structural dimension; and $\chi^2(K)$ is the aerodynamic admittance function.

Wind forces on different points of a structure are only partially correlated. It is known that the spatial correlation of turbulence in the wind reduces with an increase in distance between two points (x_1 and x_2) along the span. Here the form of the spatial cross spectrum for each point along the span is assumed as in Simiu and Scanlan (1986):

$$
S_{Q,Q}(x_1,x_2,K) = S_{Q,Q}(x,K)\exp(-CK|x_1 - x_2|/(2\pi B)) \qquad (2.7)
$$

where C is the incoherency coefficient, which is normally assumed to lie between 8 and 16 for wind, and Q stands for L, M, or D. However, it is known that buffeting forces are better correlated than the wind speed itself (Davenport et al., 1992). Therefore, a value of C equal to 4 is assumed for the partially correlated time-domain forces presented herein.

Partially-correlated time histories of buffeting forces are generated for the time-domain analysis using the form of the cross-spectrum in Equation 2.7 with C equal to 4. In principle, there are a number of methods available to generate the time histories. In the present calculations, the time history at point j along the span, $f_j(t)$, is digitally simulated as follows (Shinozuka et al., 1972):

$$f_j(t) = \sum_{m=1}^{j} \sum_{l=1}^{N} \left|H_{jm}(\omega_l)\right| \sqrt{2\Delta\omega} \cos\left[\omega_l t + \theta_{jm}(\omega_l) + \phi_{ml}\right] \tag{2.8}$$

where N is the number of points in the specified target cross-spectral buffeting force matrix, $\mathbf{S^0}(\omega)$, which is real; H_{jm} are elements of $\mathbf{H}(\omega)$, a lower triangular matrix computed from $\mathbf{S^0}(\omega)$ by the matrix relationship $\mathbf{S^0}(\omega) = \mathbf{H}(\omega)\mathbf{H}(\omega)^{\mathrm{T}}$; $\omega_l = l\Delta\omega$; $\Delta\omega = \omega_u / N$; ω_u is the upper cut-off frequency beyond which the power spectral density may be assumed to be zero; $\theta_{jm}(\omega_l) = \pi/4$ because $\mathbf{H}(\omega)$ is real; and ϕ_{ml} are random phase angles uniformly distributed between 0 and 2π.

The correlation of the wind reduces with an increase in distance between two points along the span. The correlation coefficients between the generated drag, lift, and moment forces at the midspan point on the bridge deck and the corresponding forces at other points along the span for the bridges considered are plotted in Figure 2.6. It can be seen that the agreement with the theoretical relationship is good out to a distance of about two-tenths of the span in each direction but is not as good at greater distances. It should be mentioned that the generated drag, lift, and moment forces are all symmetric about the center of the bridge. In fact, realistic buffeting winds are equally likely to be non-symmetric. However, in the analysis, the buffeting winds are taken to be symmetric to the midspan of the bridge in order to simplify the problem.

2.3. Expected Traffic Loading

Bridges are subjected to vehicle loads that generate static or dynamic forces and corresponding deflections and stresses in the bridge components. In recent years a large number of bridges have been found to have incurred damage attributed to impact and fatigue (Yen et al., 1989). Therefore, the dynamic traffic load is an important parameter in bridge design and evaluation. A large number of observations and measurements indicate that the dynamic behavior of a bridge is a function of three major factors: dynamic properties of the vehicle (mass, axle configuration, tires, speed); road roughness (approach, roadway, potholes, waves); and dynamic properties of the bridge structure (span, mass, support type, material, geometry). Since it is difficult to consider all of these

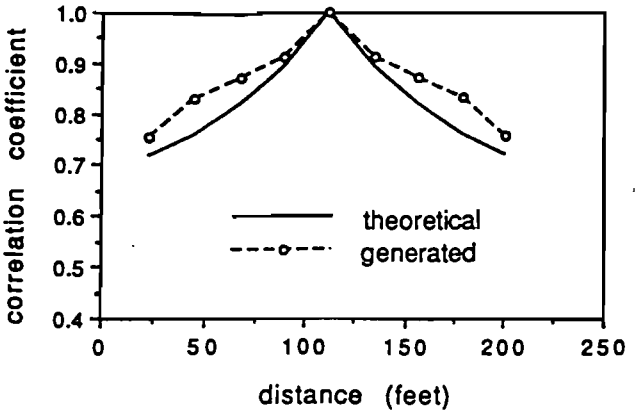

(a) Drag Force

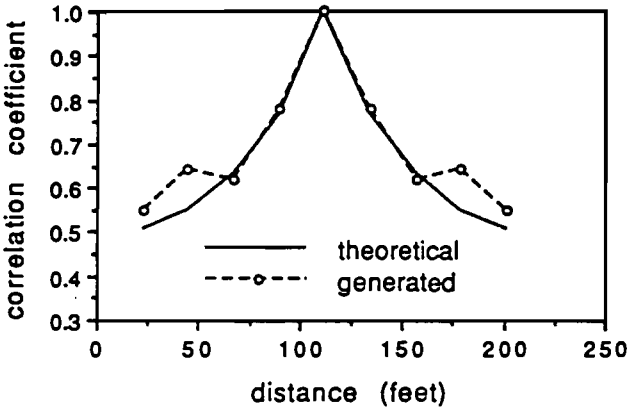

(b) Lift force

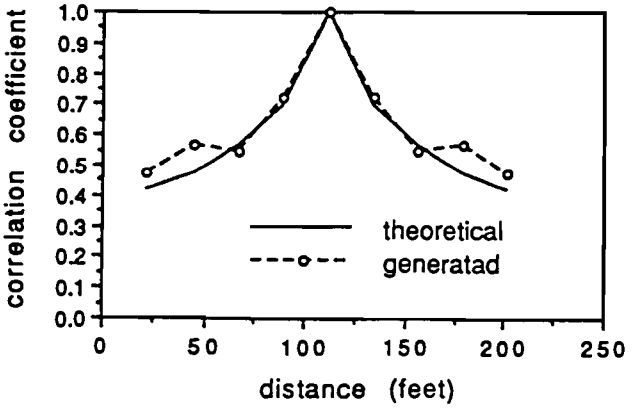

(c) Moment

Figure 2.6: Correlation Coefficients for the Bridge

factors in the bridge design, traditionally, the dynamic effects are incorporated through use of the well-known impact factor (I). An increase in the static deflections and stresses by the impact factor provides a simple method of estimating maximum deflections and stresses resulting from vehicles traveling on the bridge.

A large amount of research has been done to study the dynamic traffic loading responses of bridges, including those of Hwang et al. (1989), Gupta (1980), Yen et al. (1989), and others. Most approaches have been based on numerical methods such as the Fast Fourier Transformation (FFT) method (Yen, et al., 1989). Here, the traffic analysis is based on a finite element program. Since the natural frequencies and mode shapes of the bridge of interest have already been determined, its dynamic responses can be obtained easily if the time-dependent vehicle loading can be modeled. In this report, the vehicle loading is modeled and the dynamic responses of the bridge are obtained. Since information concerning road roughness is not available, this factor is not taken into account in the analysis. Also, details about the vehicles such as separate tire and chassis masses and spring stiffnesses are not considered.

In the traffic loading analysis, the computer code STARDYNE is used. The truck in the analysis is called a HS20-44 truck in the AASHTO specifications. It has a total weight of 320 KN (72 kips), which is allocated as follows: 36 KN (8 kips) for the front axle and 142 KN (32 kips) each for the middle and rear axles. Both distances between axles are 4.27 m (14 feet) (Figure 2.7).

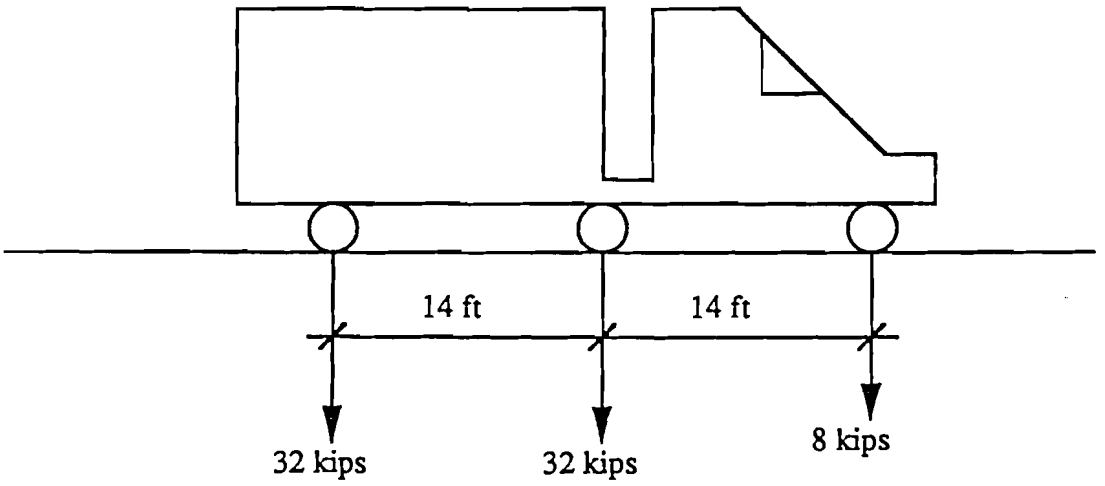

Figure 2.7: Model of HS20-44 Truck

3. Wind-Tunnel Studies

3.1. Deck-Model Description

A section model of the prototype bridge deck has been built with 1:60 geometric scale. This choice of geometric scale is based upon the dimensions of the prototype and practical considerations associated with building section models. Photographs showing the section model details are given in Figure 3.1. The material chosen is aluminum instead of wood because the depth of the section is so small it would be too flimsy if made of wood. However, the aluminum block used has been hollowed out as much as possible to make the model lighter (Figure 3.2). Two aluminum channels are added to represent the bottom chords of the prototype arches. The top of the deck of the model is covered with a rubbery material to represent the pavement geometry, including the correct amount of cant from each edge to the center. The length of the section model is chosen as 1.02 m (40 inches) to utilize most of the wind-tunnel width.

A considerable effort has been devoted to designing the railing of the section model so as to represent the prototype chain-link fence aerodynamically. The vertical columns of the chain link fence are represented by vertical rods with geometrically scaled (1:60) lengths but with differently scaled diameters. The wire mesh and the C-301 rail of the actual chain link fence are represented by seven horizontal rods spaced in the vertical direction. In the design process, the anticipated drag and moment (scaled values) due to wind flow on the chain link fence of the prototype have been closely matched to the expected drag and moment on the fence of the section model.

The end plates are made of aluminum and are attached at the ends of the section model to ensure two-dimensionality of the wind flow. Necessary accessories are attached at the ends to give the model two degrees of freedom, namely vertical and torsional (rotational) motions. A pipe of diameter 90.2 mm (0.4 inch) has been added near the bottom chord on the windward side to represent the 610 mm (24 inch) diameter water pipe on the prototype bridge. The 203 mm (8 inch) diameter pipe on one bridge is less critical than the 610 mm (24 inch) pipe, and hence has not been modeled. A picture of the full-length model is shown in Figure 3.3.

3.2. Wind-Tunnel Facility

The wind tunnel located in the Technology building at Texas Tech University was used for the experimentation. The wind-tunnel facility operates in an open loop with a maximum flow rate of around 65,000 cubic ft/min. A 5 ft wide, 4.5 ft diameter centrifugal blower (forced-draft system) drives the wind-tunnel. The blower is powered by a 50 hp,

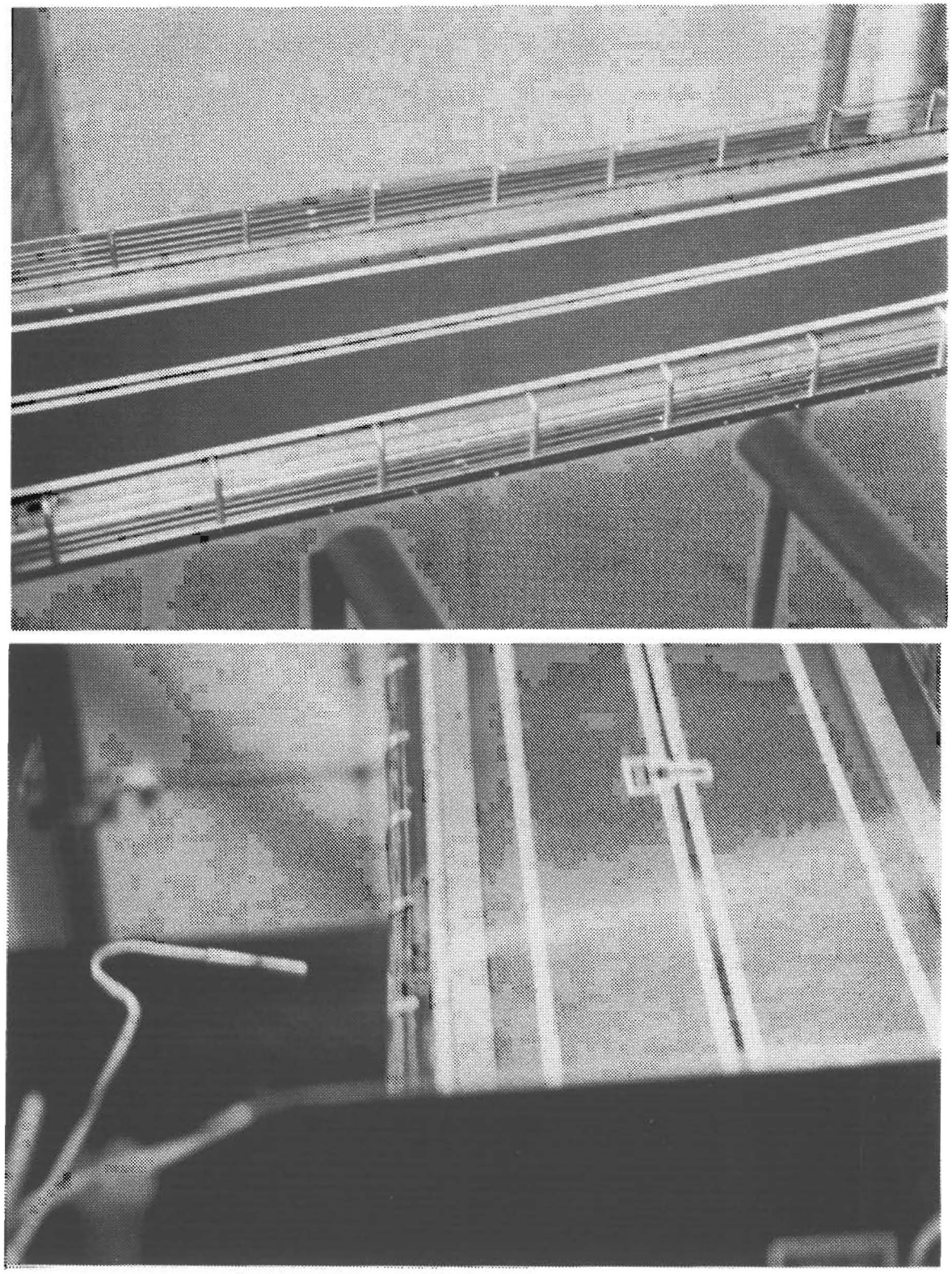

Figure 3.1: Details of the Bridge Deck Section Model

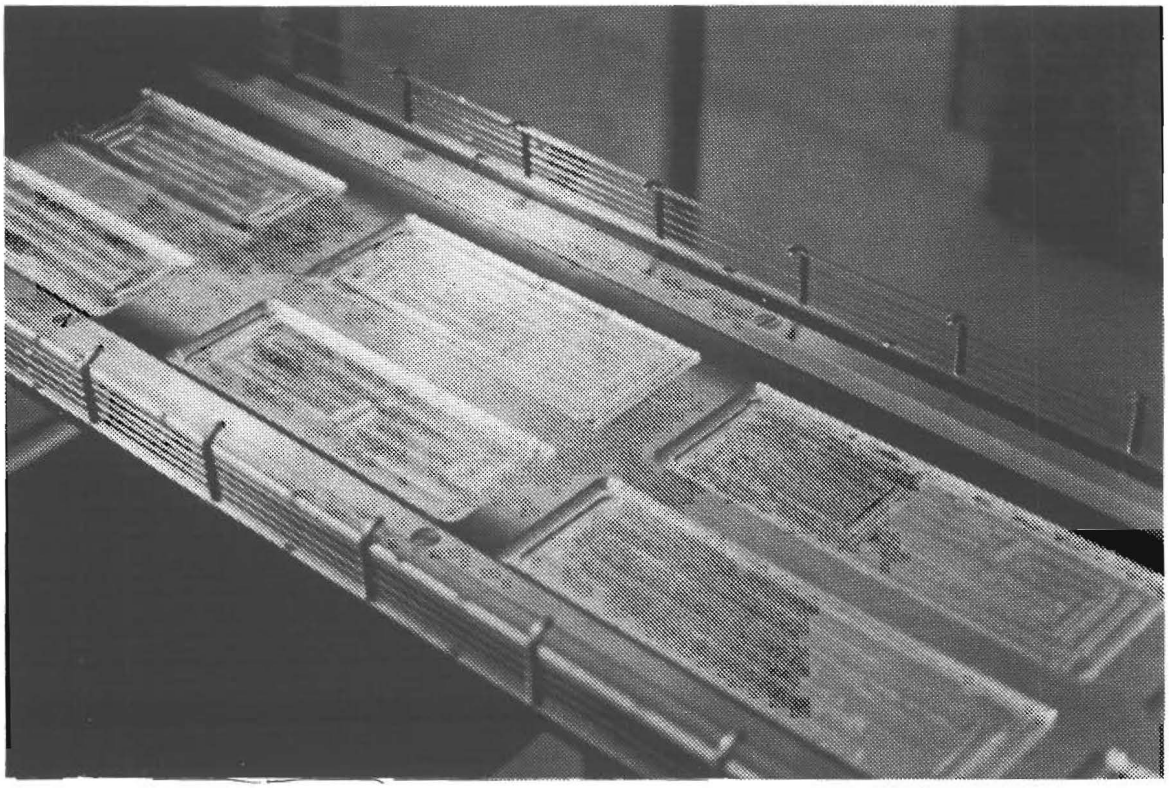

Figure 3.2: Hollowed out Aluminum Block for the Section Model

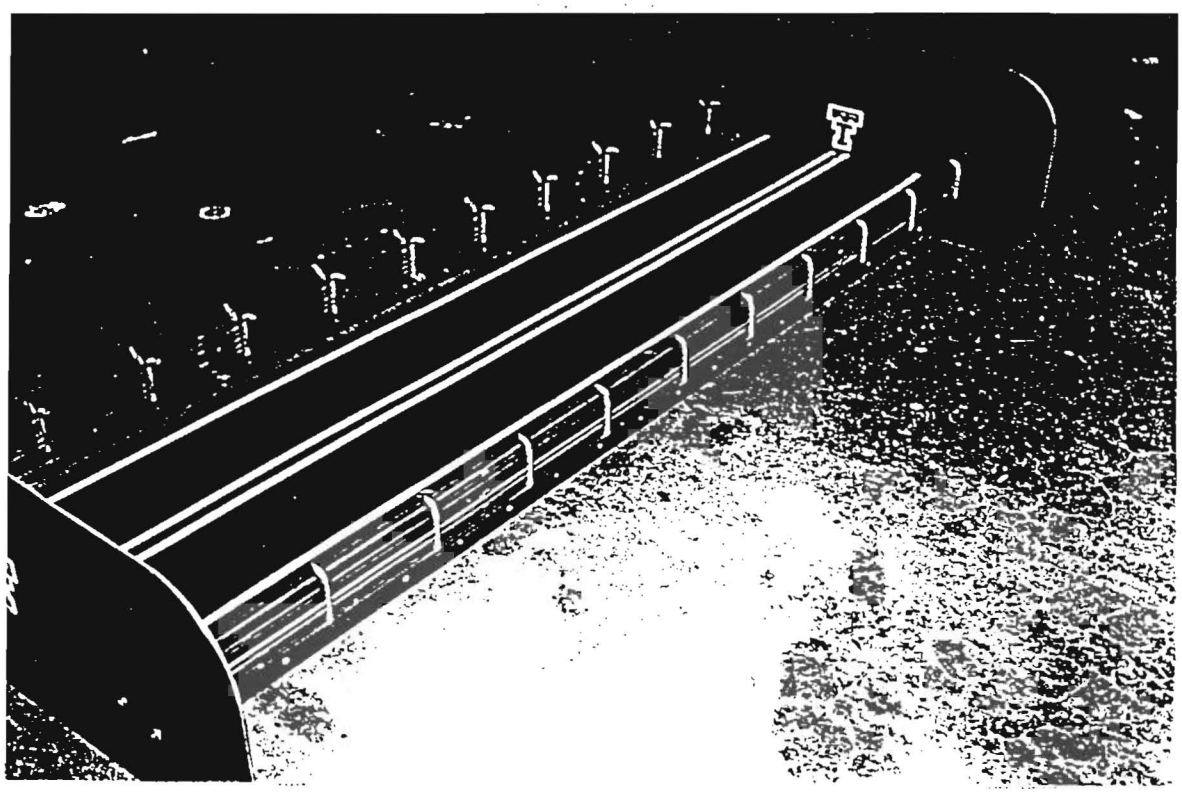

Figure 3.3: Full View of the Bridge Deck Section Model

3 phase, 220 volt motor. In order to control the flow rate (and consequently the wind speed), the blower unit has a powered actuator which opens inlet vanes from the fully-closed to the fully-open position. The actuator is controlled by a rheostat located at the test section. The wind speed can be changed continuously using this mechanism. The wind tunnel has a nozzle with a contraction ratio of 10:1 following the turbulence-reducing mesh screens and the settling chamber (Figure 3.4).

The experiments were conducted in a wind tunnel test section which is dedicated to section-model testing. The test section is equipped with all the necessary instrumentation to record aeroelastic and aerodynamic forces. The test section can be attached to the nozzle of the wind tunnel and detached when not required. The section is 3.36 m (11 feet) long with a cross-section 1.22 m (4 feet) wide and 0.92 m (3 feet) high. The bottom of the section is fixed to a wheeled support. The test model can be mounted at a distance of 2.36 m (7.75 feet) from the wind-tunnel nozzle. The section has a glass wall on one side to provide visibility. On the other wall a door is provided for easy access to the model. A hot-wire mount is fixed to the inner wall of the section which can be moved along the vertical direction.

The model suspension system and the load cell frame are fixed on the outer side of the wall. The benefit of such an arrangement is that only the model experiences the wind flow, which helps in obtaining higher accuracy of results. The suspension system is designed such that the stiffness of the model support can be changed through addition of springs or rigid bars. Provisions are made in the test section to allow movement of the model along two degrees of freedom, i.e., vertical and torsional degree of freedom, and to allow measurement of forces along the three degrees of freedom, i.e., lift (vertical), moment (torsional) and drag (along-wind). It is possible to adjust the setup to a single degree of freedom or to two degrees of freedom (vertical and torsional). Another feature of the test section is an excitation mechanism which allows the operator to give an initial amplitude to the model for any experiment including dynamic response.

3.3. Experimental Results

The experiments in the wind tunnel were carried out to determine the flutter, buffeting, and vortex-shedding response of the prototype (full scale) bridge. Three configurations of the bridge deck were tested in the wind tunnel, viz. the bridge deck with no traffic sign, with the traffic sign upstream, and with the traffic sign downstream. The results are presented in Section 8, along with the equations and calculations describing the response of the prototype bridge using the parameters determined in the wind tunnel.

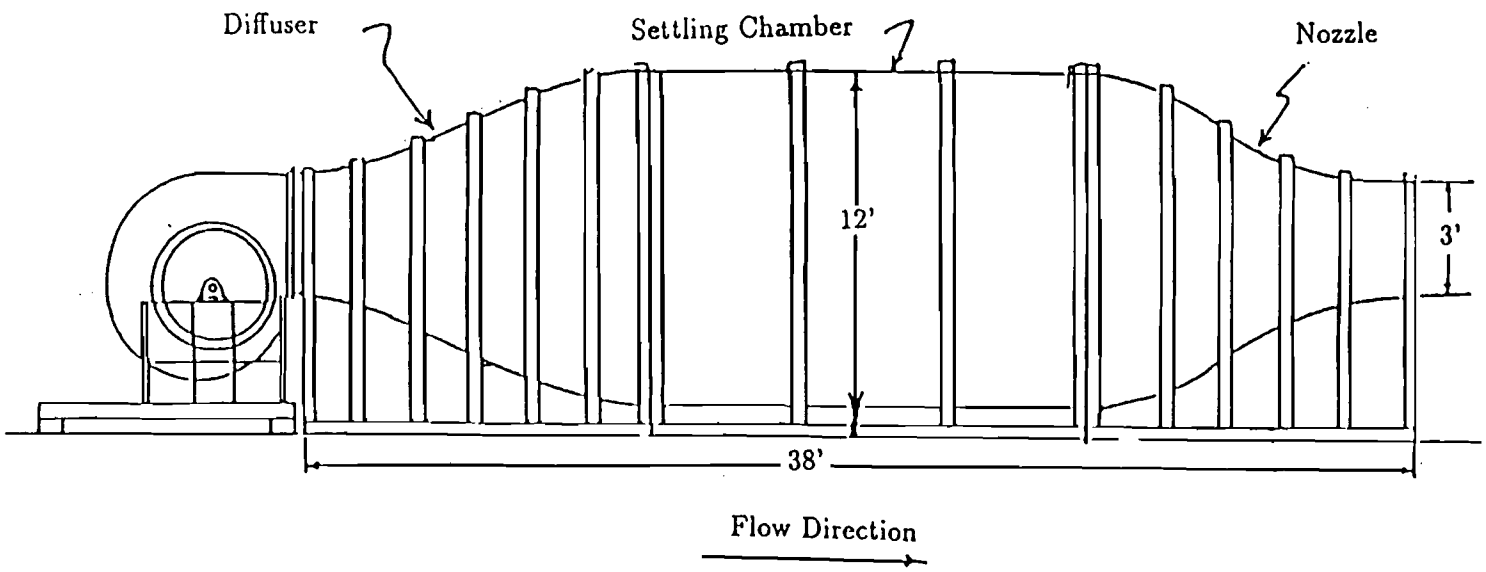

Figure 3.4: Texas Tech Wind-Tunnel Facility

4. Static Analysis

4.1. Finite Element Model Description

Analytical models of the tied arch bridge have been formulated with several finite element computer codes. The first code used was called CDA/SPRINT—a version of MSC NASTRAN that has been scaled down for a desk-top computer—marketed by the CDA Group, 6019 S. Loop E, Houston, Texas 77033. CDA/SPRINT is advantageous because of its ease in defining the structure and its graphical representation of the deflections and the modes of vibration of the structure. However, CDA/SPRINT does not have the capability of finding the transient response of the bridge when different time histories of loading are imposed at different points on the structure. Such loadings are necessary for non-coherent buffeting and for moving traffic loads on the bridge.

The second finite element program used was called ALGOR. It is a mini-computer version of SAP5 marketed by Algor, Inc., 150 Beta Drive, Pittsburgh, Pennsylvania, 15238-2932. It was found to have the desired capabilities but to be more trouble to use than other finite element programs.

The third finite element program tried was called SAP90. It was not selected for further studies because the available version only had the capacity to analyze structures with up to 100 nodes.

The finite element code finally selected for this study was called STARDYNE. This program is marketed by the Titan Corporation, 9410 Topanga Canyon Blvd., Chatsworth, California 91311. It can perform linear static, dynamic, heat transfer, composite material, fatigue, buckling, and nonlinear analyses. Particularly, its dynamic analysis capability is very strong. Stress and deflection responses can be computed for any combination of time-dependent forces that may be applied to the model. STARDYNE's integrated graphics program, called STARMAP, also allows users to build geometric models of structures easily and gives a good graphical interface. The version used in this analysis has a limit of 500 nodes. Checks were carried out between the natural frequencies and mode shapes of the U.S. 59 tied arch bridges as computed by STARDYNE, SAP90, and ALGOR. The results were found to be consistent.

Figure 4.1 shows one of the computer models of the completed bridge using STARDYNE. The elements in the model consist of quadrilateral plate elements for the bridge deck and straight beam elements for the segments of the arches, the cables, the steel construction beams, and the concrete encasement of the construction beams. A more detailed model of the bridge, shown in Figure 4.2, is used for all of the static loading

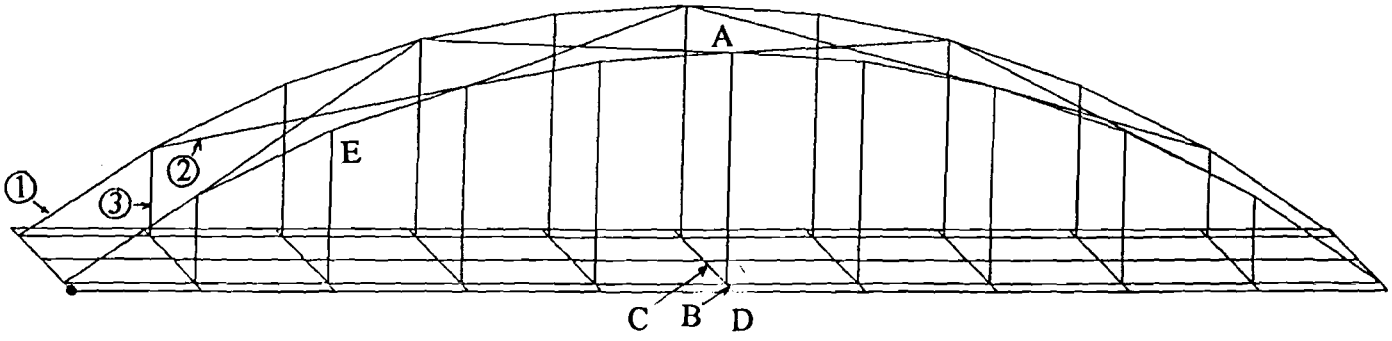

Figure 4.1: First Level Model of Completed Bridge (77 nodes) Using STARDYNE

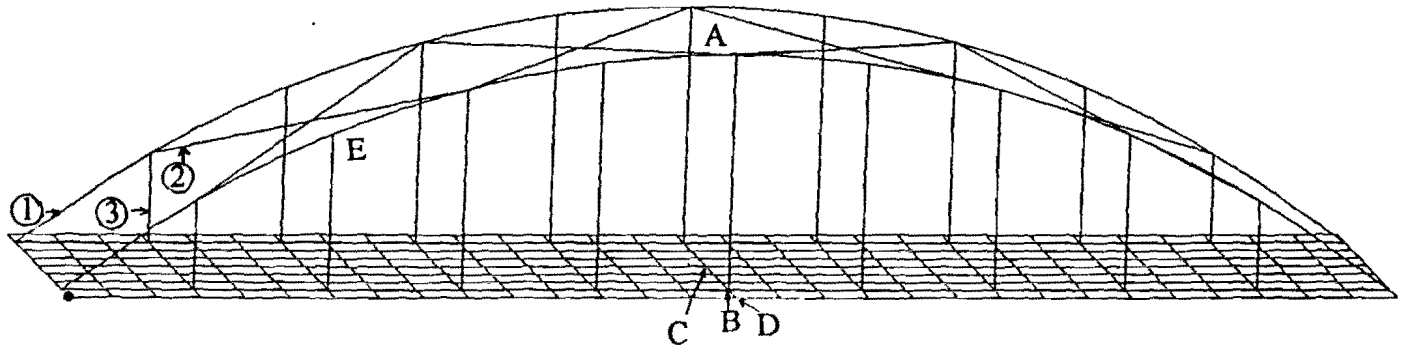

Figure 4.2: Second Level Model of Completed Bridge (341 nodes) Using STARDYNE

studies. It has 2,046 degrees of freedom. In all of the finite element computer solutions, only linear elastic response is considered.

Static and dynamic loading results have also been obtained for an important stage of partial construction in the bridge's development, that is, with both arches erected and cross-braced to each other, but with the existing bridge removed and no new bridge deck units as yet attached. The steel for both arches will be erected and the arches will be braced to each other in one weekend's operation. After this, the two arches should be almost as well supported as in the final condition. However, the long construction beams for the bridge will be vulnerable to the wind after the existing bridge is demolished and before the new bridge deck is installed so as to stiffen the steel construction beams. Temporary horizontal bracing will be required to stabilize the construction beams at this stage, which is likely to last at least a week, and perhaps several weeks. The time lag between demolition of the existing bridge and attachment of the new slab units will depend on whether consecutive weekends can be scheduled for each effort. Each effort will interrupt the high-volume traffic of the freeway below and therefore can only be carried out on a weekend.

The bracing system assumed in this study is shown in Figure 4.3. It consists of horizontal struts straight across between the construction beams at the first hanger points from each end and then at alternating hanger points in the center portions, with diagonal tension counters in the horizontal plane between all of these points. The members used for the struts during this stage were chosen by TTU as 305 mm x 305 mm x 9.5 mm (12" x 12" x 3/8") tubular members so as to limit the L/r ratio of the struts to 120, i.e., as "main members" in the steel codes. These choices were made before knowledge was gained concerning the struts designed by TxDOT, which were W12x65 wideflange sections, which have an L/r ratio of 179. This ratio is satisfactory if the members are considered to be "secondary members" because of the temporary nature of their function. The cables chosen for the diagonal tension counters were single cables of the same size as the hangers, that is, 41.3 mm ($\frac{5}{8}$-inch) bridge strand. TxDOT will use an alternate cable, a 50.8 mm (2-inch) diameter wire rope that is approximately equivalent to this bridge strand, for the hangers and for these counters, depending on the availability of the bridge strand.

4.2. Comparison to TxDOT Vertical Loading Results

Computer results have been sent to Texas Tech from TxDOT in Houston for a few vertical loading cases and static behavior. These results were requested for checking Texas Tech's computer models. The two cases with results which were used for comparison are:

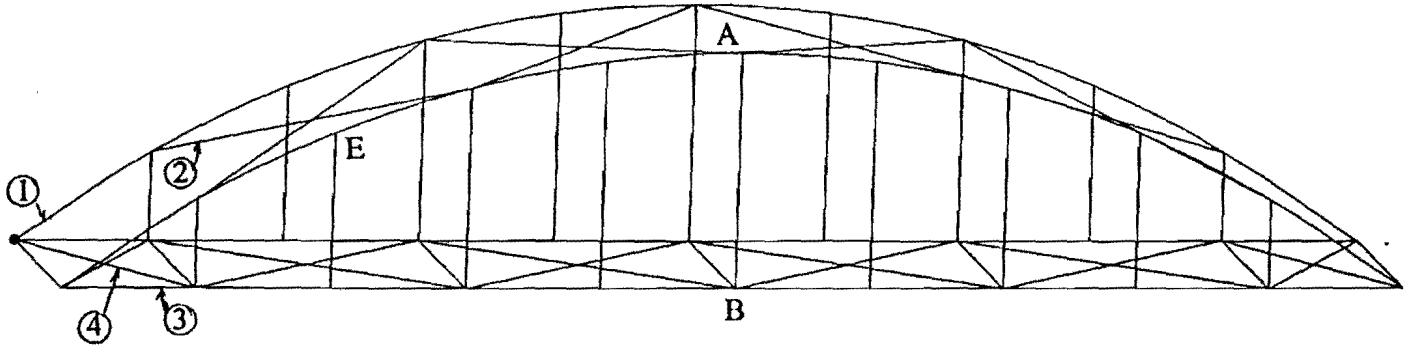

Figure 4.3: First Level Model of Partially Completed Bridge Using STARDYNE

1. full dead load plus prestress (TxDOT 2D load case 40 and 3D load case 17); and
2. loading by trucks in three adjacent lanes at midspan plus sidewalk live loading, but without the dead loads or prestessing effects (TxDOT 2D total load case 50 minus load case 40, and 3D load case 6).

Table 4.1 shows deflection comparisons for the two TxDOT loading cases. The Texas Tech results are with the detailed model of Figure 4.2, including 6 degrees of freedom per node. The point at which TxDOT deflections are given is on the construction beam at midspan on the more heavily load side. This point corresponds to point B in Figure 4.1. Table 4.1 also gives static loading results for the following points on the Texas Tech model: point A (the top of the arch), point C (the center of the bridge at midspan), and point D (the edge of the deck at midspan).

Table 4.1: Comparison of Static Midspan Vertical Deflections with TxDOT Results

Loading Case	TxDOT Deflection		Deflection of TTU Point			
	2D	3D	A	B	C	D
Dead Load Plus Prestress	-2.951 in. -74.96 mm	-2.886 in. -73.30 mm	-1.646 in. -41.81 mm	-2.375 in. -60.33 mm	— —	— —
Sidewalk Loading Plus Three Trucks at Midspan	-0.965 in. -24.51 mm	-0.834 in. -21.18 mm	-0.481 in. -12.22 mm	-0.659 in. -16.74 mm	-0.784 in. -19.91 mm	-0.592 in. -15.04 mm

Figure 4.4 illustrates the deflections in Table 4.1 as determined by Texas Tech for the first case, that of dead load plus prestress. Actually, the deck has been post-tensioned but is not composite with the steel superstructure at this stage of the construction process. The weight of the deck and the effect of the post-tensioning in the steel construction beams are included, but the steel superstructure (arches, hangers, and steel construction beams) must resist these forces. For this computation, the deck was removed and replaced with its weight, so the deck deflections in Figure 4.4 are shown for qualitative purposes only. The deflections of point A on the arch and point B on the construction beam are the ones of interest.

It may be seen from Table 4.1 that for both loading cases the Texas Tech model gives smaller deflections than the TxDOT results for the point of comparison, point B. The percentage difference is 17% for the case of dead load plus prestress and 21% for the sidewalk and truck loading. These differences are not of great concern in terms of the accuracy and consistency of the two models, but should be borne in mind in interpreting the remaining information in this report. Although the deflections differ by about 20

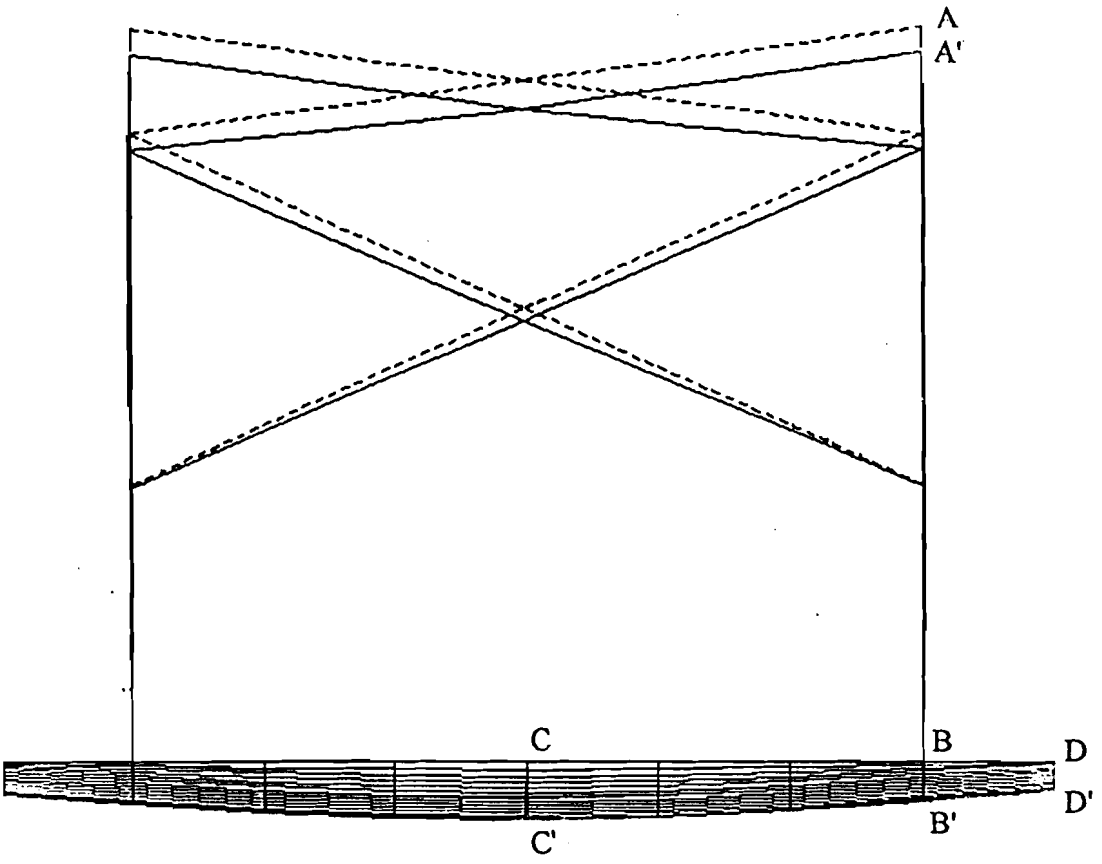

Figure 4.4: Deflections of Completed Bridge Under Dead Load Plus Prestress

percent, the member forces differ between the two models only by approximately 10 percent and the support reactions by approximately 2 percent.

4.3. Design Wind Loading

Static wind loading represents the average or steady-state effect of the wind on the bridge. The design wind loading used by TxDOT is 3.6 KPa (75 psf) on all vertical surfaces parallel to the road. In this section static responses of the partially completed bridge and the completed bridge to TxDOT's 3.6 KPa (75 psf) loads are presented. They can then be compared to the static responses to the expected buffeting winds presented in the next section.

Table 4.2 gives selected static deflection and stress results for 3.6 KPa (75 psf) wind pressures on all vertical surfaces, as used in the TxDOT design. Data are presented for the partial construction stage and for the final bridge condition as discussed earlier. The results were obtained using the most detailed meshes in the STARDYNE computer code for the complete bridge (Figure 4.2) and a corresponding mesh size for the partial construction stage of Figure 4.3. In all cases six degrees of freedom per node were included.

Table 4.2: Static Deflections and Stresses Due to Design Wind Loading (75 psf = 3.6 Kpa)
(See Figures 4.2 and 4.3 for point and member locations)

Construction Stage	Lateral Deflection			Member Stresses		
	Point	Deflection in.	mm	Member	Maximum Stress ksi	MPa
Partially Completed Bridge (Figure 4.3)	A	1.931	49.05	1 (bottom of arch)	0.667	4.602
	B	1.279	32.49	2 (bottom of cross brace)	2.270	15.66
	E	2.142	54.41	3 (end of constr. beam)	0.570	3.933
				4 (beam cross brace)	10.90	75.21
Completed Bridge (Figure 4.2)	A	0.646	16.40	1 (bottom of arch)	0.661	4.561
	B	0.007	0.18	2 (bottom brace)	1.264	8.722
	E	0.740	18.80	3 (end cable)	2.874	19.80

The results in Table 4.2 show that wind loading by itself produces stresses that are far below design levels in the completed bridge. The stresses in the deck are especially low, as expected, indicating that design wind loading should not control the design of the deck. In the completed bridge, the stresses shown must be added to the stresses from vertical loading. Since the allowable stresses are usually increased by one-third for wind loading, the combination of wind and vertical loading should not control the deck design.

The stress levels are also about the same for both of the stages of construction considered (partial and completed), indicating that the support system chosen for the partially constructed stage is adequate.

The lateral deflections in Table 4.2 are somewhat larger for the construction stage since there is no deck to stiffen the structure. However, these deflections are not excessive. The cross-bracing chosen to temporarily stiffen the construction beams at this stage causes the peak lateral deflections of these beams to be less than the peak deflections of the arch. The static wind deflections of the construction stage for 3.6 KPa (75 psf) loading are shown in Figure 4.5.

4.4. Mean Wind Loading

Static wind results are now considered for the mean wind loads described in Section 2.2. The pressure of 3.3 KPa (69.0 psf) computed in Section 2.2 for the arch is a valid number for a static design procedure, but it is not the mean pressure. The gust response factor of 1.40 included in the computation must be omitted in determining the mean pressure. Accordingly, the mean along-wind pressure on the arch is only 2.4 KPa (49.3 psf). For the deck, with a height of 5.0 m (16.5 feet) above the freeway, the design wind pressure, including the gust response factor of 1.63, is only 1.3 KPa (26.3 psf), which is a much smaller pressure than the TxDOT value of 3.6 KPa (75 psf) considered earlier. Furthermore, the mean wind pressure on the deck, found by omitting G_h, is only 0.8 KPa (16.1 psf).

Static responses to the arch and deck mean wind pressures, considering the entire arch to be loaded as heavily as the top, are given in Table 4.3. These mean or steady-state deflections due to buffeting are about one-half as large as those due to the 3.6 KPa (75 psf) design loading of Table 4.2. Similarly, the stresses in the members considered are between one-third and two-thirds of the values for 3.6 KPa (75 psf) loading.

Mean winds can develop lift or downward force and moment effects on the deck of the TxDOT completed bridge as well as lateral pressures. Since there is no deck existing at the partially completed stage, the partially completed bridge is not subjected to lift and moment effects. In the wind tunnel tests, it was found that different positions of the traffic sign changed the force coefficients of the bridge deck (see Table 8.1). In this study, four different cases are considered: 1) no sign at all, 2) sign in the windward direction for the full length of the bridge deck, 3) sign in the leeward direction for the full length of the bridge deck, and 4) sign in the windward direction for half the length of the bridge deck and in the leeward direction for the other half. A model for lift and moment

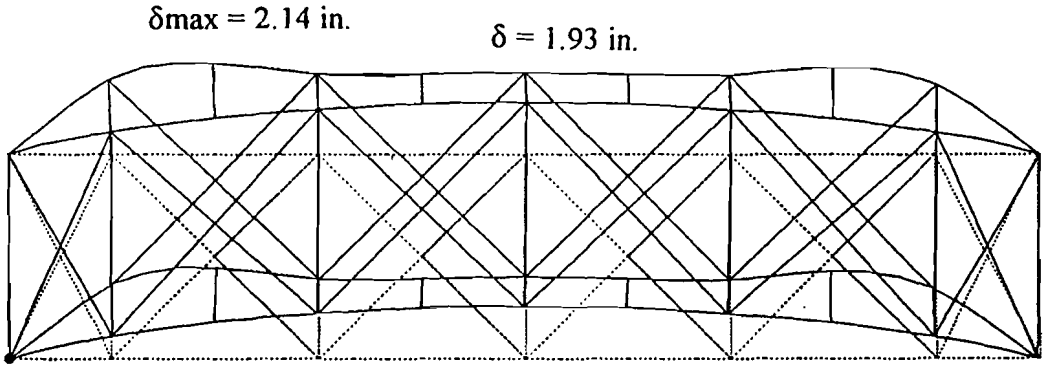

Figure 4.5: Static Wind Deflections Under 75 psf (3.6 KPa) for the Partially Completed Bridge

Table 4.3 Static Deflections and Stresses Due to Mean Wind Loading
(See Figures 4.2 and 4.3 for point and member locations)

Construction Stage	Lateral Deflection			Member Stresses		
	Point	Deflection in.	mm	Member	Maximum Stress ksi	MPa
Partially Completed Bridge (Figure 4.3)	A	0.988	25.09	1 (bottom of arch)	0.405	2.795
	B	0.337	8.56	2 (bottom of cross brace)	1.411	9.736
	E	1.096	27.84	3 (end of constr. beam)	0.380	2.622
				4. (beam cross brace)	6.276	43.30
Completed Bridge (Figure 4.2)	A	0.399	10.14	1 (bottom of arch)	0.482	3.326
	B	0.005	0.127	2 (bottom brace)	0.531	3.664
	E	0.460	11.68	3 (end cable)	2.315	15.97

effects has been formulated using properties of the deck section obtained from the wind tunnel tests. The following formulas are used:

$$L(lb/ft) = (\tfrac{1}{2}\rho U^2)BC_L \qquad \text{for the lift force, L} \qquad (4.1)$$

$$M(ft-lb/ft) = (\tfrac{1}{2}\rho U^2)B^2C_M \qquad \text{for the moment, M} \qquad (4.2)$$

where ρ is the mass density of the air (1.23 Kg/m^3 or 0.002378 slugs/ft^3), B is the width of the deck (18.3 m or 60 feet), and C_L and C_M are the lift and moment coefficients for the deck. The values of C_L and C_M for the no sign case are -0.07 and 0.04, respectively. Using the mean wind speed for the buffeting model at the height of the deck, 27.6 m/s (62.0 mph), the lift and moment forces per unit length along the deck are 1.2 KN/m (82.6 lb/ft) and 12.4 KN-m/m (2832 ft-lb/ft), respectively. The static deflections that result from these forces are given in Table 4.4. It may be seen that the maximum vertical deflection is only about one-third as great as the vertical deflections due to the static loads of Table 4.1. The associated stresses are equally small.

Table 4.4: Deflections at Midspan Due to Mean Wind Lift and Moment Loading

Deflection	Traffic Sign Position			
	No Sign	Sign Leeward	Sign Windward	Sign Half Windward and Half Leeward
Vertical (in.)	0.011	0.079	0.017	0.048
(mm)	0.279	2.007	0.432	1.219
Rotation (rad)	3.75×10^{-5}	2.72×10^{-4}	5.61×10^{-5}	1.85×10^{-4}

5. Natural Frequencies and Modes of Vibration

The natural frequencies and mode shapes of bridges are extremely important in influencing their dynamic responses to wind and traffic loadings. Also, this information is used in the calculations of dynamic response. In the response behavior, different modes come into play in different ways. The lowest lateral modes are expected to be the most important for buffeting of a bridge, since buffeting primarily produces dynamic response of the arches and small amounts of lift, moment, and drag on the deck. For vortex shedding and aeroelastic instability of the bridge, which relate essentially to the behavior of the deck in the wind, the most important modes are the lowest vertical and torsional ones. The first several frequencies and modes in vertical vibration are the most important to the dynamic response of the bridge to traffic loading.

Since the lowest frequencies of each bridge lie in the region of the wind spectrum where, from a frequency content standpoint, the spectral values are decreasing rapidly (Simiu et al., 1986), higher modes can be expected to have lower contributions to the deflections, as is typical of most structures. Accordingly, the first ten frequencies of the completed and partially constructed bridges considered are determined and tabulated in Tables 5.1 and 5.2, along with brief descriptions of the modes. These descriptions indicate whether or not the modes are symmetric or anti-symmetric about midspan and whether or not they involve torsion of the deck or lateral sway of the arch. Computer plots of the corresponding mode shapes as viewed from the side and from the end are given in Figures 5.1 and 5.2. These plots can assist in visualizing the possible types of dynamic behavior that the bridge can undergo. In the analyses to determine the frequencies and mode shapes, the vertical and horizontal vibrations are not separated. Each node has 6 degrees of freedom; therefore, the natural frequencies and mode shapes are quite accurate. Coupled modes that combine vertical, horizontal, and torsional motions are obtained.

Several striking trends of the frequencies and mode shapes of the completed bridge are found from Table 5.1 and Figure 5.1. First, all the frequencies fall in the range from about 1.0 to 5.0 Hz. As mentioned before, higher modes are expected to have lower contributions to the dynamic response. In fact, modes with frequencies above 5 Hz are not likely to be strongly excited by the wind. This principal will be seen later by examining typical wind power spectra. A key point is that both vertical and along-wind horizontal spectra have very small values above 5 Hz compared to the peak values below one Hertz. Thus, determining the first ten frequencies is appropriate for this analysis.

Another striking observation is that the first mode of the bridge is the anti-symmetric, rather than symmetric, vertical mode. This is different from beam behavior.

Table 5.1: First Ten Frequencies of the Completed Bridge

Mode No.	Frequency (Hz)	Description
1	1.38	1st Anti-Symmetric Vertical
2	2.14	1st Symmetric Vertical
3	2.27	1st Anti-Symmetric Torsional
4	2.45	1st Symmetric Lateral
5	3.02	1st Symmetric Lateral-Torsional
6	3.21	2nd Symmetric Vertical
7	4.50	2nd Symmetric Torsional
8	4.90	2nd Anti-Symmetric Vertical
9	4.94	1st Symmetric Dishing
10	5.18	1st Anti-Symmetric Dishing

Table 5.2: First Ten Frequencies of the Partially Completed Bridge

Mode No.	Frequency (Hz)	Description
1	1.53	1st Symmetric Lateral
2	1.78	1st Anti-Symmetric Vertical
3	2.00	1st Anti-Symmetric Torsional
4	2.46	1st Deck Symmetric Lateral
5	3.75	1st Symmetric Vertical
6	4.05	2nd Symmetric Torsional
7	4.76	1st Deck Symmetric Lateral
8	5.14	1st Bracing Symmetric Vertical
9	6.14	2nd Anti-Symmetric Torsional
10	6.33	1st Deck Anti-Symmetric Lateral

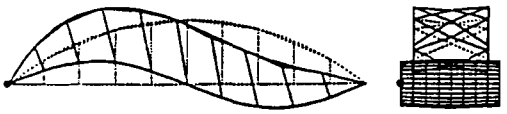

Mode No. 1: f_1 = 1.38 Hz

Mode No. 6: f_6 = 3.21 Hz

Mode No. 2: f_2 = 2.14 Hz

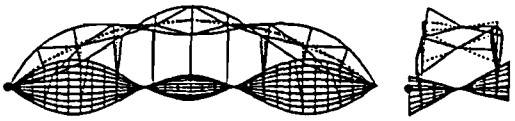

Mode No. 7: f_7 = 4.50 Hz

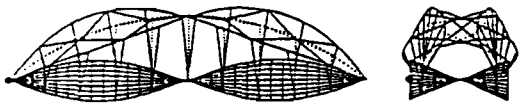

Mode No. 3: f_3 = 2.27 Hz

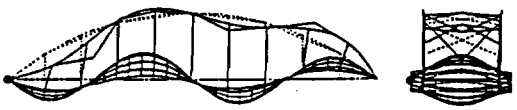

Mode No. 8: f_8 = 4.90 Hz

Mode No. 4: f_4 = 2.45 Hz

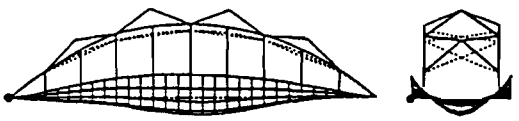

Mode No. 9: f_9 = 4.94 Hz

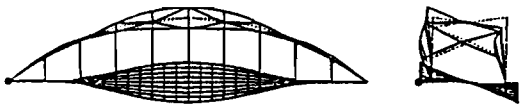

Mode No. 5: f_5 = 3.02 Hz

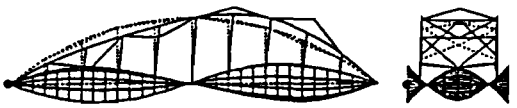

Mode No. 10: f_{10} = 5.18 Hz

Figure 5.1: First Ten Frequencies and Mode Shapes of the Completed Bridge

Mode No. 1: f_1 = 1.53 Hz

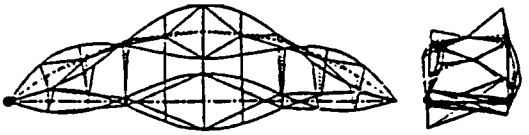

Mode No. 6: f_6 = 4.05 Hz

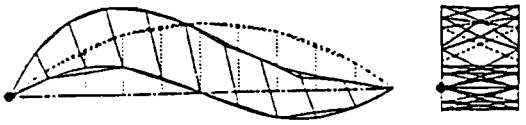

Mode No. 2: f_2 = 1.78 Hz

Mode No. 7: f_7 = 4.76 Hz

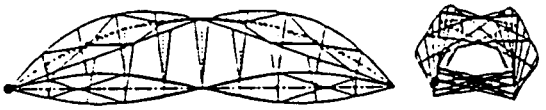

Mode No. 3: f_3 = 2.00 Hz

Mode No. 8: f_8 = 5.14 Hz

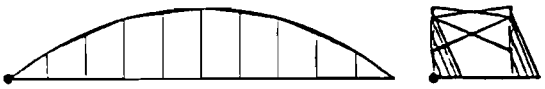

Mode No. 4: f_4 = 2.46 Hz

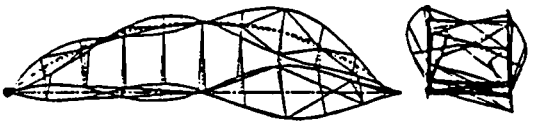

Mode No. 9: f_9 = 6.14 Hz

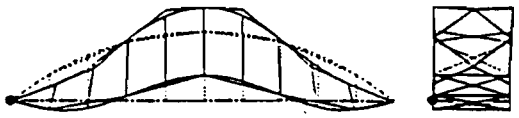

Mode No. 5: f_5 = 3.75 Hz

Mode No. 10: f_{10} = 6.33 Hz

Figure 5.2: First Ten Frequencies and Mode Shapes of the Partially Completed Bridge

This fact is expected to have particular implications for the bridge's dynamic response to moving traffic loads. With an anti-symmetric first model, a truck has the greatest tendency to excite the fundamental mode at the quarter-span point, rather than at midspan. The first symmetric vertical mode has the second lowest frequency overall. Its frequency of 2.14 Hz is influenced by the great stiffness of the arches against axial deformation, as required in symmetric vertical deflection of the structure. In the first anti-symmetric vertical mode, the arches deform primarily in bending, for which they are not so stiff.

From the results it is seen that torsional, lateral, and vertical deformations are all prominent among the ten lowest modes. The first two modes with torsion of the deck are among the group, and they are expected to be important to the vortex shedding and aeroelastic instability of the structure. They also dominate the rotational motion of the deck due to a buffeting wind. The lowest four frequencies of the bridge in purely vertical vibration fall in the range of importance for wind analysis (less than 5 Hz). For aeroelastic instability, these four vertical modes are not as critical as the lowest torsional mode at 2.27 Hz, but they still have a bearing on the deck behavior. In fact, these purely vertical modes dominate the response of the bridge due to traffic loading. Mode five is described as a lateral-torsional mode; it can be considered as a coupling of lateral and torsional modes. In this mode, when the superstructure has lateral motion in one direction, the deck has torsional motion that tends to make the superstructure sway in the opposite direction. The first mode with purely horizontal motion has a frequency of 2.45 Hz, which is twice the frequency of the first vertical mode. This mode is important in the buffeting wind analysis since it is most likely to be excited by the horizontal drag forces.

This bridge has two distinct modes which other bridges usually do not have; they are the 9th and 10th modes. In these so-called dishing modes, the structure as a whole has no lateral motion, the deck bends about its long axis, and the diagonal bracing has corresponding bending. These unusual modes are among the lowest ten due to one of the distinguishing characteristics of this structure: it has a thin deck without plate girders and floor beams to stiffen the deck, so the deck is less stiff laterally than in traditional bridges. This is another reason why the deck section of this bridge needs to be tested in a wind tunnel test in order to investigate its aeroelastic behavior.

Similar data for the frequencies and modes of the partially completed bridge are given in Table 5.2 and Figure 5.2. The structure is quite flexible and the lowest three frequencies of vibration are all less than 2 Hz. This structure is essentially just a box skeleton that is supported at its four base points. The box can vibrate vertically, laterally (lower and upper portions moving in the same directions), or in torsion (lower and upper portions moving in opposite directions).

6. Time Domain Analysis of Response to Buffeting Winds

Generally speaking, flexible bridges are subjected to three types of dynamic wind effects: aeroelastic instability, vortex shedding, and buffeting. Flutter or aeroelastic instability describes an exponentially growing response of the bridge deck, where one or more modes participate at a particularly critical wind velocity, possibly resulting in failure due to over-stressing of the main structural system. Vortices are shed from the deck at certain frequencies at different wind speeds according to the Strouhal number $St = f_s D / U$, where f_s is the frequency of vortex shedding, D is a characteristic dimension perpendicular to the flow, and U is the mean wind speed. When the frequency of vortex shedding matches one of the natural frequencies of the deck, the vortices excite that particular mode of vibration. Vibration at this wind speed is called "lock-in." The first two vertical modes of vibration are most susceptible to vortex shedding because they have the lowest frequencies.

In this study, flutter and vortex-shedding results are treated only by the frequency domain approach (see chapter 8). The time domain approach is applied in this chapter to the third type of dynamic wind effect, buffeting. Buffeting is defined as the unsteady loading of a structure by velocity fluctuations in the oncoming flow. Dynamic lift and moment on the deck go into a complete buffeting analysis, along with lateral forces. The parameters needed for lift and moment were obtained from wind tunnel tests on a section model of the bridge (see Table 8.1).

The time history of the lateral wind loading acting on the top of the arch of the completed bridge is shown in Figure 6.1. It is a statistically generated record representing the force per unit length on the arch. The arch of each bridge is only subjected to the drag force. The "buffeting" by the wind includes small amplitudes of lift and moment on the deck of the completed bridge, so the time histories of drag, lift, and moment are all applied to the structures simultaneously. The partially completed bridge is only subjected to the drag force. The force-time history at each point on the bridge for partial correlation follows the relationship present earlier in Equation 2.7. In the fully correlated calculation, the time history of the force at each point on the arch is the same and that on each point of the deck is the same. The duration of each time domain analysis is 120 seconds, which is about 50 times of the longest period of the bridge. This duration helps to ensure that the peak responses will occur within the time considered.

The time histories have been made to have a zero-mean by subtracting the mean wind values. The turbulence intensity is taken as 25 percent. The pressure time histories

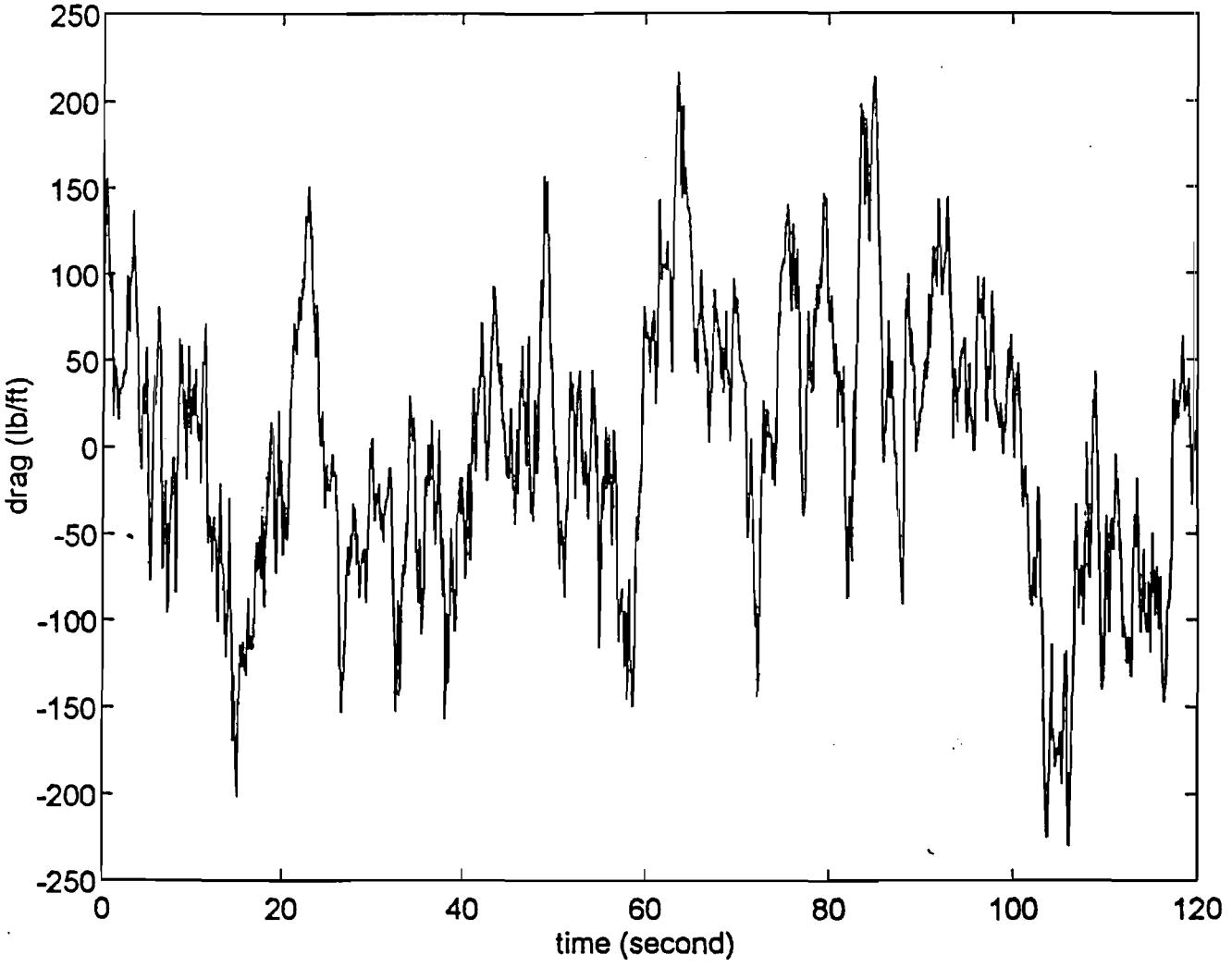

Figure 6.1: Time History of Buffeting Wind Loading at the Top of the Arch

have been generated to incorporate the wind frequency characteristics depicted in the along-wind and vertical wind spectra of Figure 6.2. They are digitized at time intervals of 0.1 seconds. Bridge damping is assumed to be one percent in all modes. The actual damping in the bridge is difficult to estimate. Highway bridge damping measurements could not be found in the literature, and no bridge quite like the one under design has been built, much less field tested. Welded steel structures are generally known to have low damping coefficients (less than 2 percent), and prestressed concrete members have less damping than ordinary reinforced concrete ones because cracks do not open and close at design levels. The damping value of one percent is considered at different points in this report to ensure that conservatively large estimates of maximum dynamic deflections are obtained.

Results for the same points and members as selected in the static analysis are presented for the dynamic analysis. Figure 6.3 shows the dynamic parts of the lateral deflection at the top of arch of the completed bridge due to both partially correlated and fully correlated fluctuating winds. The standard deviation of the deflection due to the partially correlated wind is 4.57 mm (0.18 in) and the corresponding peak value is 16.0 mm (0.63 in). The peak deflection is in the range of 3.0 to 4.0 times the standard deviation. Similar peak to standard deviation ratios are found for stresses caused by both partially and fully correlated lateral wind forces. Tables 6.1 and 6.2 give the peak dynamic deflections and stresses for both partially completed and completed bridges.

Table 6.1: Peak Dynamic Deflections and Stresses Due to Buffeting Wind Loading for Partially Completed Bridge
(See figure 4.3 for the point and member locations)

Peak Lateral Deflection			Peak Principal Stress		
Point	Partially Correlated	Fully Correlated	Member	Partially Correlated	Fully Correlated
A	1.587 in. 40.31 mm	2.524 in. 64.10 mm	1 (bottom of arch)	0.635 ksi 4.382 MPa	0.924 ksi 6.376 MPa
B	0.631 in. 16.02 mm	1.000 in. 25.37 mm	2 (bottom of arch brace)	1.902 ksi 13.12 MPa	2.754 ksi 19.00 MPa
E	1.814 in. 46.08 mm	2.906 in. 73.80 mm	3 (construction beam)	0.619 ksi 4.271 MPa	0.894 ksi 6.168 MPa
			4 (beam cross brace)	8.073 ksi 41.91 MPa	11.77 ksi 81.21 MPa

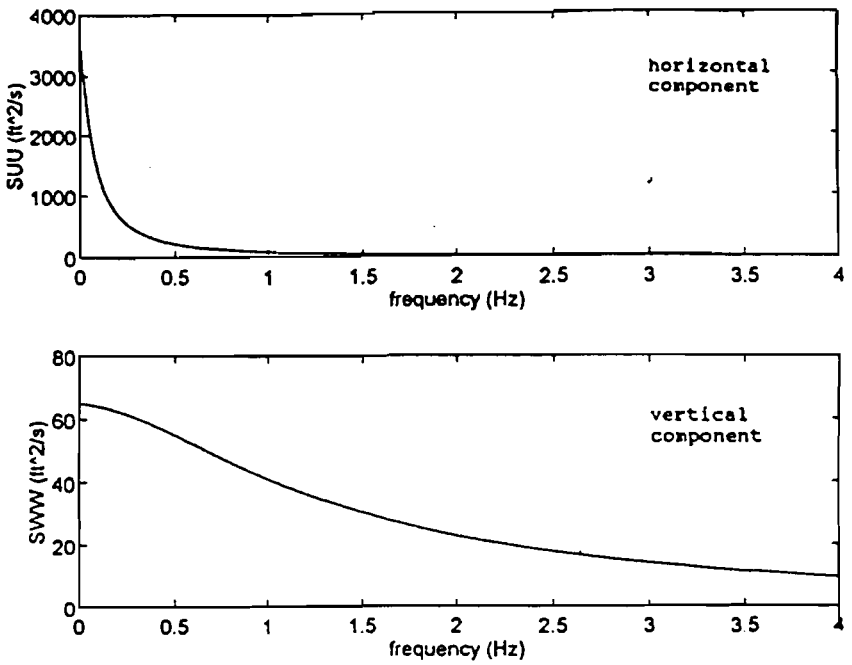

(a) Spectra for the Deck

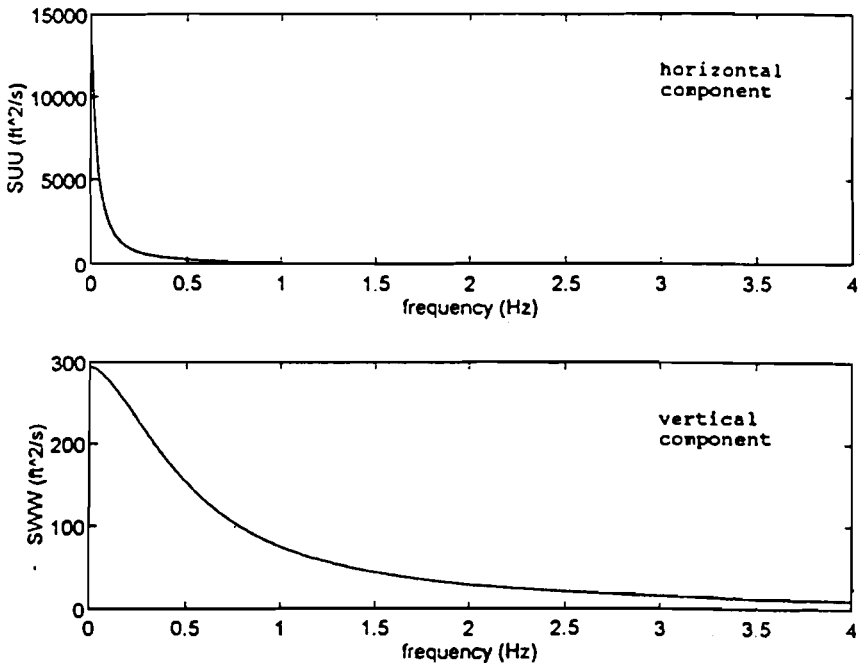

(b) Spectra for the Arch

Figure 6.2: Assumed Along-Wind and Vertical Power Spectra for the Arch and Deck

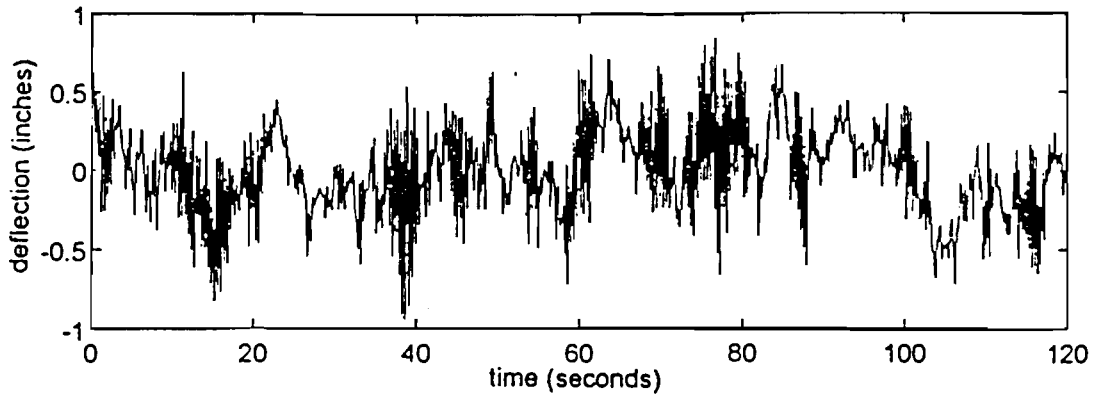

(a) Deflection due to Fully Correlated Wind

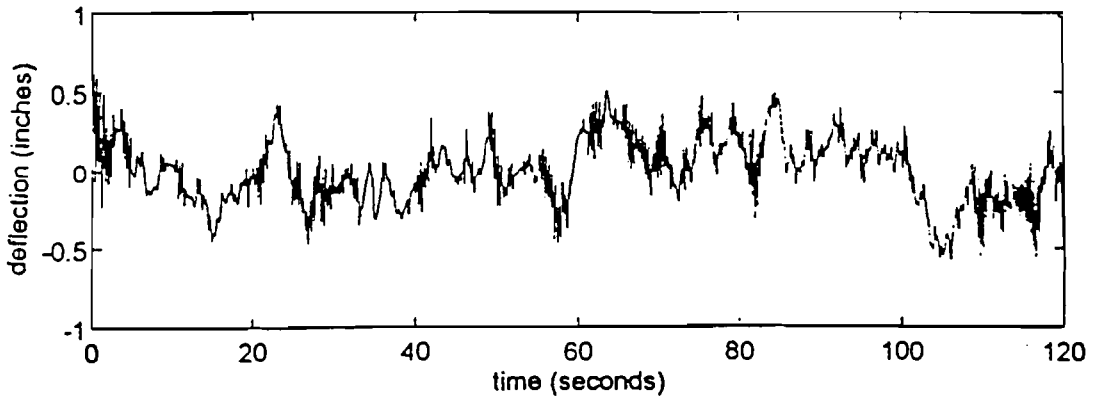

(b) Deflection due to Partially Correlated Wind

Figure 6.3: Dynamic Lateral Deflections at the Top of the Arch

Table 6.2: Peak Dynamic Deflections and Stresses Due to Buffeting Wind Loading for Completed Bridge
(See figure 4.2 for the point and member locations)

Peak Lateral Deflection			Peak Principal Stress		
Point	Partially Correlated	Fully Correlated	Member	Partially Correlated	Fully Correlated
A	0.631 in. 16.03 mm	0.982 in. 24.94 mm	1 (bottom of arch)	0.711 ksi 4.906 Mpa	1.114 ksi 7.687 MPa
B	0.010 in. 0.254 mm	0.013 in. 0.330 mm	2 (bottom brace)	0.783 ksi 5.403 MPa	1.205 ksi 8.314 MPa
E	0.682 in. 17.32 mm	0.996 in. 25.30 mm	3 (end cable)	3.406 ksi 23.50 MPa	5.171 ksi 35.68 MPa

One of the most significant features of the results in Tables 6.1 and 6.2 is the degree to which the fully correlated wind causes larger responses than the partially correlated wind. The selected dynamic deflections obtained with the fully correlated wind are consistently about 50 percent larger than with the partially correlated wind. For stresses, the table shows that the fully correlated wind induces 50 to 65 percent larger values than the partially correlated wind. These results show that the simpler model of a fully correlated wind, if used in design, could be quite conservative.

Secondly, several comparisons may be made between the mean wind deflections and stresses in Tables 4.2 and 4.3 and the peak dynamic values in Tables 6.1 and 6.2. Results for the partially correlated wind are discussed here because they are considered to be more realistic dynamic results. The peak dynamic lateral deflections due to the partially correlated wind are 50 percent larger than the mean wind values, but are all slightly smaller than the AASHTO design load deflections. When the dynamic deflections due to the partially correlated wind and static deflections due to the mean are added, however, they reach a total that is about 50 percent greater than the AASHTO design code values. When stresses rather than deflections are compared in Tables 4.2 and 6.2, it is found that the peak dynamic stresses are 50 percent larger than the mean wind stresses, and the total static and peak dynamic wind stresses are about 50 percent greater than the design wind stresses.

Gusty winds can develop lift or downward force and moment effects on the decks of bridges as well as lateral pressures. As mentioned before, the partially completed bridge is not subjected to lift and moment because the deck does not exist at that stage. Among the first ten mode shapes of the completed bridge having vertical and rotational motions of the deck, the corresponding fundamental frequencies are in the range from 1.4

Hz to 4.9 Hz. Since the modes involving deck lift and rotation are likely to be excited by the buffeting wind, the deck lift and moment effects need to be studied herein. As discussed in Section 4.4, mean wind lift and moment effects were determined by Equations 4.1 and 4.2 and are given in Table 4.4. The maximum vertical deflections and rotations due to both fully correlated wind and partially correlated wind for four different cases are tabulated in Tables 6.3 and 6.4. The lift and moment forces are applied separately and without the lateral drag force on the deck and the arches.

Table 6.3: Peak Dynamic Deflections at Midspan Due to Fully Correlated Lift and Moment

Deflection	Traffic Sign Position			
	No Sign	Sign Leeward	Sign Windward	Sign Half Windward and Half Leeward
Vertical (in.)	0.245	2.181	0.137	1.152
(mm)	6.223	55.40	3.480	29.26
Rotation (rad)	3.33×10^{-4}	4.86×10^{-3}	1.39×10^{-4}	2.50×10^{-3}

Table 6.4: Peak Dynamic Deflections at Midspan Due to Partially Correlated Lift and Moment

Deflection	Traffic Sign Position			
	No Sign	Sign Leeward	Sign Windward	Sign Half Windward and Half Leeward
Vertical (in.)	0.141	1.227	0.079	0.631
(mm)	3.581	31.17	2.007	16.03
Rotation (rad)	1.92×10^{-4}	2.68×10^{-3}	7.31×10^{-5}	1.39×10^{-4}

Dynamic deflections at point D (See Figure 4.2) of the deck of the bridge without traffic sign, under unsteady partially correlated lift and moment forces, are shown in time history form in Figure 6.4. Note that the moment effects are represented by the vertical deflections of the edge of the deck at midspan, rather than the midspan deck rotation as in Tables 6.3 and 6.4. Comparing these peak dynamic deflections to static deflections given in Table 4.4, the dynamic values are of the order of 6 times and 25 times the static values for lift and moment effects, respectively. Also, the dynamic lift deflections are of the order of 2 to 4 times the dynamic moment deflections.

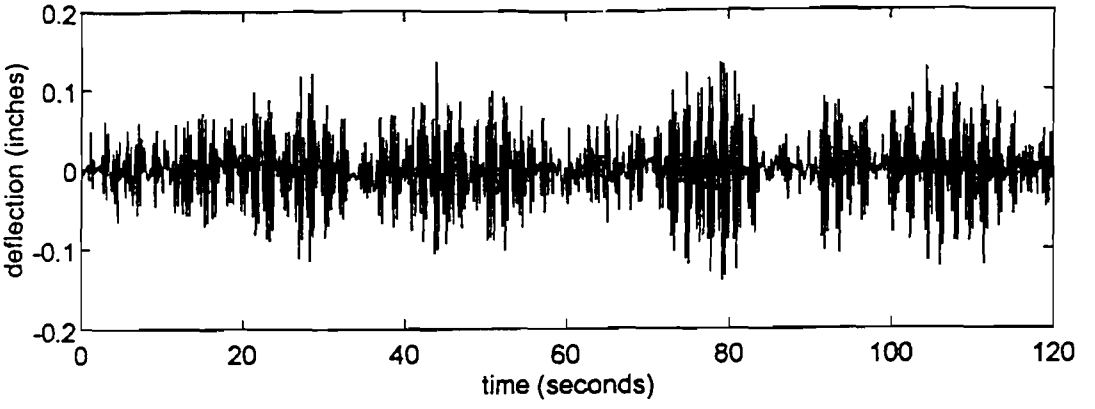

(a) Vertical Deflection due to the Lift

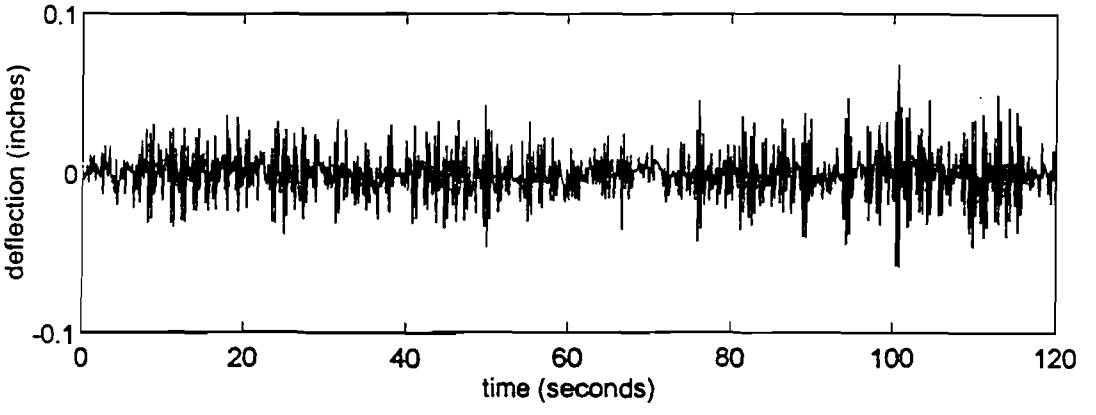

(b) Vertical Deflection due to the Moment

Figure 6.4: Dynamic Vertical Deflections of the Deck at Midspan due to Lift and Moment

7. Time Domain Analysis of Response to Traffic Loading

7.1. Static Response

The U.S. 59 bridge considered is designed to have one lane in each direction. In the static analysis, only the case in which one truck is in one lane is considered. Then, for the static case in which two trucks are side by side in adjacent lanes, the centerline deflections and stresses are simply doubled. The single truck considered is placed at every location along its lane and the resulting bridge deflections and stresses are calculated.

Since the bridge only has one lane in each direction, a new computer model is used in the traffic analysis. As shown in Figure 7.1, the deck is divided into 20 segments along the bridge and 6 segments crossing the bridge. The lines from node 43 to node 63 and from node 85 to node 105 are represented as the centerlines of the two lanes. The truck loads at all three of its axles are proportionally distributed on several nodes along these lane centerlines as concentrated loads.

The maximum static deflection for any node in the deck due to the truck at any position is 8.66 mm (0.341 in). This deflection occurs at the one-quarter point along the lane, i.e., at node 48 in Figure 7.1, and it is produced when the middle axle of the truck is at that node. It is interesting to note that the maximum deflection occurs at one of the quarter points of the bridge span, rather than at midspan, as would occur in a simply supported beam. This difference in behavior is due to the effect of the arch. The deflection of the midspan node when the truck's middle axle is at midspan is only 6.43 mm (0.253 in). Figure 7.2 shows the vertical deflection shapes of the bridge when the truck's middle axle is at the quarter span and at midspan, respectively. From Figure 7.2(a) it is seen that the deflected shape for the one-quarter point loading is anti-symmetric and very similar to the first mode shape of the bridge in vibration. There is a downward deflection in the loaded half span, an upward deflection in the other half span, and a deflection at midspan that is almost zero. The influence line for the deflection at the quarter span point due to the truck's loading is shown in Figure 7.3. The noteworthy feature is that, due to arch action, there is an upward deflection at the quarter span point when there is a downward load in the opposite half span.

The total weight of the truck is 320 KN (72 kips). Since this force is much less than the total dead load of the deck of $.37 \times 10^4$ KN (3.08×10^3 kips), the truck loading is not expected to produce the largest stress in the bridge. The static stresses in various members with the truck at the quarter span point are tabulated in Table 7.1. The maximum stress occurs in the hanger immediately adjacent to the truck and is only

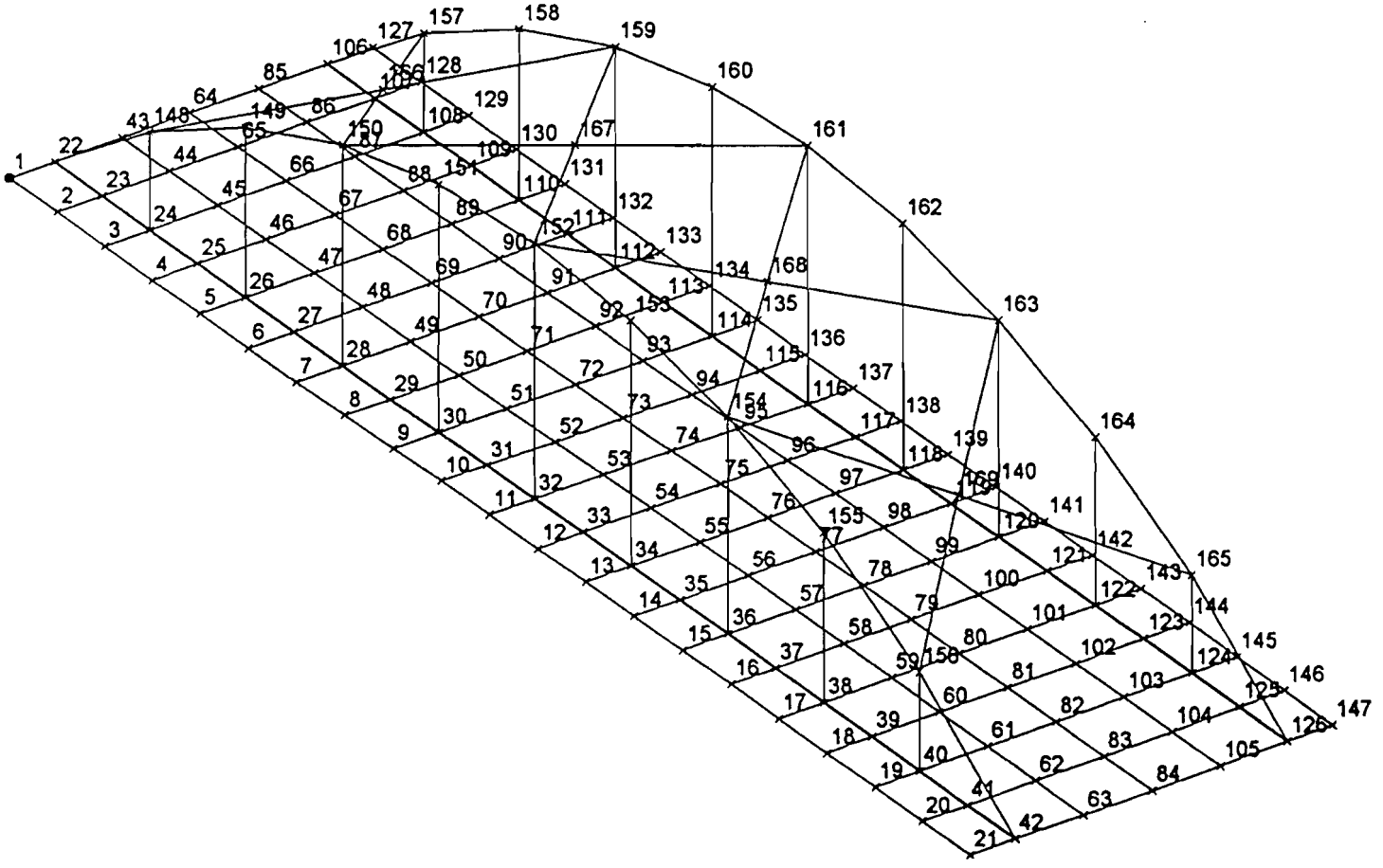

Figure 7.1: Computer Model of the Bridge for Traffic Analysis

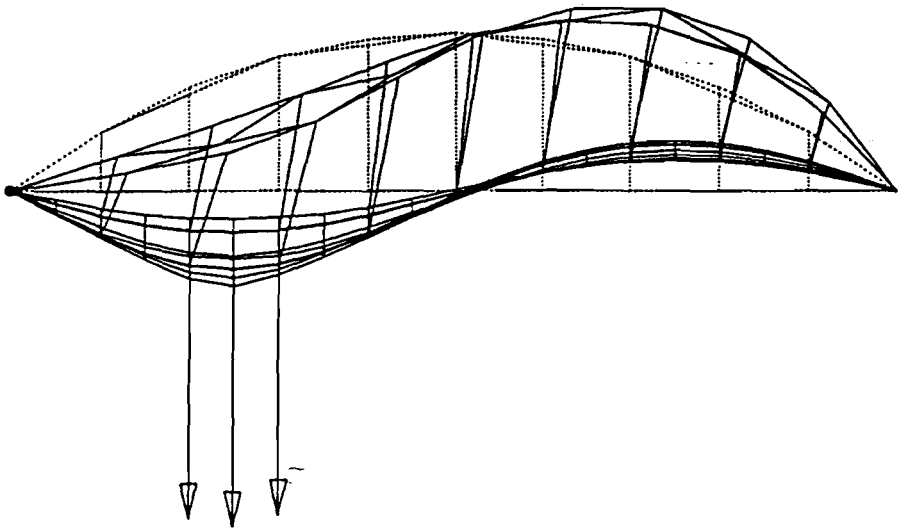

(a) One-quarter Span Point

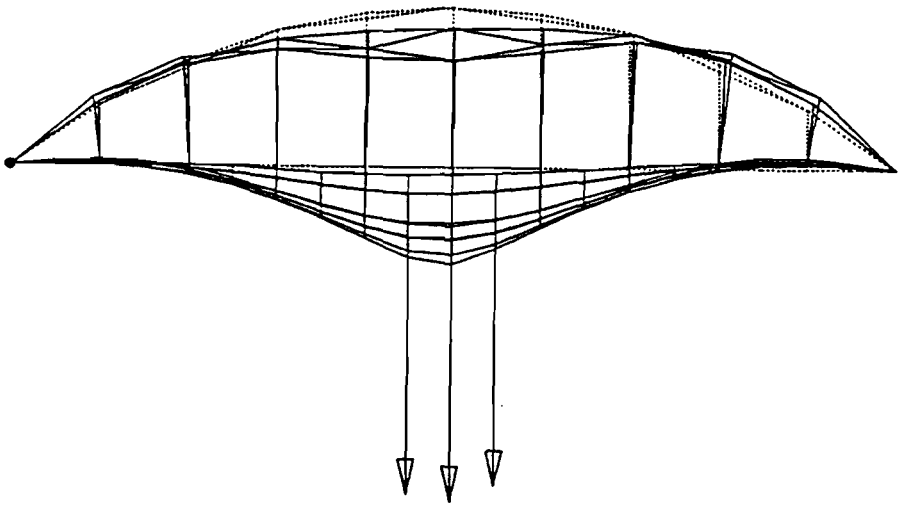

(b) Midspan Point

Figure 7.2: Static Deflection Shapes due to a Single Truck

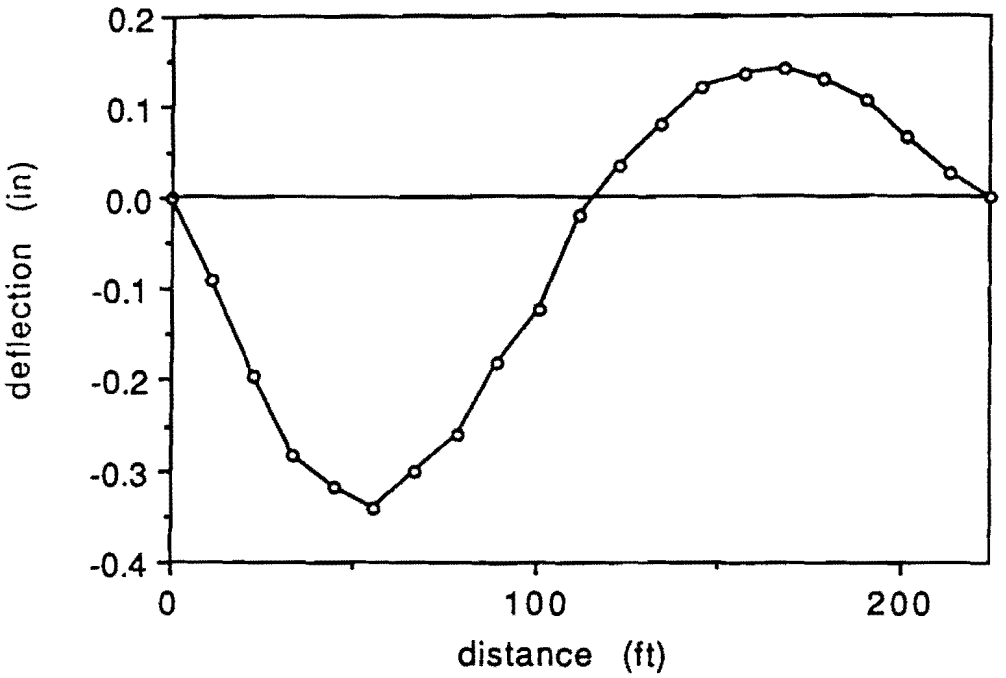

Figure 7.3: Influence Line of Quarter Span Point due to a Single Truck

2.48×10^4 KPa (3.59 ksi). The static stresses due to the truck at other positions have the same order of magnitude as the stresses given in this table.

Table 7.1: Static Normal Stresses Due to Single Truck at the Quarter Span Point

Member	Maximum Normal Stress	
	Ksi	MPa
1 (Deck quadrilateral plate element under truck)	0.221	1.525
2 (Top pf arch)	0.387	2.670
3 (Near side hanger between middle and rear axles)	3.586	24.74
4 (Construction beam immediately to side of truck)	0.022	0.152
5 (Arch cross-brace above truck)	0.128	0.883

7.2. Dynamic Response

New frequencies and mode shapes have been determined from the new computer model having 979 degrees of freedom (see Figure 7.1). The first 10 frequencies and corresponding mode shapes are almost the same as those given in Table 5.1 and Figure 5.1. Because the truck weight is fairly small compared to the dead weight of the deck, the bridge is not subjected to strong torsional motion. Therefore, the modes involving torsion of the deck are not likely to be excited. However, the first three purely vertical modes do come into play. They are the most important ones.

In the studies of dynamic response presented herein, several cases involving one or more trucks traveling in the same or opposite directions are considered. Also, two different vehicle speeds, 13.41 m/s (30 mph) and 26.82 m/s (60 mph), are considered in each case. One percent damping is assumed in all modes.

For a particular node i along a lane in which a truck is traveling, the truck is assumed to apply a force to the node only if one of its axles is between node (i-1) and node (i+1). Otherwise, the node has no axle force acting on it. This representation of the loads can be called a "stringer model" along the span. Also, the loads from the left and right side wheels are assumed to be concentrated at the node in the center of the lane. As an example, the traffic loading force-time history for one node, the midspan point on the near lane (point 53 in Figure 7.1) is shown in Figure 7.4 for a truck moving from left to right at a speed of 30 mph (13.41 m/s). There is an initial increase in the nodal load when the front axle of the truck passes node 52, which is 3.42 m (11.2 feet) from the midspan node. Then when the middle axle passes node 52, it also begins applying an increasing load on node 53, while the front axle, now past node 53, is applying a decreasing load to it. Later, the load on node 53 from the middle axle begins to decrease when it passes this

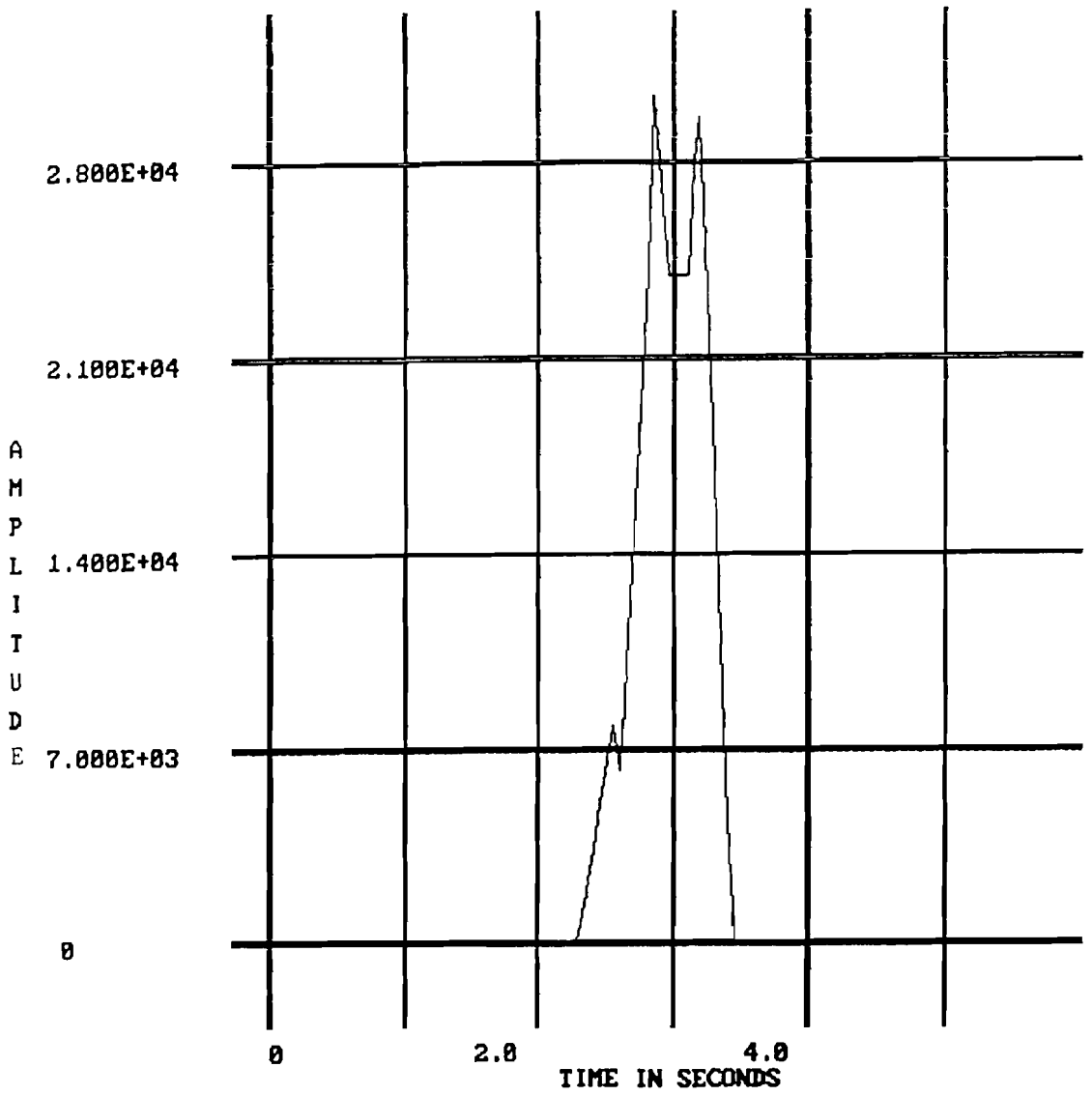

Figure 7.4: Time History of Truck Loading at Midspan for 30 mph Vehicle Speed

node. This occurs at a time when neither of the other axles exerts any load on the node, since they are 4.27 m (14 feet) away to the front and rear. Then when the rear axle passes node 52 and the middle axle is still between nodes 53 and 54, the net force on node 53 increases once more. A second peak load is reached when the rear axle passes node 53. Finally, no loads are exerted on node 53 when the rear axle passes node 54. A similar explanation applies to the time history for the 26.82 m/s (60 mph) truck speed in Figure 7.5, but the times involved are all shorter.

Figures 7.4 and 7.5 do not show the exact peak forces for either truck speed because the chosen time steps do not catch the axles exactly when they pass node 53. The time interval is chosen as 0.05 seconds in the analysis. However, the values shown correctly reflect the loads at node 53 at the times used in the dynamic analyses. Corresponding time histories are generated at other nodes to provide the complete loading on the bridge in each moving load analysis.

In the following paragraphs, responses of the bridge to several cases of moving trucks loading are presented. The different cases involve different situations of one or two trucks moving in the same or opposite directions. The more elementary cases are useful in understanding the dynamic behavior of the bridge under the action of the trucks, while the more complicated cases help in identifying the worst possible stresses.

Case 1 - Single Truck.—In the first case considered one truck passes over the bridge from left to right in the lane on the near side in Figure 7.1. Figures 7.6 and 7.7 give dynamic acceleration, velocity, and deflection time histories at the quarter span point for the two speeds considered (13.41 and 26.82 m/s (30 and 60 mph)), and Figures 7.8 and 7.9 give corresponding time histories at the midspan point. For both truck speeds, the maximum deflection is found to be downward and to occur at the quarter span point along the bridge. This maximum deflection is 8.43 mm (0.332 in) for the 13.41 m/s (30 mph) speed and 8.56 mm (0.377 in) for the 26.82 m/s (60 mph) speed. The peak deflections at midspan are only 5.84 mm (0.230 in) for both speeds.

At a speed of 13.42 m/s (30 mph), the time required for the truck to pass completely off the bridge is 5.72 seconds. Figure 7.6 shows that there are small residual accelerations and velocities but virtually zero residual displacements at the quarter span point after the truck has left the bridge. In fact, the overall response is basically a static response—the peak deflection occurs just about the time when the truck's middle axle passes over the quarter point (at 1.59 seconds), and this is the location of the truck that produces the maximum static deflection there. Moreover, the peak dynamic deflection for the 13.41 m/s (30 mph) speed is slightly smaller than that for static loading (8.43 mm (0.332 in) versus 8.66 mm (0.341 in)).

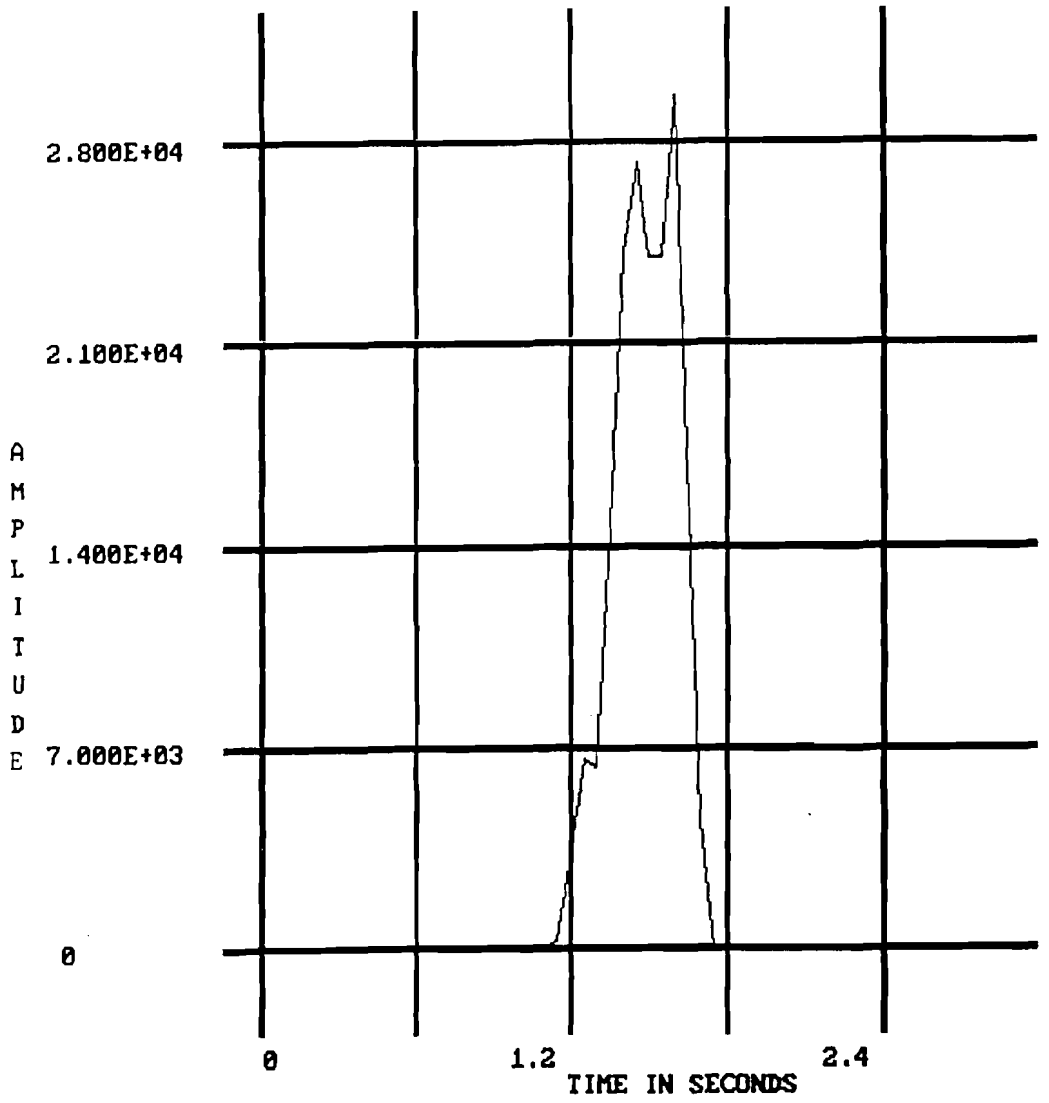

Figure 7.5: Time History of Truck Loading at Midspan for 60 mph Vehicle Speed

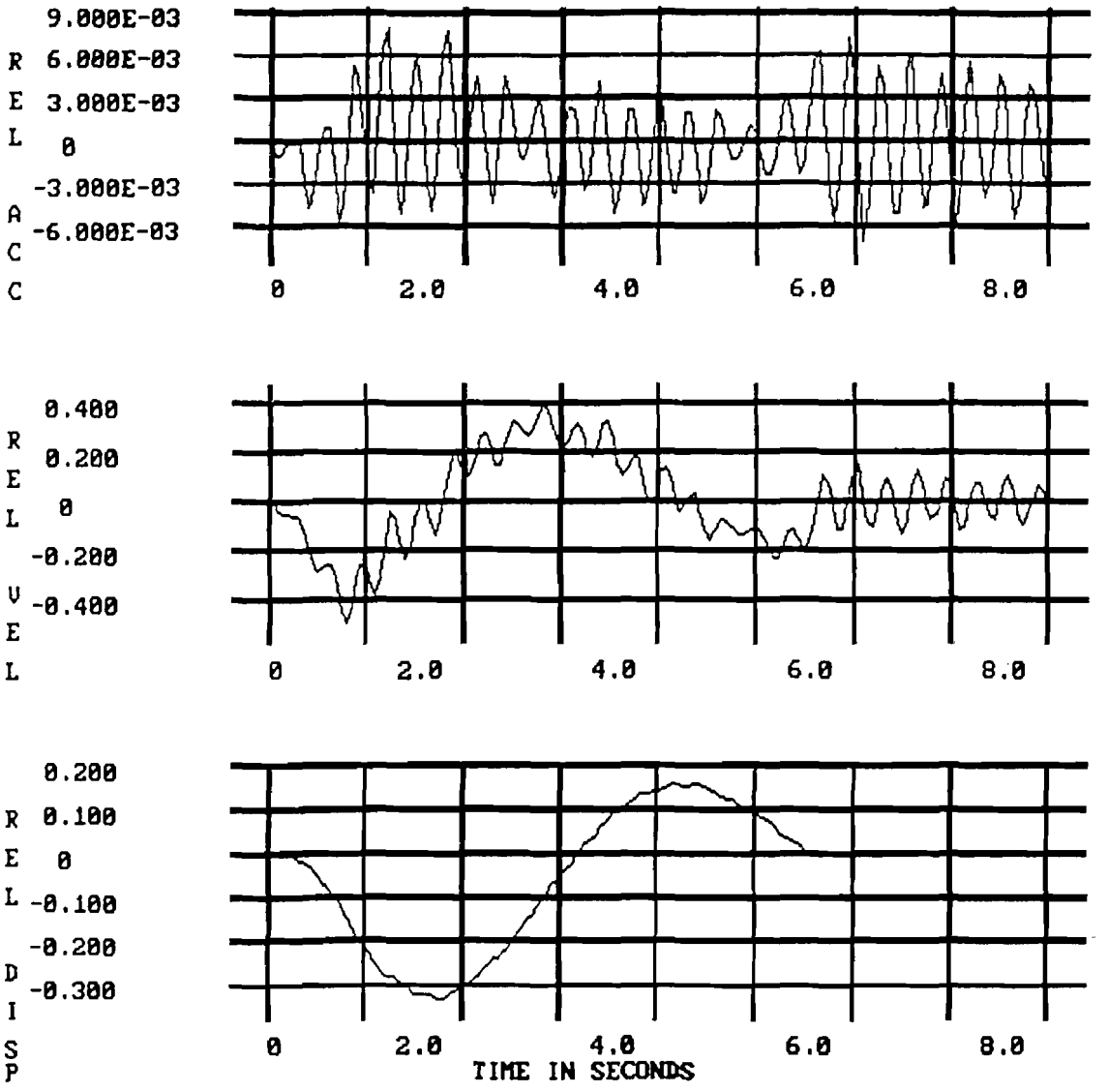

Figure 7.6: Dynamic Response of Quarter Span Point for One Truck Traveling at 30 mph

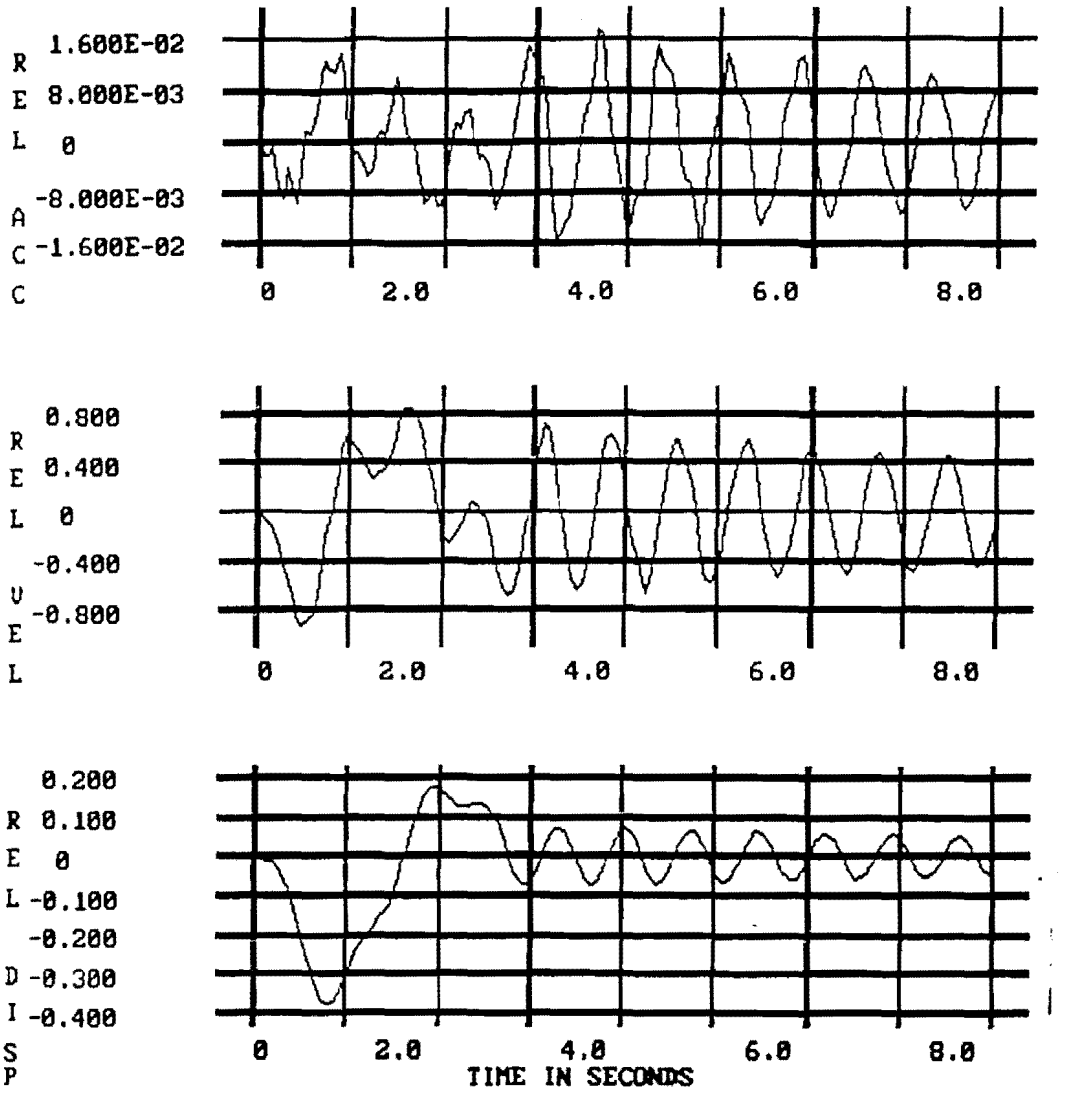

Figure 7.7: Dynamic Response of Quarter Span Point for One Truck Traveling at 60 mph

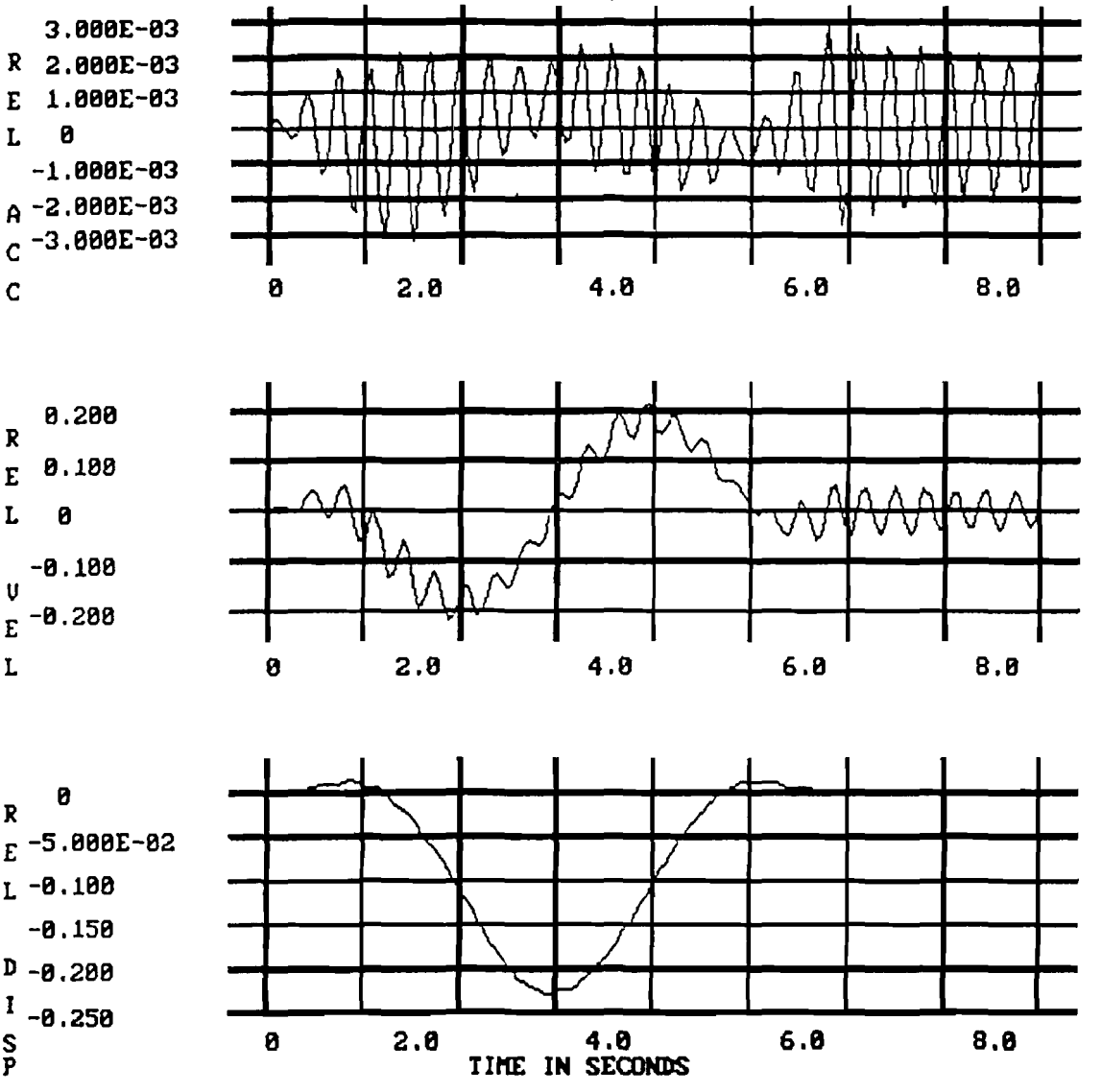

Figure 7.8: Dynamic Response of Midspan Point for One Truck Traveling at 30 mph

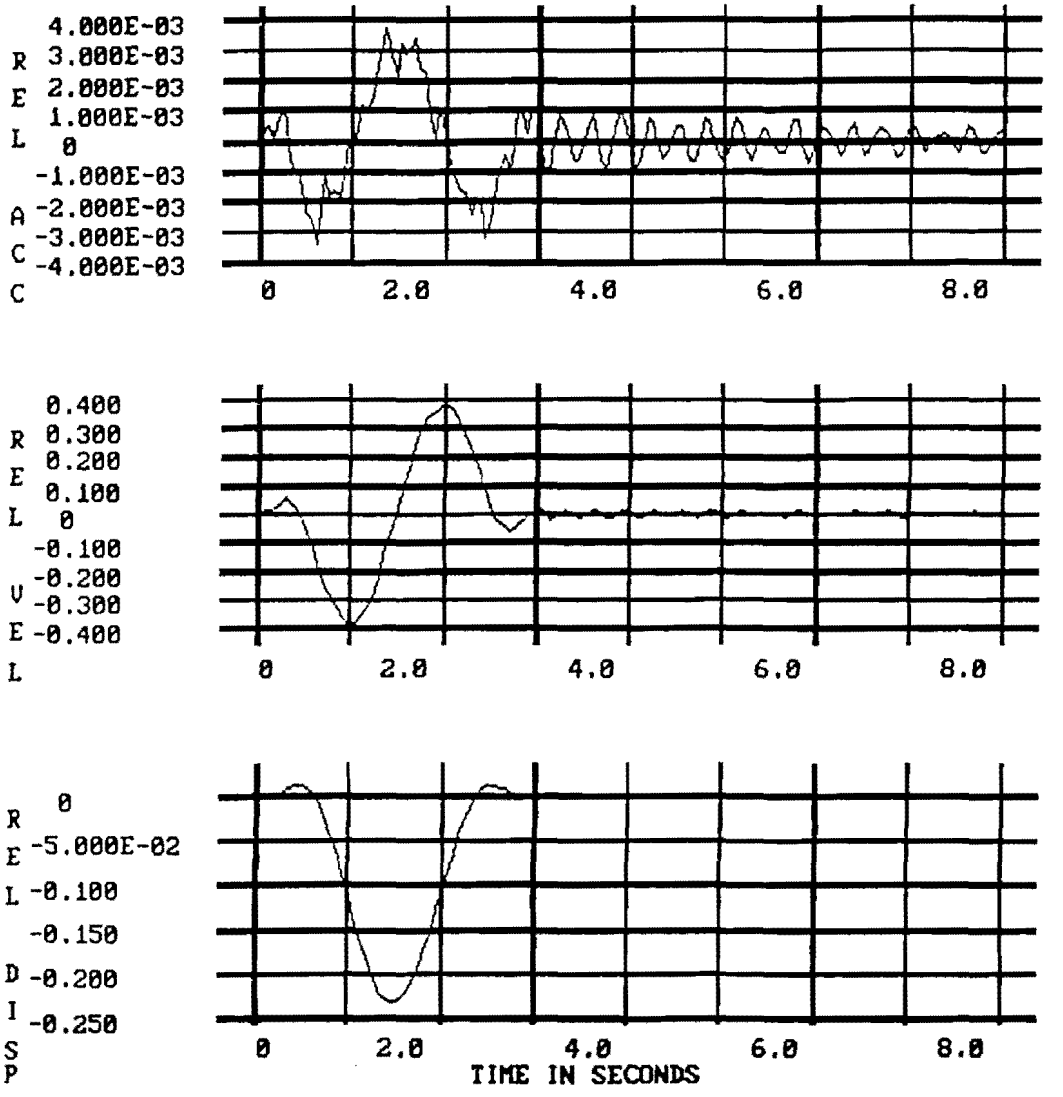

Figure 7.9: Dynamic Response of Midspan Point for One Truck Traveling at 60 mph

This lack of dynamic response can be understood in terms of the natural frequencies and mode shapes of the bridge. First of all, only the vertical modes (modes 1, 2 and 6 of Figure 5.1), and not the torsional ones, seem to be excited even slightly by the purely vertical truck loading. Secondly, in terms of mode shape, for the anti-symmetric fundamental mode to be easily excited it would need to have an upward load at the three-quarter span point at the same time as a downward load at the quarter span point. Third, in terms of frequency content or partial resonance, the first mode would be excited far more if the purely downward truck loading acted first on one half span and then on the other half span in rhythm with the fundamental period, that is, if it moved from the quarter-span point to the three-quarter-span point in half the fundamental period. However, the half period is 0.36 seconds and at the 13.41 m/s (30 mph) speed the time for the truck to move the stated distance is 2.55 seconds. In other words, the truck speed is about seven times slower than the speed that would optimize the contribution of the first mode. As a result, there is little participation of the first mode.

With regard to the symmetric second mode, it would be optimally excited if the time for the truck to move to the center of the span were about one-fourth of its natural period, with the load getting off the bridge within half the period. However, one-fourth the second period is only 0.115 seconds and the time for the truck to reach midspan at 13.41 m/s (30 mph) is 2.55 seconds. Thus, from the frequency standpoint, the second mode is not excited to any significant degree either. However, the single downward load of the truck does correlate more with the symmetric second mode shape than with the anti-symmetric first mode shape.

Finally, the sixth mode, with its second symmetric mode shape in vertical deflection, would be excited most from a frequency standpoint if the truck traveled approximately two-thirds the length of the bridge in one full period. The full period is 0.314 seconds and the time to travel the stated distance is 3.39 seconds, again indicating little participation of this mode. The time histories of velocity and acceleration in Figure 7.6 show a definite oscillation at about 3 Hz superimposed on the dominant traces corresponding to the pseudo-static responses. These superimposed oscillations appear to be at the sixth mode frequency of 3.21 Hz.

For the 26.82 m/s (60 mph) truck speed, the times required for the truck to travel the various distances just discussed are all cut in half, but they are still much longer than the times required for optimal modal participation. All three modes do participate slightly more than for the 13.41 m/s (30 mph) speed, but the first mode is the one excited the most. This can be seen by the residual oscillations at the fundamental frequency of 1.4 Hz in Figure 7.7. The greater participation of the first mode also causes the peak dynamic

deflection at the quarter point to be ten percent higher than the corresponding static deflection (9.58 mm(0.377 in) vs. 8.66 mm(0.341 in)). Since the 26.82 m/s (60 mph) speed is an upper bound on the speed anticipated to occur on the bridges in question, the "impact factors" for one truck on these bridges should be about 1.10.

The dynamic deflections at midspan shown in Figures 7.8 and 7.9 are not significantly larger than the static deflections; that is, the overall behavior is essentially static. At the 26.82 m/s (60 mph) speed the lack of residual oscillations at midspan (Figure 7.9) in contrast to the 2.54 mm (0.1 in) oscillations at the quarter span point (Figure 7.8) confirms that the bridge is left vibrating in the anti-symmetric first mode after the truck leaves the bridge.

Case 2 - One Truck Following Another in the Same Direction.—According to traffic safety guidelines, the minimum safe distance between a vehicle and the one behind it is one car length (approximately 6.10 m (20 feet)) for every 4.47 m/s (10 mph) of speed. With this guideline, the safe separation distance for a speed of 13.41 m/s (30 mph) is 18.3 m (60 feet), or about one-fourth the total length of the bridge, and the safe separation distance for a speed of 26.82 m/s (60 mph) is 36.6 m (120 feet), or about half the bridge length. These separation distances are taken herein from the rear axle of the lead truck to the front axle of the following truck. For the 13.41 m/s (30 mph) speed the second truck enters the bridge 2.0 seconds later than the first one; the delay time for the 26.82 m/s (60 mph) speed is 1.68 seconds.

Deflection time histories for the quarter span point and for the midspan point with one HS20-44 truck following another in the same lane are given in Figures 7.10 and 7.11. The deflection traces have more than two peak values in these cases. The maximum deflection remains about the same as with one truck for the 13.41 m/s (30 mph) speed, 8.51 mm (0.335 in), but it is nine percent greater than for one truck at the 26.82 m/s (60 mph) speed, becoming 10.41 mm (0.410 in). At the full 36.6 m (120 feet) separation distance for the 26.82 m/s (60 mph) speed, the second truck is close to the quarter span point when the first one is at the three-quarter span point. At this instant, each tends to cause an upward deflection at the location of the other, thus reducing the peak deflection. Instead, the peak deflection occurs when only the first truck is on the bridge, that is, it is the same as for the one truck case (Case 1). For the 13.41 m/s (30 mph) speed the frequency of the oscillations in the velocity and acceleration traces is again close to the 6th mode frequency of 3.21 Hz., and the first mode appears to barely be excited. For the 26.82 m/s (60 mph) speed, on the other hand, the residual oscillations are again at the fundamental frequency of 1.4 Hz.

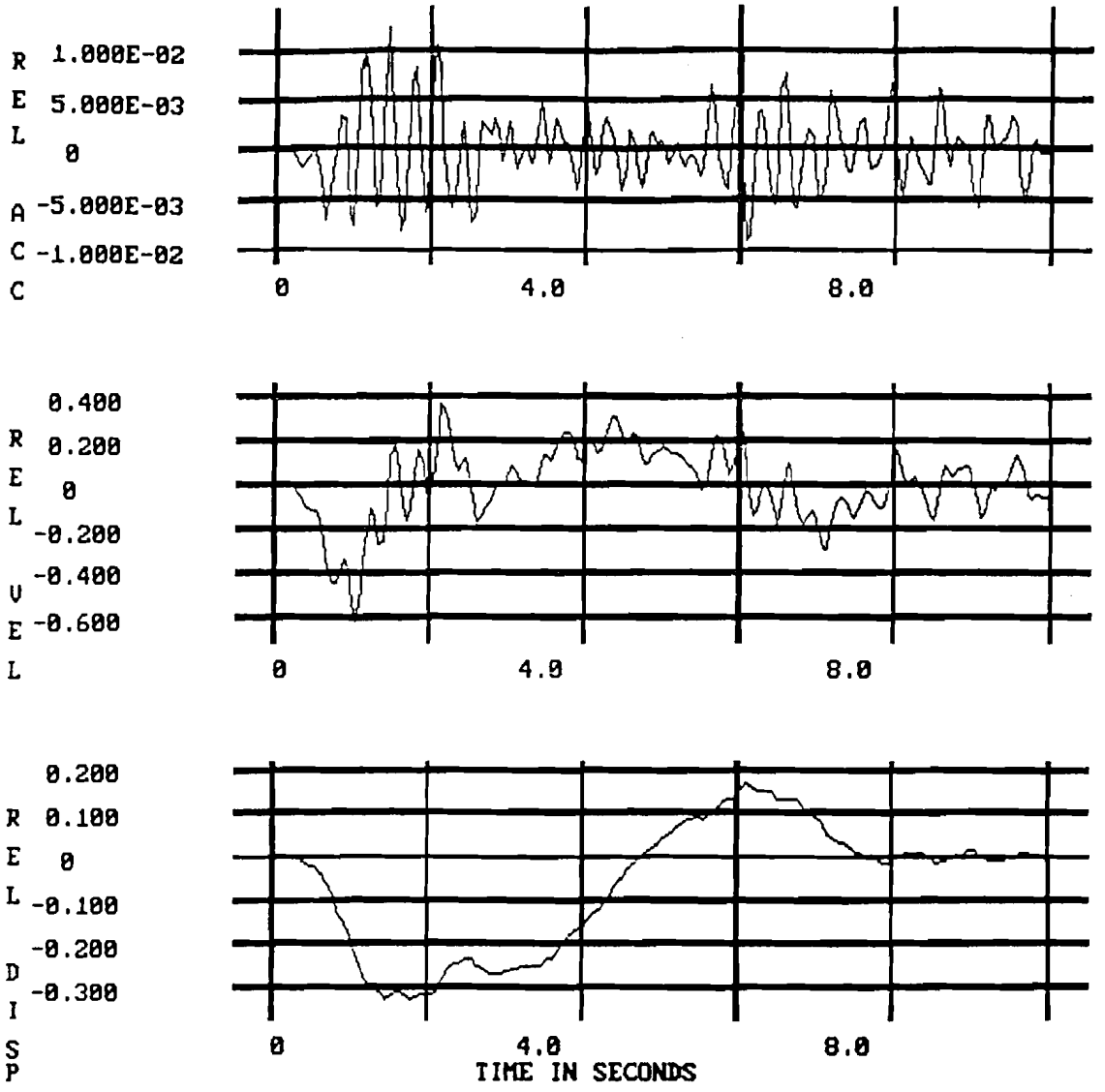

Figure 7.10: Dynamic Response of Quarter Span Point for Two Trucks Following with Full Separation at 30 mph

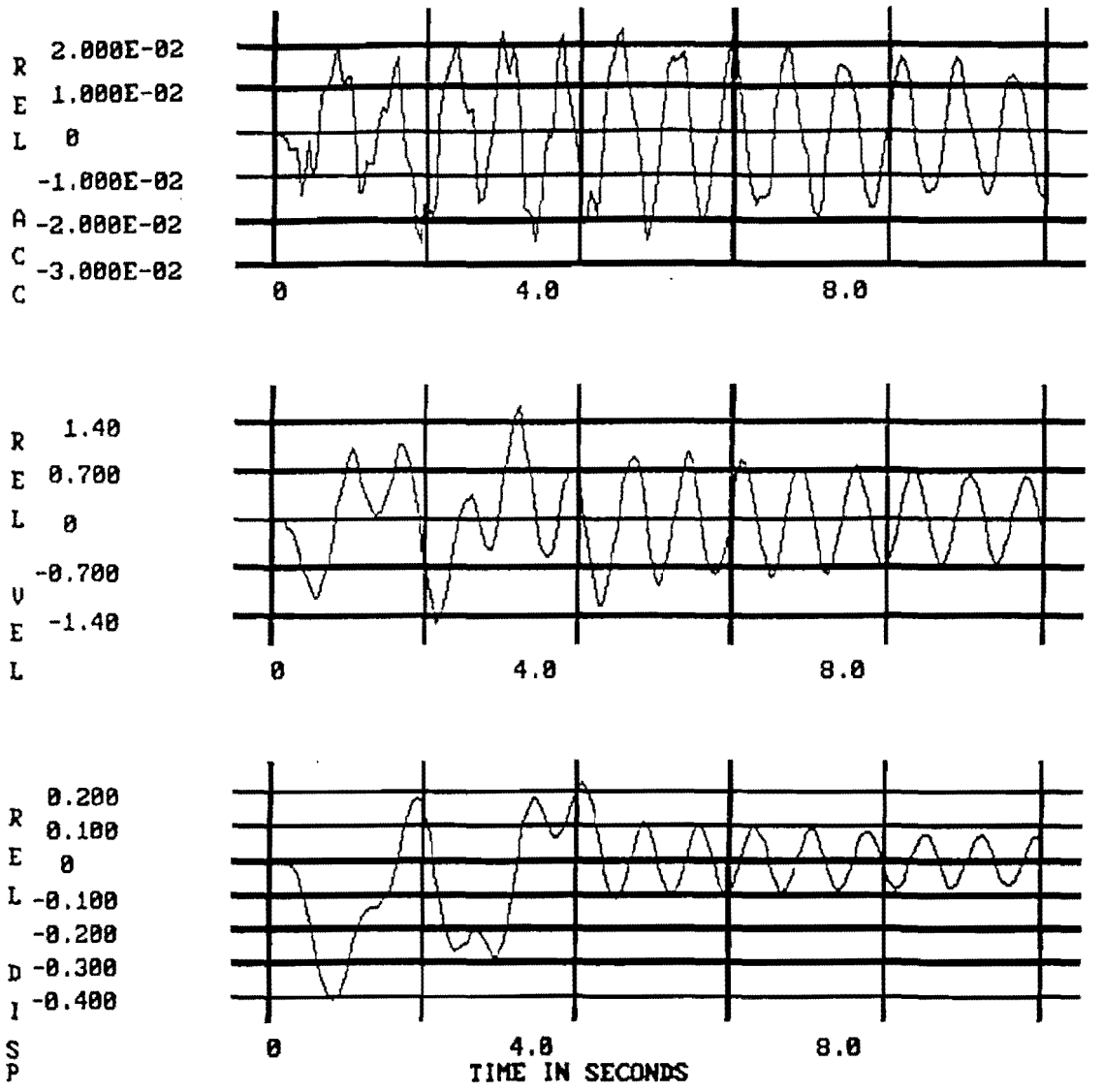

Figure 7.11: Dynamic Response of Quarter Span Point for Two Trucks Following with Full Separation at 60 mph

If the distance between the two trucks is only half the safe distance, or 9.15 m and 18.3 m (30 feet and 60 feet) for the 13.41 and 26.82 m/s (30 and 60 mph) speeds, respectively, the second truck is only 1.32 seconds behind the first one for the 13.41 m/s (30 mph) speed and 1.00 seconds behind for the 26.82 m/s (60 mph) speed. As shown in Figure 7.12, for the 13.41 m/s (30 mph) speed the maximum deflection is 11.71 mm (0.461 in) and the time history has just one peak value. This 30% increase over the one truck peak deflection is due to the fact that the second truck influences the quarter point deflection before the deflection caused by the first truck decreases. As shown in Figure 7.13 for the 26.82 m/s (60 mph) speed, the time history has more than two peak values and the absolute peak is almost the same as for the greater separation distance case.

All of this behavior reflects the fact that the distance between trucks is the most important influence, not the time delay between their effects, since the response of the bridge to each truck is close to a static response.

Case 3 - Two Trucks Passing in the Same Direction.—The deflections when two trucks are traveling in the same direction and are parallel to each other in adjacent lanes, such as one passing the other while on the bridge, are obtained by simply doubling the deflections due to a single truck (Case 1).

Case 4 - Two Trucks Meeting at the Midspan Point—When two trucks pass over the bridge in opposite directions, entering it at exactly the same time and traveling at the same speed, they meet at the midspan point, and the deflection behavior of the bridge is different from any considered so far. The time histories of the deflections at the quarter span point are shown in Figures 7.14 and 7.15 for the two speeds considered. Note that for both speeds when the two trucks are at the two quarter-span points each tends to reduce the deflection at the location of the other. This condition is the same as for the previous case of a 36.6 m (120-foot) spacing between two trucks traveling at 26.82 m/s (60 mph) in the same direction (Figure 7.10). The resulting quarter span deflections are only about half the values for one truck. The maximum deflection in this case occurs at midspan, rather than at one of the quarter-span points, and it is twice the midspan deflection for one truck. The two maximum deflections are 11.63 mm (0.458 in) and 11.79 mm (0.464 in). for the 13.41 and 26.82 m/s (30 and 60 mph) speeds, respectively.

Case 5 - Two Trucks Meeting at the Quarter Span Point—Another possibility for trucks traveling in opposite directions is for them to pass each other at one of the quarter-span points. It was found previously for the single truck case that the maximum deflection occurred at one of these points, so when two trucks meet at one of these points, the bridge is expected to have its maximum deflection. Time histories of the deflections at the quarter span point are shown in Figures 7.16 and 7.17 for two trucks passing each other

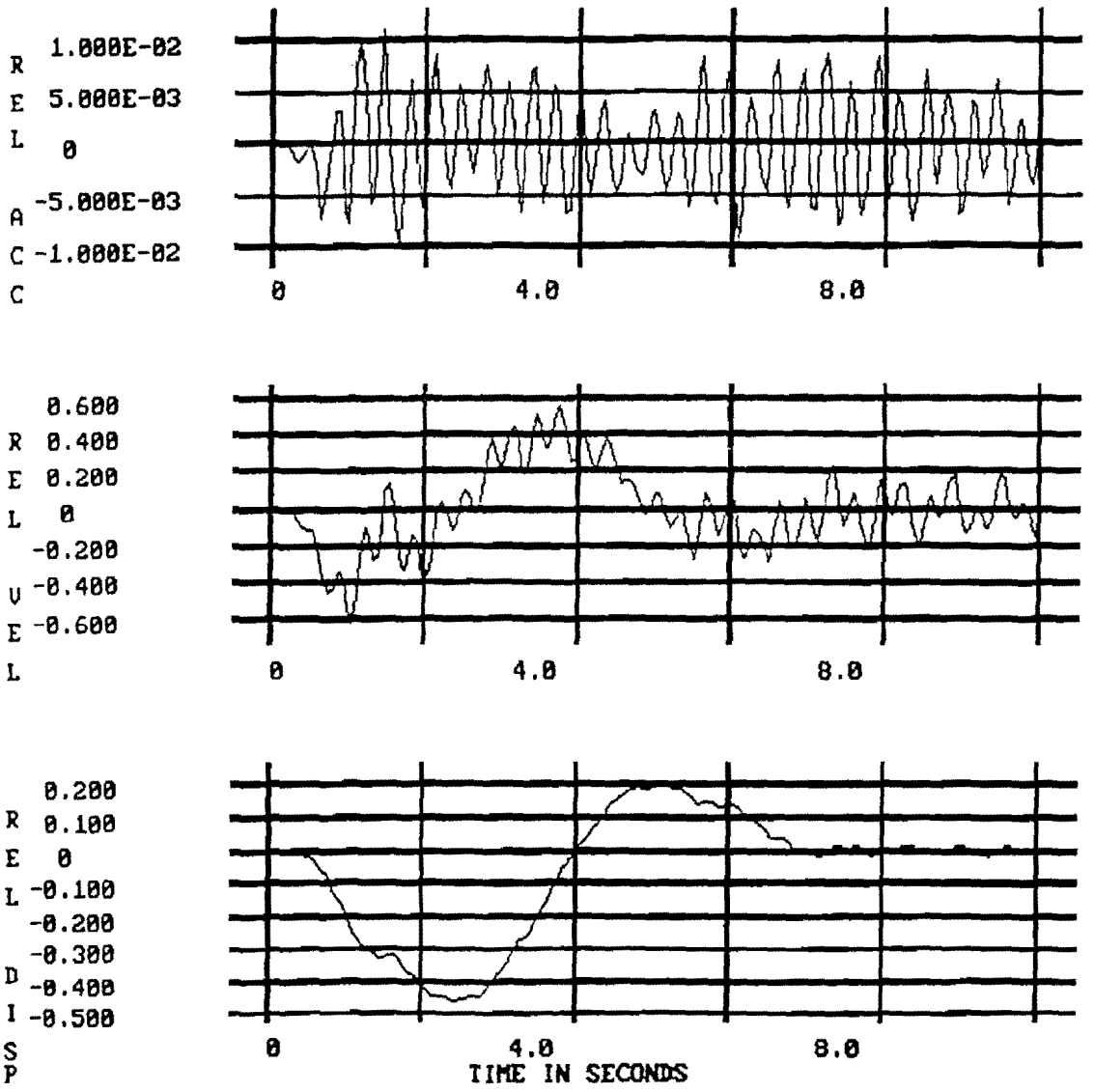

Figure 7.12: Dynamic Response of Quarter Span Point for Two Trucks Following with Half Separation at 30 mph

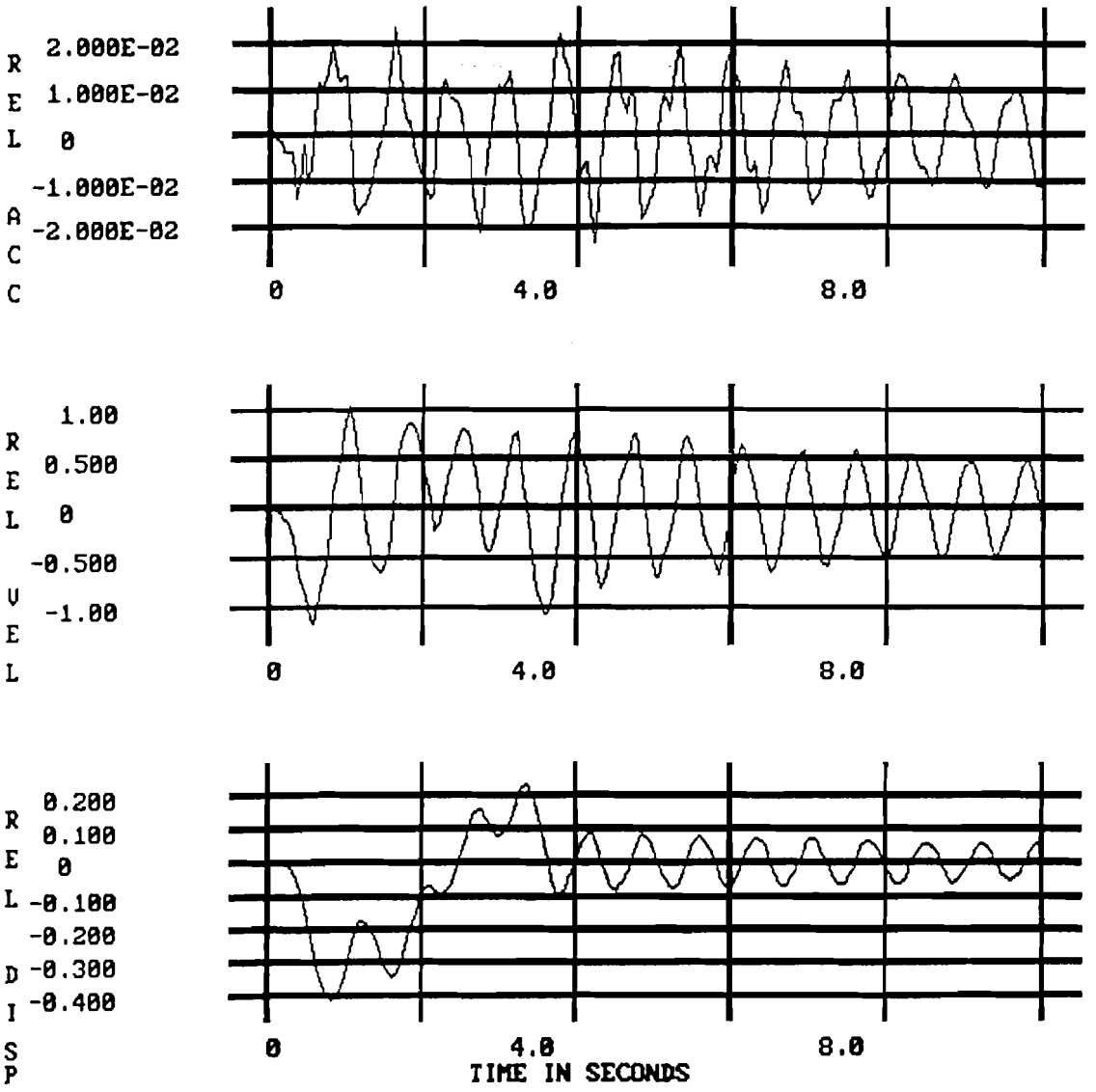

Figure 7.13: Dynamic Response of Quarter Span Point for Two Trucks Following with Half Separation at 60 mph

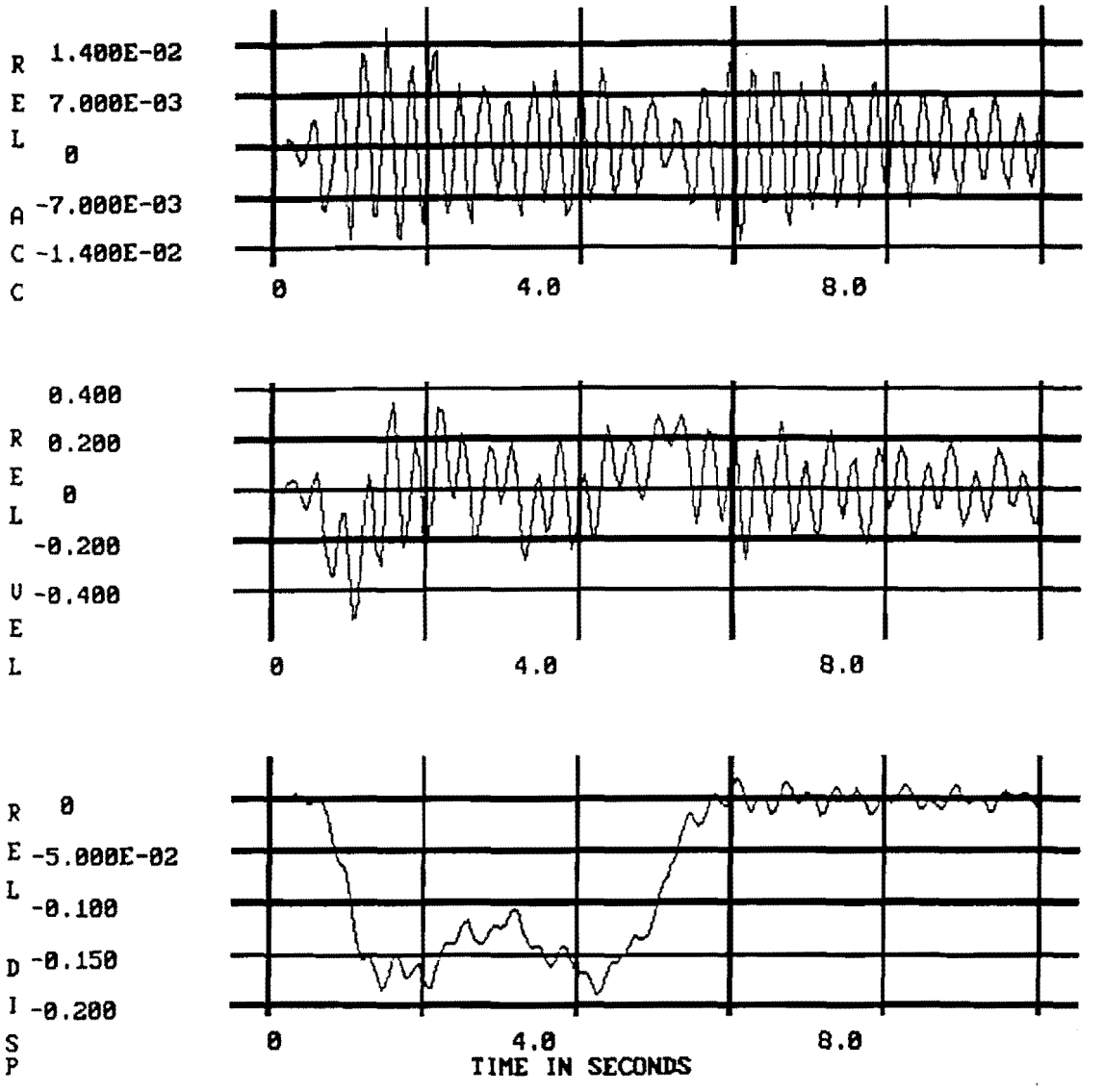

Figure 7.14: Dynamic Response of Quarter Point for Two Trucks Meeting at Midspan at 30 mph

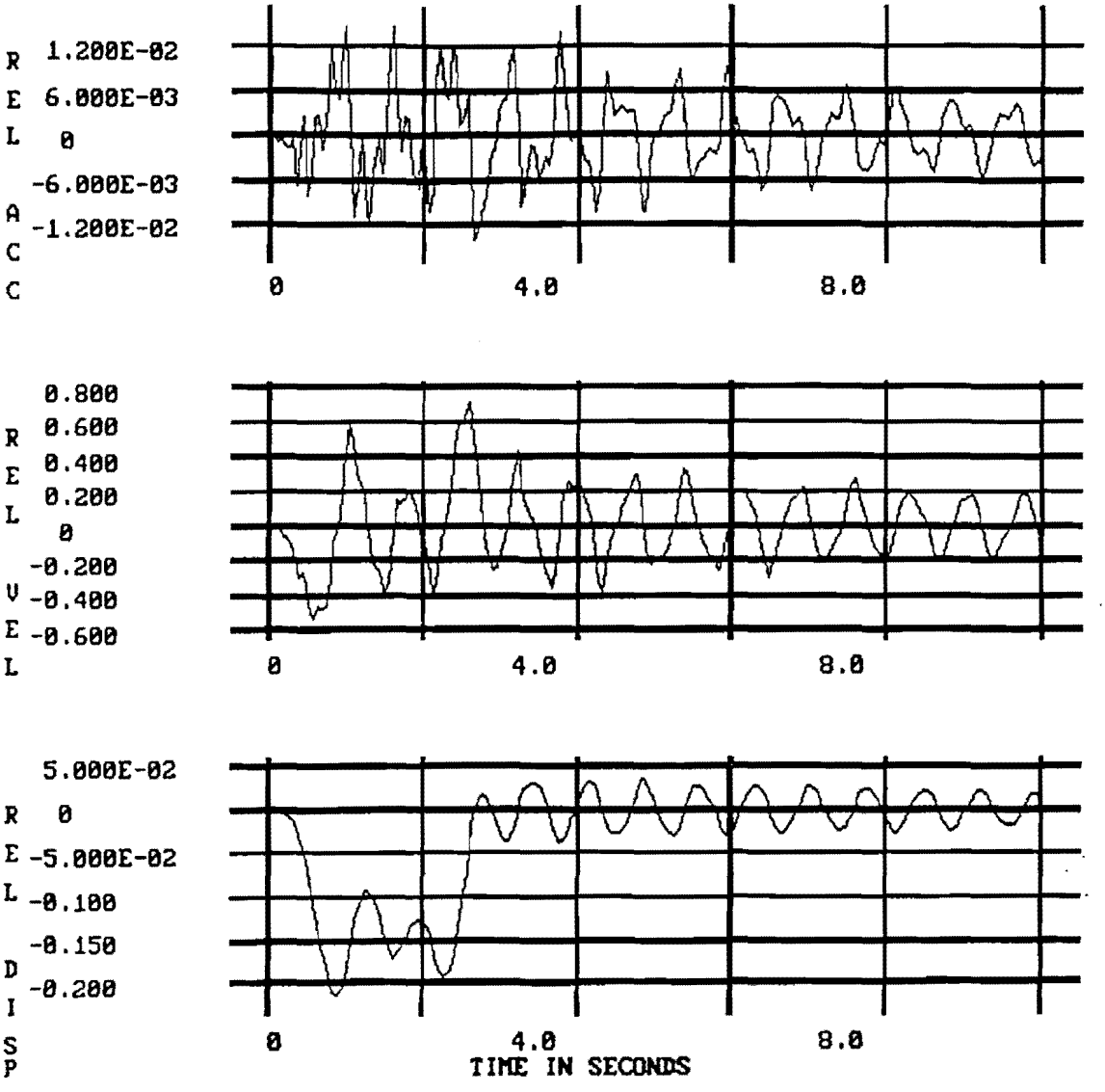

Figure 7.15: Dynamic Response of Quarter Point for Two Trucks Meeting at Midspan at 60 mph

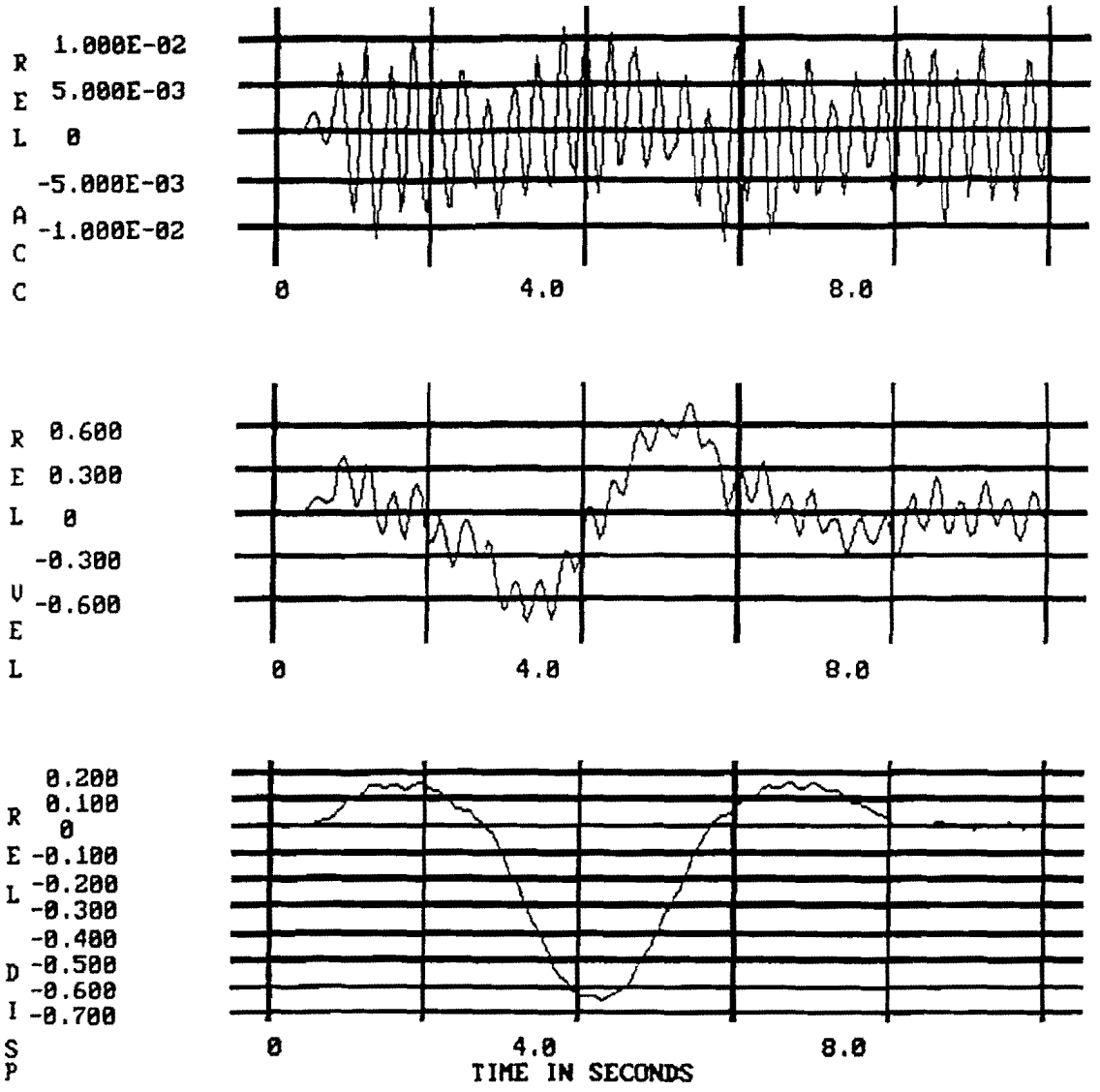

Figure 7.16: Dynamic Response of Quarter Span Point for Two Trucks Meeting There at 30 mph

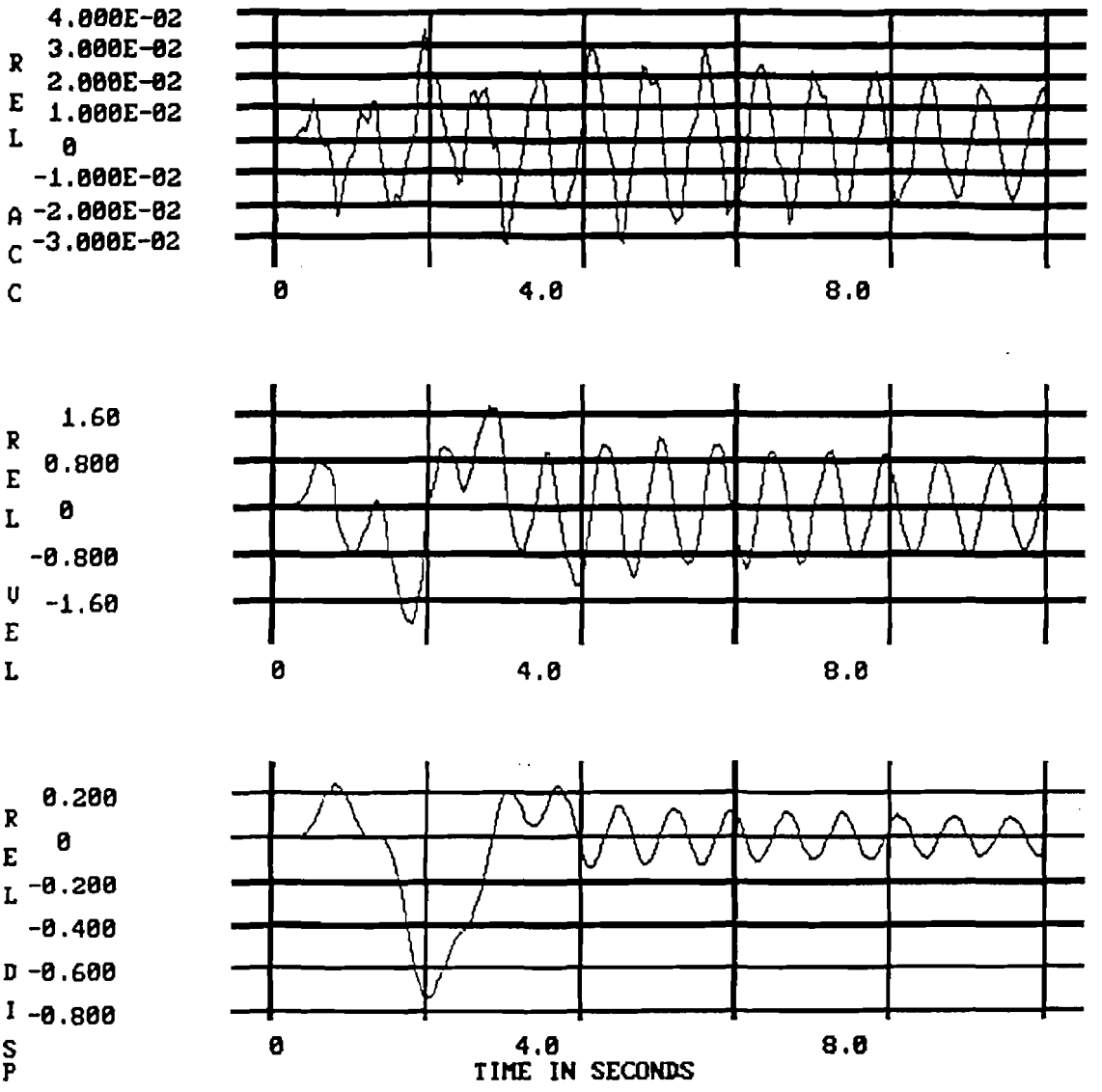

Figure 7.17: Dynamic Response of Quarter Span Point for Two Trucks Meeting There at 60 mph

other at the quarter span point. The maximum downward deflections at this point are 16.59 mm (0.653 in) and 18.85 mm (0.742 in), for the 13.41 m/s (30 mph) and 26.82 m/s (60 mph) speeds, respectively. The maximum values are essentially the same as for two trucks moving side by side (Case 3). As before, after the trucks exit the bridge, it vibrates in the 6th overall mode for the 13.41 m/s (30 mph) speed and in the first mode for the 26.82 m/s (60 mph) speed.

Summary of Peak Deflections.—Table 7.2 gives the deflections at the quarter span point and at the midspan point along the center line of the deck for all of the cases considered.

Table 7.2: Peak Dynamic Centerline Deflections Due to Traffic Loading

Case No.	Description	(unit)	30 mph speed		60 mph speed	
			1/4 span Point	Midspan Point	1/4 Span Point	Midspan Point
1.	Single Truck	in.	-0.332	-0.229	-0.377	-0.231
		mm	-8.433	-5.817	-9.576	-5.867
2.	Two trucks following:					
	- full safe separation	in.	-0.335	-0.221	-0.410	-0.232
		mm	-8.509	-5.613	-10.41	-5.893
	-half safe separation	in.	-0.461	-0.339	-0.412	-0.223
		mm	-11.71	-8.611	-10.46	-5.664
3	Two trucks passing	in.	-0.664	-0.458	-0.754	-0.464
		mm	-16.87	-11.63	-19.15	-11.79
4	Two trucks meeting at midspan	in.	-0.189	-0.458	-0.213	-0.464
		mm	-4.801	-11.63	-5.410	-11.79
5	Two trucks meeting at the 1/4 span point	in.	-0.653	-0.227	-0.742	-0.231
		mm	-16.59	-5.766	-18.85	-5.867

In dynamic analysis using the STARDYNE program, calculation of stresses in addition to deflections requires a significant amount of extra computer time. Since the dynamic deflections due to traffic loading are found to be very close to corresponding static deflections, dynamic stresses are not obtained directly herein. Rather, they are estimated from the dynamic deflection magnitudes and the degree of agreement between the deflected shapes in the static and dynamic cases. Figure 7.18 compares the influence lines of the deflections of the quarter span point due to a single truck traveling over the bridge at different speeds. The similarity in the three deflection shapes is another indication of how small the dynamic effects are for this particular bridge and type of traffic

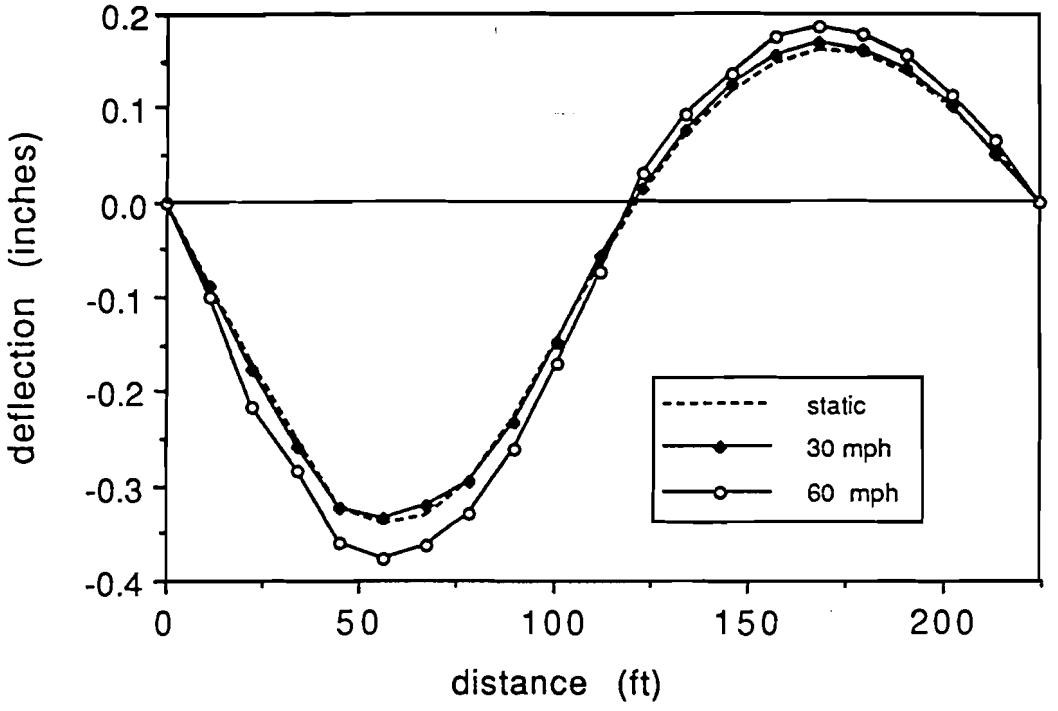

Figure 7.18: Comparison of Deflections of Quarter Span Point Between Static and Dynamic Responses

loading. The similarity also shows that the dynamic stresses will be very close to the static stresses. The ten percent increase in the peak dynamic deflections over the static deflections for the 26.82 m/s (60 mph) speed can be used to estimate the worst dynamic stresses as 1.1 times the static stresses.

Overall, the traffic loading results show that the U.S. 59 bridges considered do not have strong dynamic responses since they are relatively stiff and the vehicle speeds are not very high.

8. Frequency Domain Analysis

8.1. Flutter Instability

8.1.1. Background

Flutter instability describes an exponentially growing response of the bridge deck in which one or more modes participate at a particular critical wind velocity resulting in failure due to overstressing of the main structural system. Flutter instability of the TxDOT bridge is assessed in this report using a set of flutter-derivative coefficients calculated from wind-tunnel experiments. The flutter derivatives are dimensionless coefficients which are functions of reduced frequency $K=\omega B/U$, where U = mean wind speed, ω = frequency in rad/s, and B = deck width. The levels of aeroelastic damping and aeroelastic stiffness due to the wind-deck interaction depend on these coefficients, which are strictly functions of the shape of the cross section and hence, can be obtained only through wind-tunnel testing. Since the first few modes are uncoupled, there is a possibility of having the aeroelastic damping drive the deck to flutter instability, i.e., damping-driven flutter.

The modified damping-driven flutter criterion is as follows (Scanlan, 1978):

$$H_1^*(K)G(h_i,h_i)+H_2^*(K)G(\alpha_i,h_i)+A_1^*(K)G(h_i,\alpha_i)+A_2^*(K)G(\alpha_i,\alpha_i)\geq\frac{4\varsigma_i I_i\omega_i}{\rho B^4\omega} \quad (8.1)$$

where

$$(\frac{\omega_i}{\omega})^2=1+\frac{\rho B^4}{2I_i}\left[H_3^*(K)G(\alpha_i,h_i)+H_4^*(K)G(h_i,h_i)+A_3^*(K)G(\alpha_i,\alpha_i)\right] \quad (8.2)$$

and where $G(r_i,s_i)=\int_0^l r_i(x)s_i(x)dx$ are the modal integrals in which $r_i,s_i = h_i$ or α_i are the vertical and torsional displacement components of the ith mode shape, l is the length of the bridge, ω is the frequency in radians per second of the ith mode of vibration, I_i is the generalized mass of the ith mode of vibration, H_j^* and A_j^*, j=1...4 are the flutter derivatives, ζ_i is the mechanical damping ratio of the ith mode of vibration, B is the deck width, and ρ is the air density.

8.1.2. Experimental Results

The experiments for determining aeroelastic instability were conducted for vertical and torsional degrees of freedoms. The time history of the decaying response of the

model was recorded by releasing the model with an initial amplitude at a certain wind speed. The recorded data were then used to calculate the modified damping and stiffness of the model due to the wind flow. These values of damping and stiffness were used to calculate the flutter derivatives of the model (Scanlan, 1978). The most important ones are A_2^*, A_3^*, H_1^*, *and* H_4^*, which are shown in Figure 8.1 as functions of the dimensionless wind speed, K, for all three sign configurations considered (no sign, leeward sign, and windward sign). The experiments were carried out at several wind speeds to generate curves of the type shown, thus revealing, among other things, the wind speed at which one of the derivatives may change sign.

It is seen that only the windward sign configuration shows a negative damping in the torsional degree of freedom (see the plot of A_2^* in Figure 8.1(b)). All other configurations show positive damping in both vertical and torsional degrees of freedom. Also, it turns out that A_1^*, H_2^*, and H_3^* do not play a significant role in the response of the bridges considered because the lowest natural modes do not have coupling between the vertical (h) and torsional (α) deflections. Thus, values of the latter flutter derivatives were not determined experimentally.

8.1.3. Flutter Analysis

Flutter analysis of the full-scale bridge was carried out using Equations 8.1 and 8.2 for two different configurations. The first configuration was the one without the traffic sign. The results of the no sign experiments were used for this configuration. The second configuration was one with the traffic sign in the windward direction for half the length of the bridge deck and in the leeward direction for the other half. The results of the windward sign and leeward sign experiments from the wind tunnel were appropriately used in the analysis to simulate this configuration.

For the bridge with no signs it was found that flutter instability will never develop at any wind speed. For the configuration with windward and leeward signs on opposite ends of the bridge, mode number 5 (the 1st symmetric torsional mode) is the most vulnerable to flutter among all the modes of vibration, but it yields a wind speed for potential flutter that is so high that it is physically unrealizable. In the calculations the natural frequencies and mode shapes for both bridge configurations were taken from the finite-element analysis discussed in Section 5 of this report. The deck width B was 18.3 m (60 ft) as furnished by TxDOT. The values of the critical damping ratios ζ_i for all the modes were uniformly assumed to be 0.5%, a conservative (low) estimate.

The conclusion from the flutter instability analysis is that the bridge deck is aeroelasticity stable.

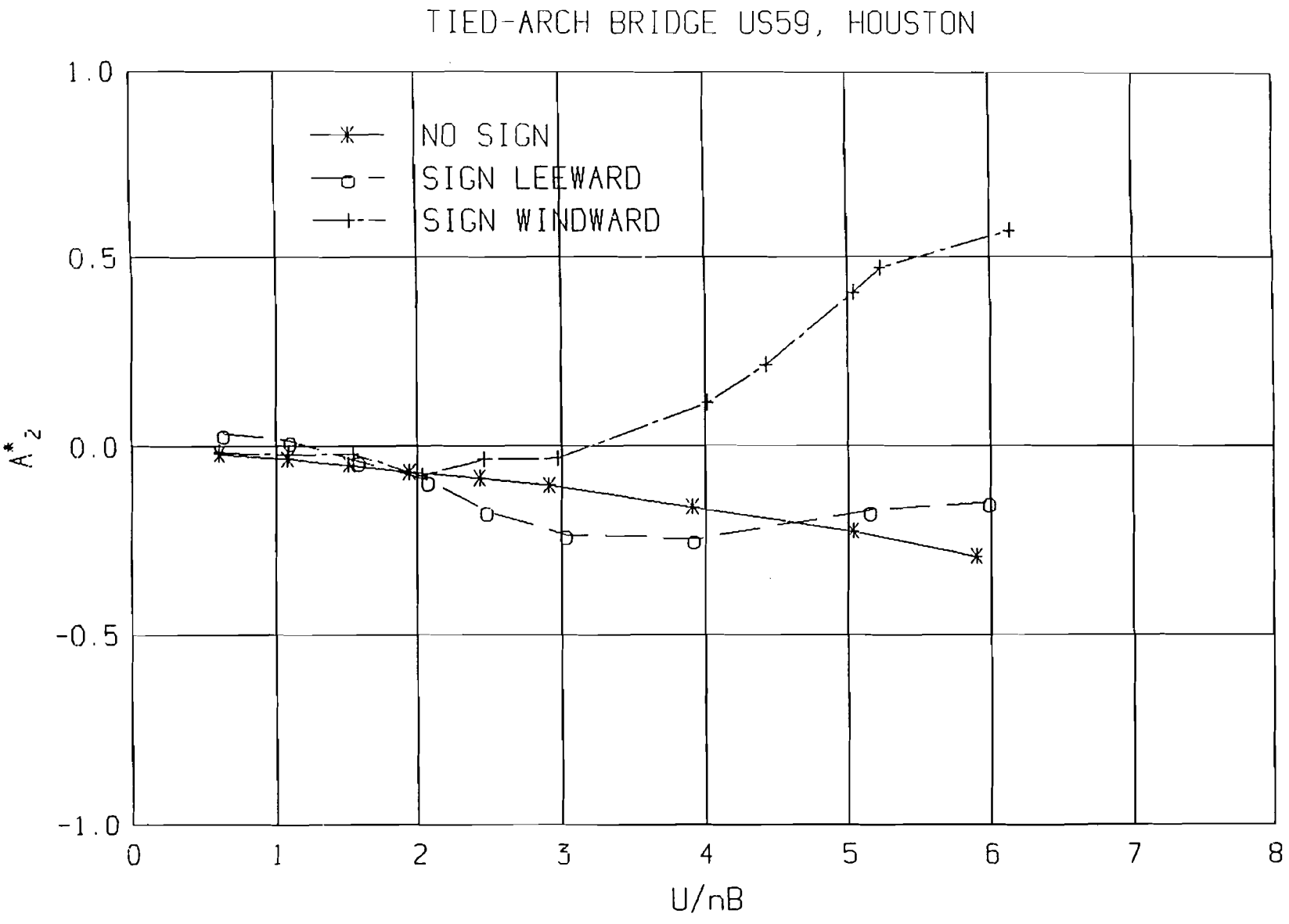

Figure 8.1(a): Flutter Derivative A_2^* vs. Wind Speed

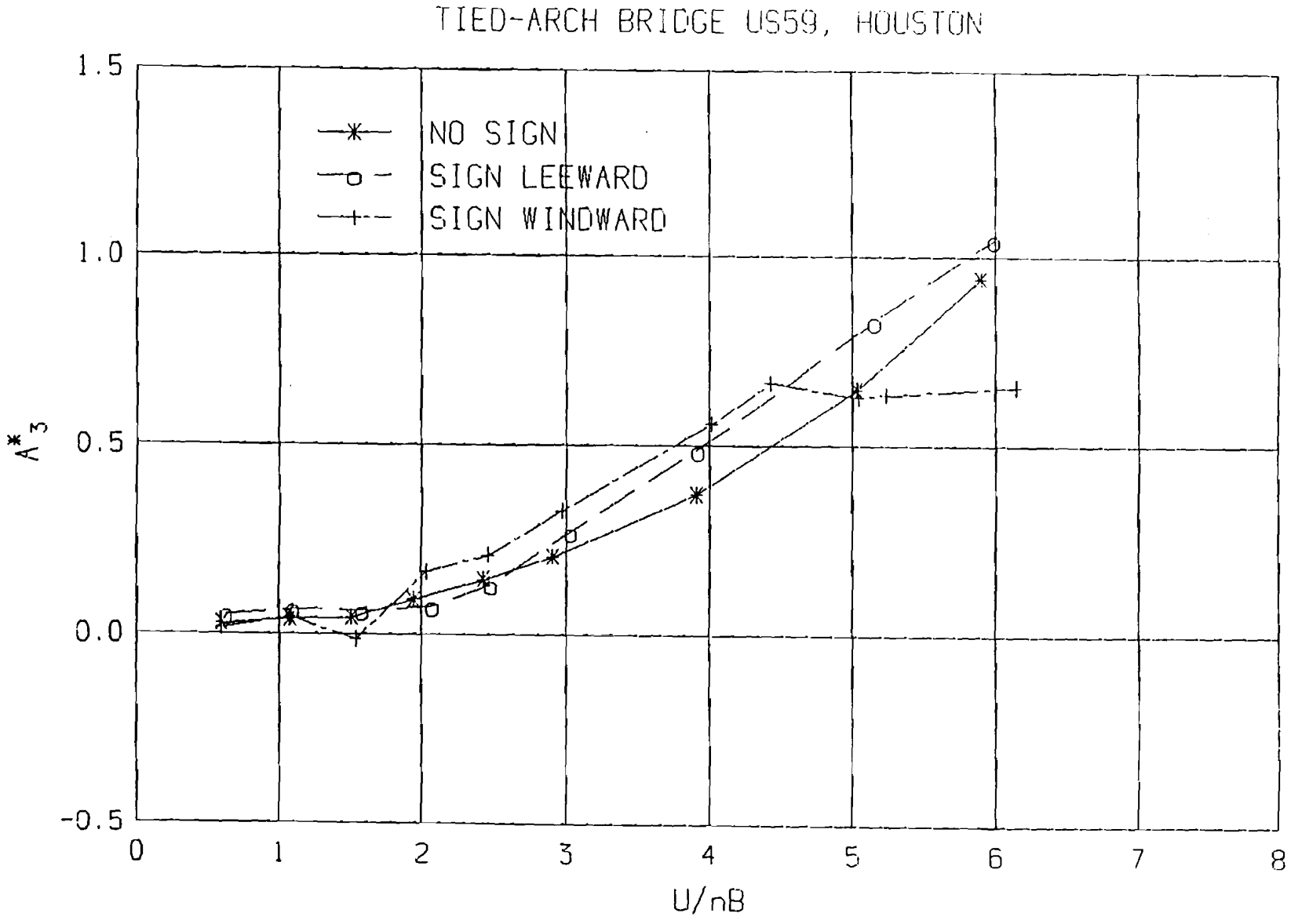

Figure 8.1(b): Flutter Derivative A_3^* vs. Wind Speed

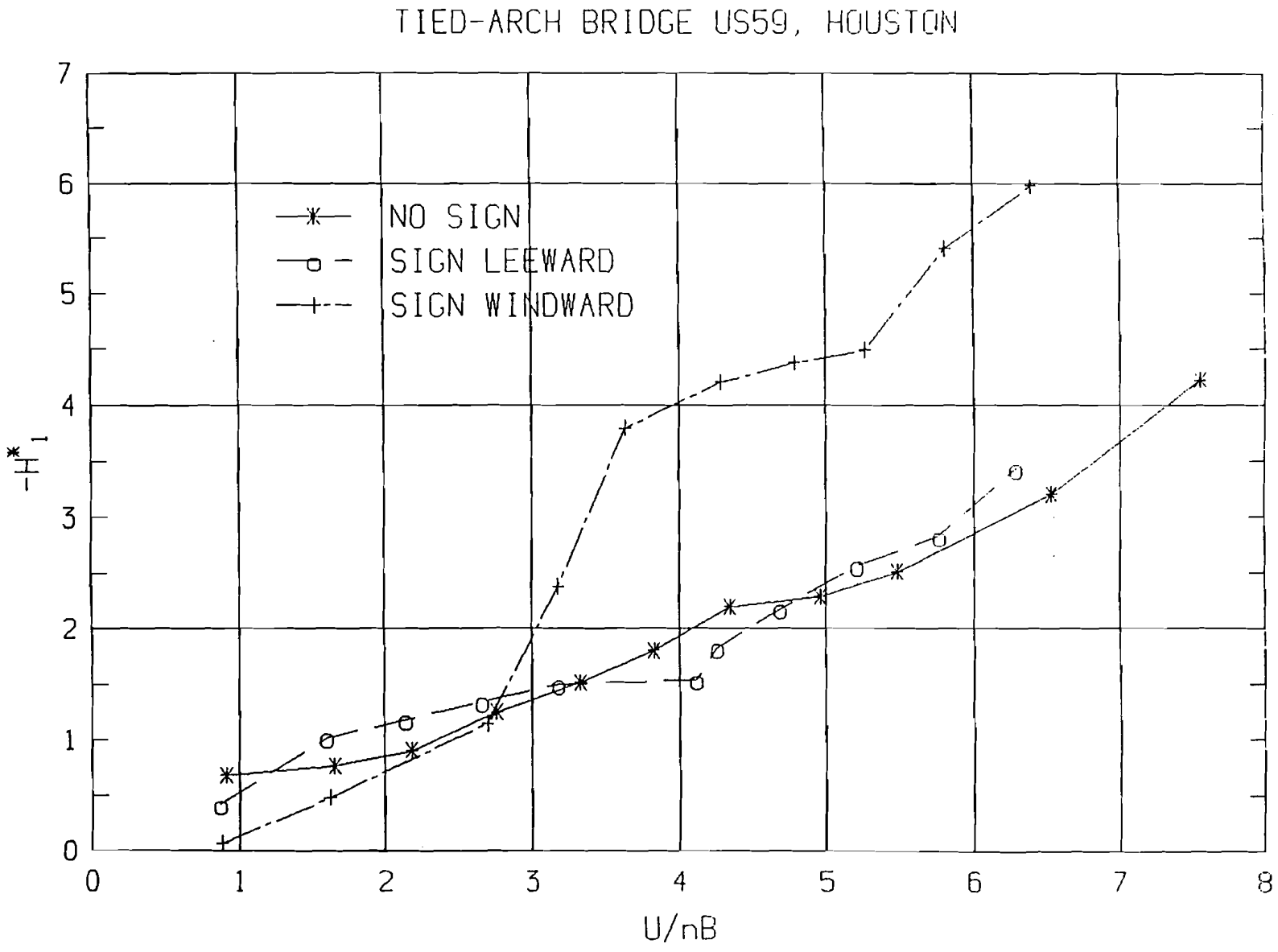

Figure 8.1(c): Flutter Derivative H_1^* vs. Wind Speed

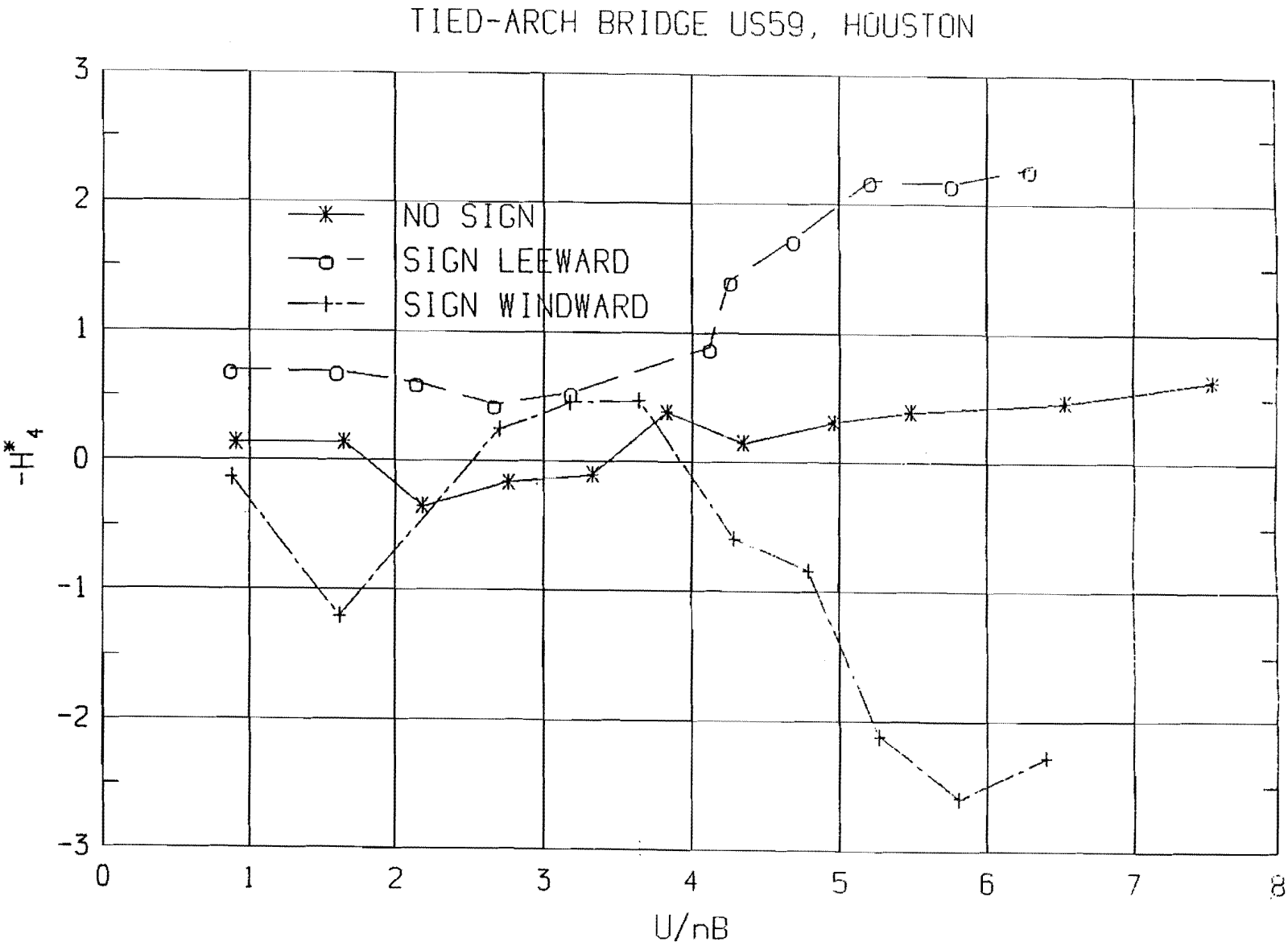

Figure 8.1(d): Flutter Derivative H_4^* vs. Wind Speed

8.2. Buffeting Response of the Deck

8.2.1. Background

A frequency-domain method is used in this section to calculate the buffeting response of the deck. Earlier, a time-domain method was used to predict the buffeting response of the deck and the arch at various construction stages.

Buffeting forces act on a bluff body like a bridge deck or arch because of fluctuations in the wind speed, i.e., wind turbulence. These forces are also influenced by turbulence induced by the bluff body itself as described by Equation 2.6. To account for the body-induced turbulence, an aerodynamic admittance function $\chi(n)$ needs to be found for each of the three forces, i.e., the lift, moment and drag forces.

8.2.2. Experimental Results

The first wind tunnel experiments for buffeting involved determination of the static coefficients of drag, moment and lift as well as the slopes of these coefficients with a variation with the angle of attack, α. The model was rigidly fixed to the force balance and steady state drag, moment and lift forces were measured for different wind speeds and different angles of attack to achieve this objective. The values of the coefficients obtained are presented in Table 8.1.

Table 8.1: Static Aerodynamic Coefficients

Bridge Component	Coefficient	No Sign	Windward Sign	Leeward Sign
Deck	C_L (A)	-0.07	-0.15	-0.69
	C_M (B)	0.04	0.60	0.29
	C_D (A)	0.11	0.22	0.22
	$C_L' (=dC_L/d\alpha)$	4.98	0.00	6.03
	$C_M' (=dC_M/d\alpha)$	2.35	0.00	2.57
Arch	C_L	0.00	0.00	-1.38
	C_M	0.00	0.00	0.00
	C_D	2.90	2.90	2.90

Notes. (A) Normalized by deck width B= 18.3 m (60 ft)

(B) Normalized by B^2

(C) Normalized by arch depth D= 0.965 m (38.0 in)

Admittance functions were determined in the wind tunnel using the dynamic model by measuring the fluctuating response under a turbulent wind. Turbulence in the wind was generated with two different grids (see Figure 8.2). In each case the turbulence intensity of both fluctuating wind components (u and w) was in the range of 8 to 10%. For the configuration of the deck with the windward sign, the admittance functions were found to be 3.0, 0.5, and 10.0 for lift, moment and drag, respectively, at the natural frequency of the model. The admittance function of the arch was assumed to be 5.0 for drag. The same values were used for all sign configurations considered in order to be conservative.

8.2.3. Buffeting Analysis

In the buffeting analysis, the mean vertical response, mean rotational or torsional response, and mean lateral or along-wind response of the deck—plus the mean lateral response of the arch—are computed. The corresponding mean square responses are also calculated to estimate the maximum excursion from the mean value. Quantities used in the analysis include the equivalent design wind speeds U calculated in Section 2.2 of this report, the assumed spectra of along-wind and vertical-wind turbulence given in Section 2.2, the first ten modes of vibration presented in Table 5.1, the force coefficients shown in Table 8.1, the admittance functions reported in Section 8.2.2, and the flutter derivatives shown in Figure 8.1. The flutter derivatives influence the buffeting response by modifying the mechanical damping ratios and the natural frequencies. The set of flutter derivatives used for the flutter instability analysis are also used in the buffeting calculations. The analysis is carried out for both of the bridge deck configurations described earlier, that is, with no signs and with windward and leeward signs on opposite halves of the deck. However, the only results presented are for the latter case, which is much more critical. The results are reported in graphical and tabular form and compared with the time domain results of Section 6.

The frequency domain buffeting analysis begins by using the spectra of along-wind and vertical-wind turbulence (Equations 2.1 and 2.2) to obtain the spectra of the buffeting responses. Then the mean square values of the responses are obtained. Although it is known that in the field the spatial correlation of wind turbulence reduces with increased distance between points along the span, the turbulence is assumed to be fully correlated along the span in the present calculations. This assumption gives a conservatively high estimate of the response. Calculations are carried out with U varying from 8.9 m/s (20 mph) to 35.8 m/s (80 mph), with along-wind turbulence intensities I_u of 25% and 40%, and with a mechanical damping ratio ζ_i of 1.0% in all modes. As indicated earlier, the first ten modes of vibration are used to calculate the total response. The resulting standard

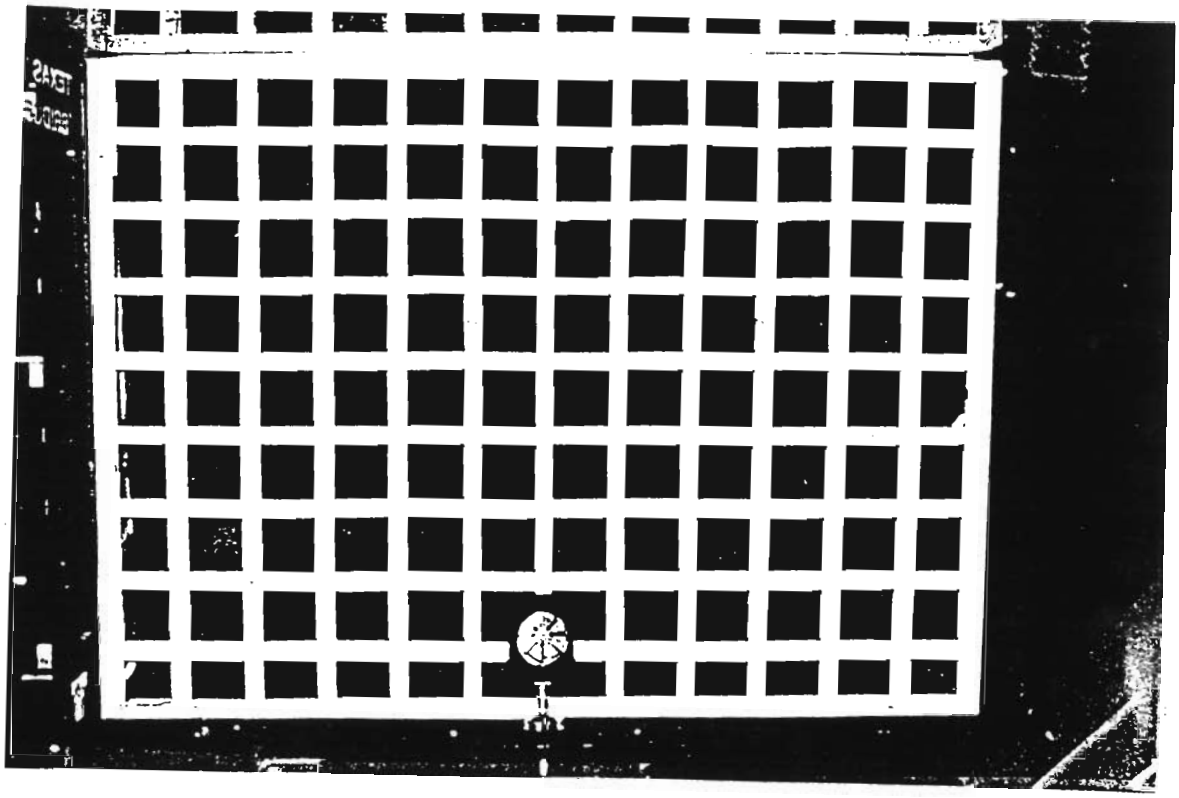

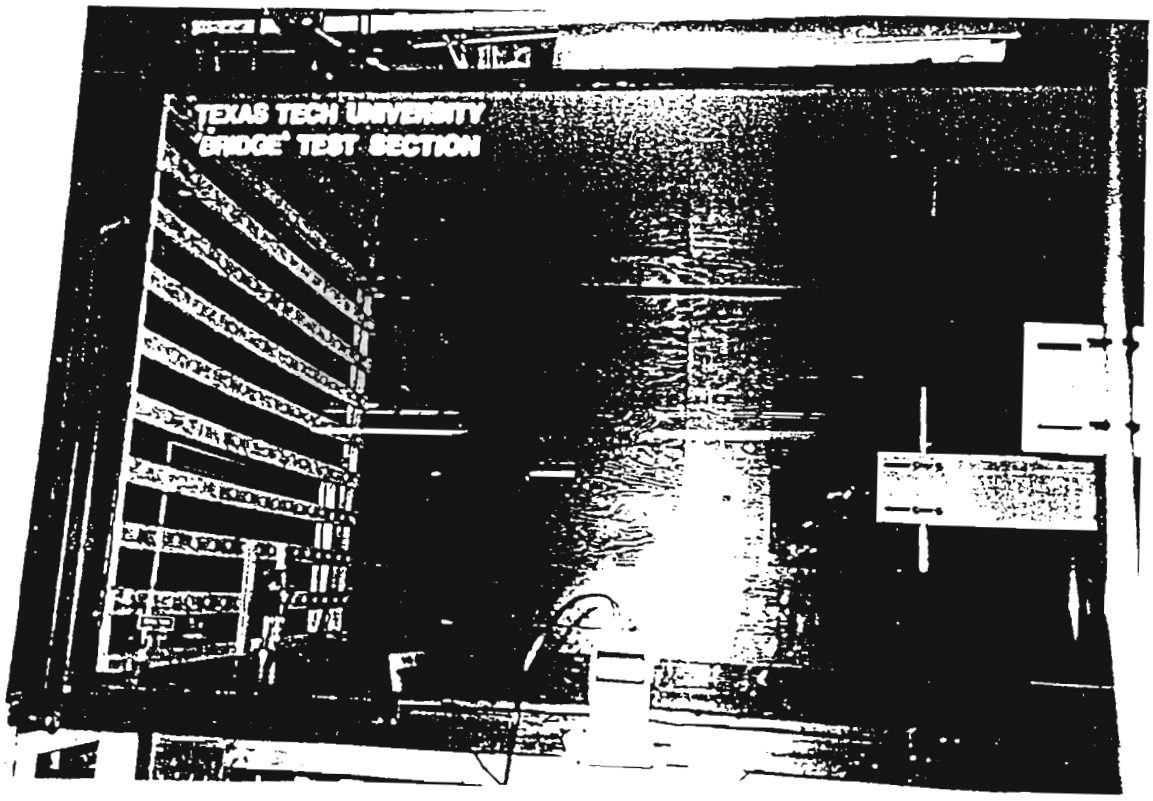

Figure 8.2: Two Different Grids for Wind Tunnel Turbulence

deviations σ_h of the maximum vertical response h and the standard deviations σ_α of the maximum torsional response α are listed in Table 8.2 for the different combinations of U and I_u, considered.

Table 8.2: Standard Deviation of the Vertical Buffeting Response (σ_h) and Torsional Buffeting Response (σ_α) of the Deck by the Frequency Domain Method

U	σ_h		σ_α	
	I_u=25%	I_u=40%	I_u=25%	I_u=40%
20 mph 8.9 m/s	6.9 E-3 ft 2.1 mm	1.2 E-2 ft 3.6 mm	2.4E-4	4.9E-4
40 mph 17.9 m/s	3.4 E-2 ft 10.4 mm	7.5 E-2 ft 22.9 mm	1.1E-3	2.3E-3
60 mph 26.8 m/s	4.2 E-2 ft 12.8 mm	8.6 E-2 ft 26.2 mm	3.0E-3	6.0E-3
80 mph 35.8 m/s	0.106 ft 30.5 mm	0.27 ft 82.4 mm	5.1E-3	1.0E-2

At a design wind speed of U = 26.8 m/s (60 mph), the largest standard deviations of the deck displacements in Table 8.2 are σ_h^{max} = 26.2 m (0.086 ft) and σ_α^{max} = 0.006 radians. These values correspond to the higher turbulence intensity I_u = 40%. Since the first ten modes of vibration (see Table 5.1) have no lateral deflection component (drag component) of the deck, the deck's lateral displacement is close to zero. The probability that the vertical or rotational response of the deck lies within a certain range of its mean can be found if the probability distribution function (PDF) is assumed to be a normal distribution. In the absence of knowledge of the PDF, usually the Chebyshev inequality is used, which states that the probability that the occurrence of any variable x is within $\bar{x}$-$c\sigma_x$ and $\bar{x}+c\sigma_x$ bounds is $1-1/c^2$, where σ_x is the standard deviation of x. If c is taken as 3.5, then the probability becomes 0.92. Therefore, there is a 92% probability for the response to be within the following bounds:

$$\begin{aligned} h_{max} &\le \bar{h} + 3.5 \times \sigma_h^{max} \\ \alpha_{max} &\le \bar{\alpha} + 3.5 \times \sigma_\alpha^{max} \\ p_{max} &\le \bar{p} + 3.5 \times \sigma_p^{max} \end{aligned} \qquad (8.3)$$

where $\bar{h}$, $\bar{\alpha}$, and $\bar{p}$ are the mean vertical, torsional and lateral deflections, respectively, given in Table 4.4.

The largest expected peak responses based on Equation 8.3 and the standard deviations in Table 8.2 are of interest, especially at the design speed U for the deck of 27.6 m/s (62 mph). This windspeed is close to the 26.8 m/s (60 mph) case in Table 8.2. At this wind speed Equation 8.3 gives peak values of h and σ as 0.09 m (0.303 ft) and 0.021 radians, respectively.

The main method used in the buffeting studies of this report is the time domain approach, as presented in Section 6. It is instructive to compare the time domain results to corresponding values obtained using the frequency domain method. In the time domain analysis, the only cases considered had 1% damping in all modes of the bridge and a wind turbulence intensity of 25%. Also, the only mean wind speed U considered was 27.6 m/s (62 mph), which is closest to the 26.8 m/s (60 mph) wind speed considered in Tables 8.2. The resulting peak deflections were given in Table 6.3. The associated standard deviations of the vertical deflection and rotation of the deck for the case of a fully correlated wind are 8.9 mm (0.029 ft) and 7.41×10^{-4} radians, respectively. For a partially correlated wind, the corresponding standard deviations are 3.8 mm (0.015 ft) and 4.06×10^{-4} radians, respectively.

The comparison of results obtained from the time domain and frequency domain methods is based on the same force coefficients as determined in the wind tunnel. The lines in Figure 8.3 show the standard deviations of the deck rotation, α, and vertical deflection, h, as functions of the design wind speed U. The smaller turbulence intensity considered (25%) produces smaller responses (the solid line), and the larger turbulence intensity produces larger responses (the dashed line). For comparison, the dynamic responses of the deck as obtained in the time domain, but changed from peak value to standard deviation form, are also shown in the figure. Reading across at 26.8 m/s (60 mph) in part (b) of the figure for the vertical deflection, the time domain response with full correlation is found to be slightly smaller than the frequency domain response given by the solid line for the same conditions (full correlation, $I_u = 25\%$, and $\zeta_i = 1\%$). The time domain results for partial correlation are even smaller, but do not match any of the frequency domain results, which are all for full correlation.

For the deck rotation in part (a) of Figure 8.3, it is seen that the standard deviation obtained from the time domain analysis with a fully correlated wind is only one-fourth as large as the corresponding result from the frequency domain analysis. The only fundamental difference between the two methods is in the aeroelastic effects included in the frequency domain analysis. However, flutter derivatives accounted for only in the frequency domain analysis should not have a large effect at the wind speed of 26.8 m/s (60 mph) considered in the comparison. The non-dimensional wind speed U/nB is only 0.65

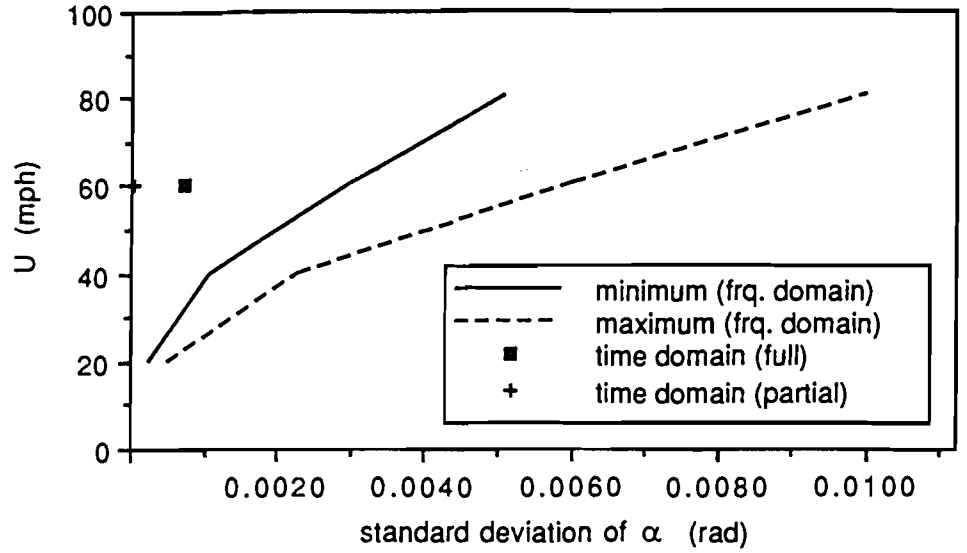

(a) Rotation on the Deck

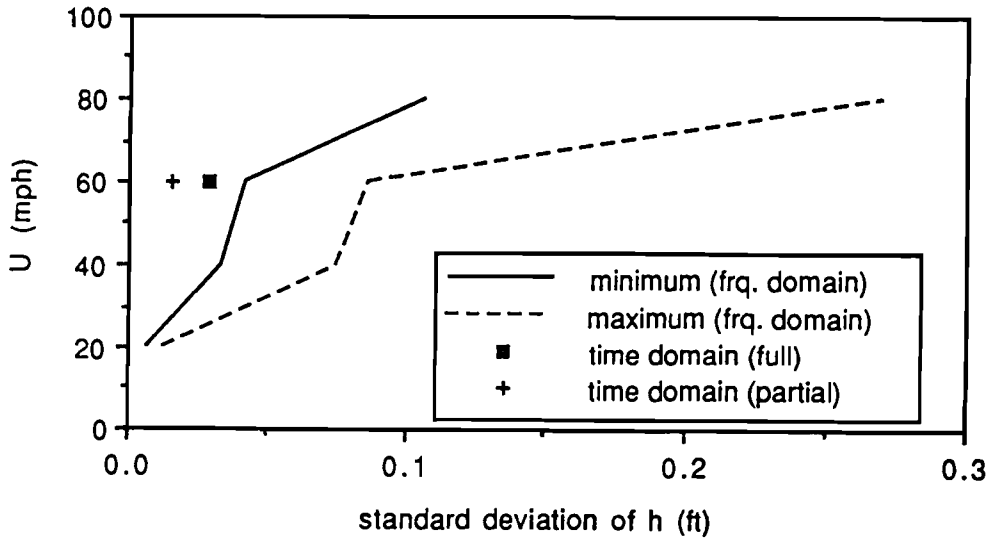

(b) Vertical Deflection on the Deck

Figure 8.3: Comparison of Standard Deviations Between Time and Frequency Domain Analyses

for the third mode and 0.49 for the fifth mode at 26.8 m/s (60 mph). Figure 8.1 shows that all of the flutter derivatives are small at this value of U/nB. Aeroelastic damping does have a greater effect on the deck's vertical deflection, h, than on its twist, α, because the more dominant first two modes involve only vertical deflections.

For this particular structure, the peak dynamic vertical and rotational deflections (as obtained in the time domain) are approximately 3.5 times the standard deviations of these deflections. This result confirms the frequently used estimates in frequency domain analysis that the peak deflections or stresses should be in the range from 3 to 4 times the standard deviations.

8.3. Vortex-Induced Response of the Deck

8.3.1. Background

Vortices will be shed from the deck at certain frequencies (f_s) and at different wind speeds according to the Strouhal number, which is defined for any cross section as follows.

$$St = f_s D / U \tag{8.4}$$

where f_s is the frequency of vortex shedding, D is a characteristic dimension perpendicular to the flow, and U is the mean wind speed. The wind tunnel experiments on the section model determined its Strouhal number to be 0.14. When the frequency of vortex shedding matches one of the natural frequencies of the deck, the vortices will excite that particular mode of vibration. Vibration at this wind speed is called "lock-in."

The amplitude of vibration at the lock-in wind speed can be calculated using Equations 8.5 and 8.6:

$$Y(x) = D\xi_0 \Phi(x) \tag{8.5}$$

and

$$\xi_0 = \frac{2}{\sqrt{\varepsilon}} \sqrt{\frac{\phi_2}{\phi_4}} \left[1 - \frac{4\pi m \zeta St}{\rho D^2 Y_1} \right]^{1/2} \tag{8.6}$$

where $\Phi(x)$ is the mode shape, $\phi_2 = \int \Phi^2(x)\frac{dx}{L}$ and $\phi_4 = \int \Phi^4(x)\frac{dx}{L}$, ζ is the critical damping ratio, ρ is the air density, m is the mass per unit length, and Y_1 and ε are experimentally obtained parameters.

8.3.2. Experimented Results

The vortex-shedding experiments were conducted at the lock-in speed, i.e., the wind speed at which the frequency of vortex shedding is equal to the natural frequency of the model. The time history of the response was recorded at the lock-in speed and the parameters of vortex shedding Y_1 and ε were identified from the data. The value of the parameter Y_1 for the deck with the windward sign is 16.0; with the leeward sign it is 13.0. The value of the parameter ε for the deck with the windward sign is 1,250; with the leeward sign it is 2,630.

8.3.3. Vortex-Shedding Analysis

The lock-in wind speeds at which the first two modes may be excited are U = 119 ft/s = 36.3 m/s (81.0 mph) for the first mode, and U = 185 ft/s = 56.3 m/s (126 mph) for the second mode, using the natural frequencies obtained from the finite-element study. The lock-in wind speed for the third mode is physically unrealizable. Although persistent winds of 36.2 m/s (81 mph) and 56.3 m/s (126 mph) are not very common, the first two modes are used for response calculations.

To use Equations 8.5 and 8.6, values of the two parameters Y_1 and ε must be known for the deck. These parameters depend on the deck shape and the mechanical damping ratio ζ and have been obtained experimentally from the wind-tunnel test, as indicated above.

Steady-state vortex-excited amplitudes of vibration are listed in Table 8.3 for both the first and second modes of vibration and damping ratios of 0.5 and 0.75 percent. All the results are for signs in the windward and leeward positions on opposite halves of the bridge. Because the first mode is anti-symmetric, full correlation of the vortices over partial spans on either side of the center point are assumed for the first mode in this calculation. Full correlation of the vortices over the entire span of the bridge is assumed for the second mode because it is symmetric. These assumptions are illustrated graphically in Figure 8.4; they are reasonable for the present purpose. The mode shapes used are from the finite-element study discussed earlier. It can be seen from Table 8.3 that the maximum amplitudes of vertical deck deflection of 0.092 m (0.30 ft) in the first mode at the lock-in wind speed of 36.3 m/s (81 mph) and of 0.09 m (0.27 ft) in the second mode

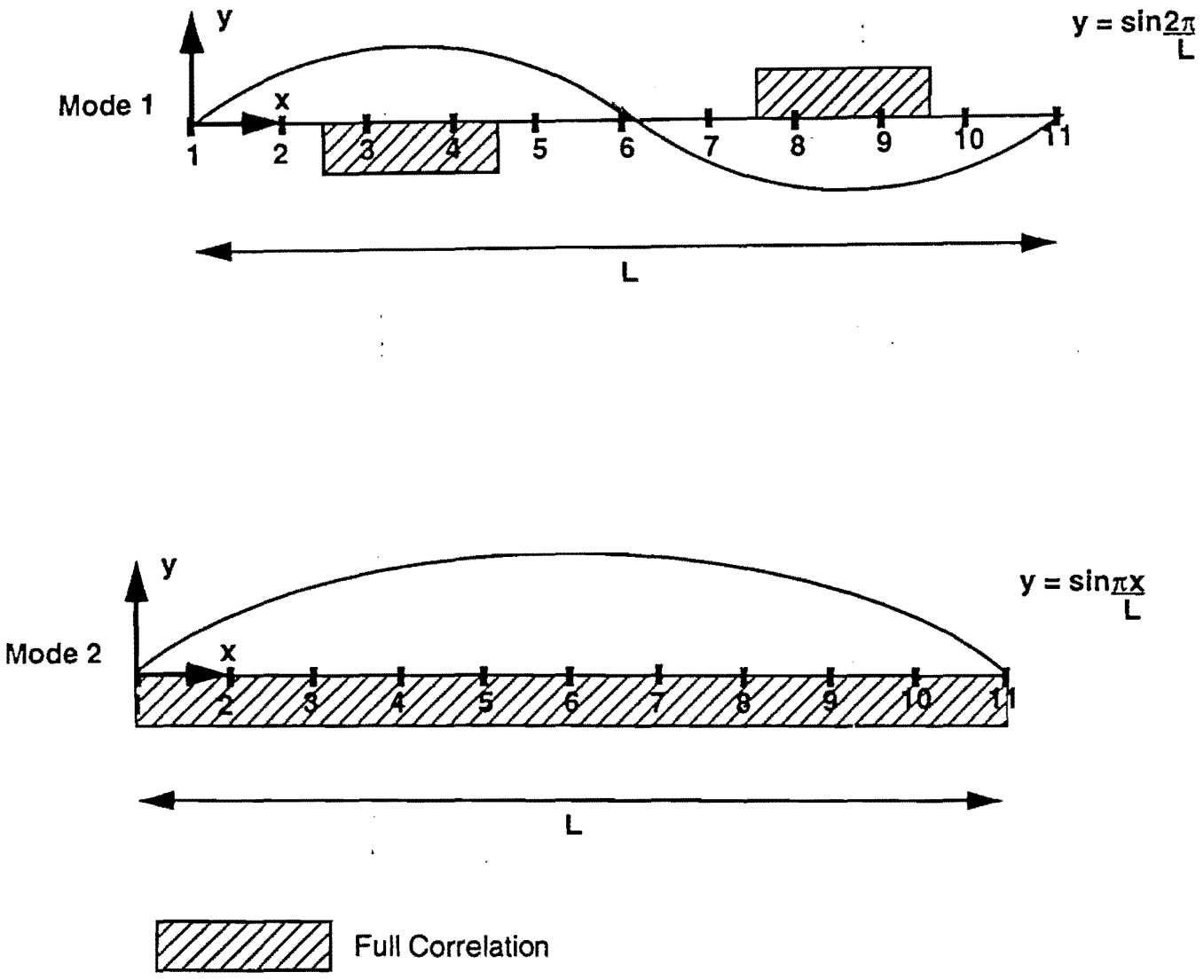

Figure 8.4: Span-wise Correlation of Vortices Shed from the Deck

at the lock-in wind speed of 56.3 m/s (126 mph) result for the same combination of parameters. The maximum amplitude in the first mode of vibration will occur at each quarter point of the span and the maximum amplitude in the second mode of vibration will occur at the midspan point of the bridge.

Table 8.3: Vertical Deflection of the Deck due to Vortex-Shedding (with Traffic Signs)

Mode	St	U	Sign Position	Y_1	ζ	ε	Amplitude	σ_h
1	0.14	81.0 mph 36.1 m/s	Windward Leeward	16 13	0.50%	1250 2630	0.30 ft 0.09 m	0.21
1	0.14	81.0 mph 36.1 m/s	Windward Leeward	16 13	0.75%	1250 2630	0.20 ft 0.06 m	0.14
2	0.14	126.0 mph 56.2 m/s	Windward Leeward	16 13	0.50%	1250 2630	0.27 ft 0.08 m	0.19
2	0.14	126.0 mph 56.2 m/s	Windward Leeward	16 13	0.75%	1250 2630	0.18 ft 0.05 m	0.13
1,2					$\geq$ 1.00%		0.00	0.00

* Note: Both windward and leeward sign positions are used for analysis of the bridge configuration (i.e., sign half windward and half leeward).

The standard deviation of a sinusoidal response of amplitude A is $A/\sqrt{2}$. Therefore, under the worst conditions, the standard deviation of the response in the first mode is equal to 0.06 m (0.21 ft). This standard deviation should be added to the mean vertical lift displacement to get the total excursion as in the buffeting analysis (Equation 8.3). The maximum excursion of the vertical response at mid-span corresponding to U=36.1 m/s (81 mph) can be calculated using Equation 8.3 as 0.24 m (0.79 ft), where the mean response is taken from Table 4.4. It needs to be mentioned that this value of the maximum excursion is an extreme value estimate based on certain assumed statistics and a high confidence limit.

The above calculations give an upper bound of approximately 0.25 m (0.8 ft) on the amplitude of vibration due to vortex shedding. Normally, the damping ratio for a concrete structure like the bridge deck is assumed to be more than 2 percent. An increase in the damping ratio will either decrease the calculated amplitude or completely eliminate the anticipated vibration. The bottom line of Table 8.3 indicates that for a damping ratio of 1.0% or greater there will be no vortex shedding vibration.

8.4. Vortex-Induced Response of Deck Hangers

8.4.1. Background

There are nine sets of hangers on each side of the deck which transfer the load from the deck to the arch. Each set of hangers consists of two bridge strands which are separated by 305 mm (12 inches) center to center. Each bridge strand is made of multiple wires and has an outer diameter of 41.3 mm (1.625, or ⅝ inches). The properties of the bridge strand and the tensile loads carried by the hangers were furnished by TxDOT.

The susceptibility of each of these hangers to vortex-shedding excitation is examined in this section. The procedures for calculating the natural frequencies and mode shapes of the hangers, the lock-in wind speeds, and the amplitudes of vibration are given first. It is found that motion due to vortex-shedding will take place only if the critical damping ratio of the hanger is below 0.05%. A damping ratio of 0.02% is assumed for the present calculation, which is a very low (conservative) number.

The formula for calculating the frequency of vibration ω (rad/s) of a hanger having mass per unit length m and length L and carrying a tensile load T is given by

$$\omega = \frac{n\pi}{L}\sqrt{\frac{T}{m}}, \qquad \text{n= 1,2,3.... mode number} \tag{8.6}$$

The above formula is modified if the flexural rigidity EI of the hanger is included in the calculation of frequency. The modified formula is

$$\omega = \frac{n\pi}{L}\sqrt{\frac{T}{m} + \frac{n^2\pi^2 EI}{mL^2}}, \qquad \text{n= 1,2,3.... mode number} \tag{8.7}$$

When EI is negligible, Equation 8.7 takes the same form as Equation 8.6. The corresponding mode shapes of the hanger are

$$\Phi_n(x) = A \times \sin(\frac{n\pi x}{L}), \qquad \text{n= 1,2,3.... mode number} \tag{8.8}$$

The following values are used for calculating the fundamental frequency of the hanger located at the center of the span (hanger no. 5):

m = mass per unit length = 0.014 slugs/in (81.0 N/m) = 5.55 lb/ft.

T = Tensile Force = 330.1 kN (74.2 kips)

L = Length = 9.91m (32.5 ft)

A = Metallic Area = 1025.8 mm^2 (1.59 in$^{2)}$

D_e = Equivalent diameter based upon A = 36.1 mm (1.42 in)

E = 1.65 x 10^8 KPa (24 x 10^6 psi)

I = 8.32 x10^4 mm^4 ($\pi D_e^4/64$ = 0.20 in.$^{4)}$

The frequencies (f_n) calculated for hanger 5 using Equations 8.6 and 8.7 are 10.22 Hz and 10.25 Hz, respectively. It was decided to use Equation 8.6 for all the hangers because the frequencies calculated using Equation 8.6 differed very slightly from those calculated using Equation 8.7.

The Strouhal number (St) of a circular cross section is 0.2 for Reynolds numbers (Re) from 500 to 10^4. There are two cables in a side-by-side configuration in each set of hangers. The ratio of the distance between hangers (E = 305 mm or 12 in) to the diameter of each hanger (D = 41.28 mm or 1.625 in.) is 7.4. It is known that as long as E/D is greater than 4.0, the vortices shed from one hanger will not interfere from those shed by the other hanger. Hence, the calculation can consider only one hanger.

Using Equation 8.4, $U = f_nD/St$ = 10.22×1.625/(0.20×12) = 2.11 m/s (6.92 ft/s) is the lock-in speed for hanger number *5* in its first mode. Similarly, the first mode lock-in speed for each hanger is calculated and tabulated in Table 8.4.

Table 8.4: Dynamic Response of the Hangers

Hanger No.	Length	Tension	f_n (Hz)	U	Y_{max}
1,9	16.25 ft 4.96 m	76.3 kips 339.4 kN	20.74	9.60 mph 4.29 m/s	0.12 in. 3.05 mm
2,8	23.75 ft 7.24 m	81.7 kips 363.4 kN	14.68	6.80 mph 3.04 m/s	0.12 in. 3.05mm
3,7	30.00 ft 9.15 m	77.1 kips 343.0 kN	11.29	5.20 mph 2.32 m/s	0.12 in. 3.05 mm
4,6	31.25 ft 9.53 m	75.0 kips 333.6 kN	10.69	4.90 mph 2.19 m/s	0.12 in. 3.05 mm
5	32.50 ft 9.91 m	74.2 kips 330.1 kN	10.22	4.70 mph 2.10 m/s	0.12in. 3.05 mm

8.4.2. Analysis of Vortex-Induced Responses of Deck Hangers

The amplitudes of vibration of the different cables at the lock-in wind speed can be calculated using Equations 8.5 and 8.6 in which D = 4.13 mm (1.625 in). If it is assumed that vortices are fully correlated over the entire length of the hanger in Equation 8.6, then

ϕ_2= 0.500 and ϕ_4= 0.375. The parameters Y_1 and ε are taken as 4.96 and 624.0, respectively, for a circular cross section (Goswami 1991). Assuming a damping ratio ζ of 0.02 %, Equation 8.5 gives the value of the amplitude of steady-state vibration Y_{max} at mid-height of the hanger as 3.05 mm (0.12 in.). The same calculation can be repeated by assuming that vortices are correlated only over the middle third of the length of the hanger. The amplitude of vibration for this case is 2.54 mm (0.10 in.).

Table 8.4 lists the calculated values of the natural frequencies (f_n), the lock-in wind speeds (U), and amplitudes of vibration (Y_{max}) at the mid-height location of the hangers, assuming fully-correlated vortex shedding over the entire span of each hanger. In every case, Y_{max} = 3.05 mm (0.12 inch) because the steady-state vibration amplitude due to vortex shedding is dependent only upon three parameters, namely, mass per unit length, diameter, and the assumed damping ratio of the hanger, which are taken to be the same for all the hangers. If it is assumed that the vortices are correlated only over the middle third of the hanger, then the values of the amplitudes reduce marginally to 2.54 mm (0.10 inch).

It can be concluded from the above analysis that even with a very low assumed damping ratio, the maximum amplitude of vibration is only 3.05 mm (0.12 inch). Hence, the expected motion of any hanger, if it vibrates at all, will be imperceptible and should not be a problem.

9. CONCLUSIONS

A comprehensive set of investigations of the proposed arch bridges over U.S.59 in Houston has been carried out to determine their potential susceptibility to wind and traffic loadings. Wind tunnel tests on a geometrically scaled model of the bridge deck have been conducted to determine the pertinent parameters for buffeting, vortex shedding and flutter behavior. Then, analyses for all three of these types of dynamic wind behavior, as well as for static wind and static and dynamic traffic loading effects, have been conducted.

Analyses in the frequency domain using the flutter parameters determined in the wind tunnel show that the bridge deck will be aeroelastically stable (not susceptible to flutter instability) except at unrealistically high wind speeds of over 68 m/s (150 mph). Even this condition is possible only for the bridge deck with a 3.1 m (10-foot) traffic sign attached to the upwind side. Analyses in the frequency domain with the vortex shedding parameters determined in the wind tunnel show that, while vortex shedding can occur at wind speeds of 36 m/s (81 mph) and 56 m/s (126 mph), the so-called "lock-in" wind speeds for the first and second vertical modes of vibration, vortex shedding will not produce deflections or stresses of concern. Flutter and vortex shedding studies are not needed for the partially completed stage of the bridge (when the existing bridge has been removed and the new deck has not yet been installed) because the thin deck that is potentially susceptible to these problems is not present.

Studies have been carried out in both the frequency and time domains to determine the buffeting wind behavior of the bridges. The time domain analyses have utilized the finite element code STARDYNE and have included both fully correlated and partially correlated winds on the completed bridges. Also, these studies have treated the buffeting wind response of a typical bridge in its partially completed stage. Conservatively low fractions of critical damping of 0.5 to 2.0 percent have been assumed for all modes of vibration. These computations show that even buffeting from a turbulent lateral wind with a basic wind speed of 40 m/s (90 mph), which is the standard design wind in Houston, will only produce stresses in the completed bridge of 14 MPa (2 ksi). Although a detailed fatigue analysis has not been performed, stresses of this magnitude should not create fatigue problems in the completed bridge. For the partially completed bridge, the peak buffeting stresses could be as high as 104 MPa (15 ksi) in the temporary horizontal braces. However, there still should not be a fatigue problem because of the very short time over which this stage of construction will be subjected to the wind. Frequency domain calculations of the buffeting response of the completed bridge agree reasonable well with the time domain results. Comparison between the two show that the common assumption

that the peak response will be between 3 and 4 times the root mean square response is valid.

Studies of the expected vibration of the hanger cables due to vortex shedding reveal that the different cables may vibrate at wind speeds in the range from 2.2 to 4.4 m/s (5 to 10 mph), but only with an amplitude of 3.0 mm (0.12 in.), irrespective of their different lengths. This amplitude of vibration should not cause a problem. It is based on an assumed damping ratio of 0.02 percent, which is a very low value. If the actual damping ratio is 0.5 percent or higher, then the cables should hardly vibrate at all.

Time domain studies of the bridge under stationary and moving traffic loads indicate that the bridge will basically behave in a static manner. The largest dynamic amplification factor, or impact factor, found was 1.10. Several combinations of one and two HS20-44 trucks moving in the same and opposite directions were considered in the traffic loading analysis.

The overall conclusion from this project is that the proposed arch bridges over U.S. 59 in Houston should not have any problems with wind or traffic loadings.

REFERENCES

AASHTO (1977), "Standard Specifications for Highway Bridges," American Association of State Highway and Transportation Officials, Twelfth edition.

ASCE (1990), "Minimum Design Loads for Buildings and Other Structures," ASCE 7-88, American Society of Civil Engineering, New York, NY.

Barton, F. W., T.T. Baber, P.S. Duemmel, and W. T. Mckeel (1991), "Field Test of a Cable-Stayed Bridge," *Transportation Research Record 1290*, pp. 243-251.

Blevins, R. D. (1984), *Applied Fluid Dynamics Handbook*, Van Nostrand Reinhold Company, Inc., New York.

Bryja, D. and P. Sniady (1991). "Spatially coupled Vibrations of a Suspension Bridge under Random Highway Traffic," *Earthquake Engineering and Structural Dynamics*, Vol. 20, pp. 999-1010.

Chan, T. H. T. and C. O'Connor (1990), "Vehicle Model for Highway Bridge Impact," *Journal of Structural Engineering*, Vol. 116, No. 7, pp. 1772-1793.

Davenport, A.G., King, J.P.C. and Larose, G.L. (1992), "Tautstrip Model Tests," Proceedings of First International Symposium on Aerodynamics of Large Bridges, A. Larsen, ed., Copenhagen, Denmark.

Goswami, I. (1991), *Vortex-Induces Response of Circular Cylinders*, Thesis submitted in conformity with the requirements for Doctor of Philosophy, Dept. of Civil Engg., The Johns Hopkins University, Baltimore, MD.

Gupta, R. K. (1980), "Dynamic Loading of Highway Bridges," *Journal of the Engineering Mechanics Division*, Vol. 106, No. EM2, pp. 377-394.

Hwang, E.-S. and A.S. Nowak, (1989), "Dynamic Analysis of Girder Bridges," *Transportation Research Record 1223*, pp.85-92.

Kovacs, I. (1994), "Synthetic Wind for Investigations in Time-Domain," ASCE Structures Congress XII, 1994.

Scanlan, R. H. (1978), "State-of-the-Art Methods for Calculating Flutter, Vortex Induced, and Buffeting Response of Bridge Structures," Federal Highway Administration Report No. FHWA/RD 80/50.

Scanlan, R. H. (1988), "On Flutter and Buffeting Mechanism in Long-Span Bridges," *Probabilistic Engineering Mechanics*, Vol. 3(1), pp. 22-27.

Shinozuka, M. and Jan, C.M. (1972), "Digital Simulation of Random Processes and Its Applications," *Journal of Sound and Vibration*, Vol. 25(1), pp. 111-128.

Simiu, E. and Scanlan, R. H. (1986), *Wind Effects on Structures,* Second Edition, Wiley-Interscience Publications, New York.

Yen, B.T. and L. L. Y. Lai (1989), "Evaluation of Bridge Vibration Through Field Measurement of Strains," *Transportation Research Record 1223*, pp. 101-106.